ISTANBUL TECHNICAL UNIVERSITY ★ GRADUATE SCHOOL

PERFORMANCE ASSESSMENT OF NONLINEAR ACTIVE DEVICES TO DESIGN BROADBAND MICROWAVE POWER AMPLIFIERS VIA VIRTUAL GAIN OPTIMIZATION

Ph.D. THESIS

Sedat KILINÇ

Electronics and Communication Engineering Department

Electronics Engineering Programme

APRIL 2023

ISTANBUL TECHNICAL UNIVERSITY ★ GRADUATE SCHOOL

PERFORMANCE ASSESSMENT OF NONLINEAR ACTIVE DEVICES TO DESIGN BROADBAND MICROWAVE POWER AMPLIFIERS VIA VIRTUAL GAIN OPTIMIZATION

Ph.D. THESIS

Sedat KILINÇ
(504152206)

Electronics and Communication Engineering Department

Electronics Engineering Programme

Thesis Advisor: Prof. Dr. Ismail Serdar OZOGUZ
Thesis Co-Advisor: Prof. Dr. Bekir Siddik Binboga YARMAN

APRIL 2023

İSTANBUL TEKNİK ÜNİVERSİTESİ ★ LİSANSÜSTÜ EĞİTİM ENSTİTÜSÜ

DOĞRUSAL OLMAYAN AKTİF ELEMANLARIN PERFORMANS ANALİZİ VE SANAL KAZANÇ OPTİMİZASYONUYLA GENİŞBANDLI MİKRODALGA GÜÇ KUVVETLENDİRİCİSİ TASARIMI

DOKTORA TEZİ

Sedat KILINÇ
(504152206)

Elektronik ve Haberleşme Mühendisliği Anabilim Dalı

Elektronik Mühendisliği Programı

Tez Danışmanı: Prof. Dr. İsmail Serdar ÖZOĞUZ
Eş Danışman: Prof. Dr. Bekir Sıddık Binboğa YARMAN

NİSAN 2023

Sedat KILINÇ, a Ph.D. student of ITU Graduate School student ID 504152206, successfully defended the thesis/dissertation entitled "PERFORMANCE ASSESSMENT OF NONLINEAR ACTIVE DEVICES TO DESIGN BROADBAND MICROWAVE POWER AMPLIFIERS VIA VIRTUAL GAIN OPTIMIZATION", which he prepared after fulfilling the requirements specified in the associated legislations, before the jury whose signatures are below.

Thesis Advisor :	**Prof. Dr. İ. Serdar ÖZOĞUZ** Istanbul Technical University	....
Co-advisor :	**Prof.Dr. B. Sıddık YARMAN** Istanbul University-Cerrahpaşa	....
Jury Members :	**Prof. Dr. Ahmet AKSEN** Işık University	....
	Prof. Dr. Fırat KAÇAR Istanbul University-Cerrahpaşa	....
	Assoc. Prof. Dr. Metin YAZGI Istanbul Technical University	....
	Assoc. Prof. Dr. Tufan C. KARALAR Istanbul Technical University	....
	Assoc. Prof. Dr. Oğuzhan KIZILBEY TUBITAK National Metrology Institute	....

Date of Submission : 26 January 2023
Date of Defense : 26 April 2023

To humanity and science,

FOREWORD

I would first of all like to express my sincere gratitude to my thesis co-advisor, Professor Sıddık B. YARMAN. He has been a constant source of encouragement during my graduate studies, providing me with a very pleasant and productive research environment without which this thesis would not have been possible. I would also like to acknowledge the numerous professional advancement opportunities he has provided. I have learned a great deal from him.

I would also like to express my sincere gratitude to my advisor Prof. Dr. Serdar ÖZOĞUZ for his very precious support and encouragement. Whenever I need support and guidance throughout my dissertation studies, his office was always open.

I give my thanks to Prof. Dr. Fırat KAÇAR (from Istanbul University-Cerrahpasa) for his academic guidance, encouragement, and support.

Special thanks are extended to Prof. Dr. Ahmet AKSEN and Assoc. Prof. Dr. Metin YAZGI for their valuable suggestions, discussions, and for serving on the steering committee of the thesis.

Gratitude is extended to Asst. Prof. Dr. Koray GÜRKAN (from Istanbul University-Cerrahpasa) who helped me with manufacturing the printed circuit boards for prototypes.

Finally, I owe my thanks to my family for their continuous support and endless patience.

January 2023

Sedat KILINÇ
(Electronics and Communication
Engineer, M.Sc.)

TABLE OF CONTENTS

Page

ABBREVIATIONS

BW	**:** Bandwidth
DE	**:** Drain Efficiency
FM	**:** Fictitious Double Matching Problem
FM	**:** Fictitious Matching
GaN	**:** Gallium Nitrate
GBWL	**:** Gain Bandwidth Limitation
HEMT	**:** High Electron Mobility Transistor
IMN	**:** Input Matching Network
LMS	**:** Least Mean Squared
LP	**:** Load Pull
MSE	**:** Mean Squared Error
OMN	**:** Output Matching Network
PA	**:** Power Amplifier
PAE	**:** Power Added Efficiency
PD	**:** Power Delivery
PI	**:** Power Intake
PPP	**:** Power Performance Product
PR	**:** Positive Real
PRF	**:** Positive Real Function
RF	**:** Radio Frequency
RF-LST	**:** Real Frequency Line Segment Technique
RFT	**:** Real Frequency Technique
SP	**:** Source Pull
TPG	**:** Transducer Power Gain
VGO	**:** Virtual Gain Optimization

SYMBOLS

$\boldsymbol{C}$	: Capacitance
$\boldsymbol{L}$	: Inductance
$\boldsymbol{R}$	: Resistance
$\boldsymbol{X}$	: Reactance
$\boldsymbol{Z}$	: Impedance
$\boldsymbol{K}$	: Immittance
$\boldsymbol{P_{av}}$	: Available power
$\boldsymbol{P_{in}}$	: Input power
$\boldsymbol{P_{out}}$	: Output power
$\boldsymbol{f}$	: Frequency
$\boldsymbol{\omega}$	: Angular frequency
$\boldsymbol{\eta}$	: Drain efficiency
[**E**]	: Equilazer block
$\boldsymbol{\lambda}$	: Richards variable
$\boldsymbol{p}$	: Laplace variable
$\boldsymbol{\Omega}$	: Ohm
$\boldsymbol{Z_L}$	: Realizable load impedance
$\boldsymbol{Z_{LP}}$	: Load pull impedance
$\boldsymbol{Z_S}$	: Realizable source impedance
$\boldsymbol{Z_{SP}}$	: Source pull impedance

LIST OF TABLES

Page

LIST OF FIGURES

Page

PERFORMANCE ASSESSMENT OF NONLINEAR ACTIVE DEVICES TO DESIGN BROADBAND MICROWAVE POWER AMPLIFIERS VIA VIRTUAL GAIN OPTIMIZATION

SUMMARY

In this thesis, we proposed a structured set of sequential procedures to design broadband microwave power amplifiers. A power amplifier is a major building block in transceivers for wireless communications. The output stage of a transmitter, amplifies the modulated electrical signal over a power amplifier connected to an antenna. To design solid-state microwave power amplifiers, active devices such as radio frequency (RF) power transistors are used. Nowadays, it is a common practice to employ Gallium Nitrate (GaN) transistors in RF power amplifier designs due to their high electron mobility and high-power delivering capacity. In practice, power amplifier design process starts with careful selection of the power transistor considering the design parameters such as the required output signal power to be delivered, drain/power-added efficiency of the amplifier, transducer power gain over the specified bandwidth, etc.

Once the power transistor is selected, its nonlinear behavior is characterized by determining the optimum source-pull (SP) and load-pull (LP) impedances to design an RF power amplifier for optimum gain and efficiency. As they are obtained, these impedances may not be realizable network functions over the desired frequency band to yield the input and the output matching networks for the amplifier. Therefore, in this thesis, first, we introduce a new method to test if a given impedance is realizable. Then, a novel “Real Frequency Line Segment Technique” based numerical procedure is introduced to assess the gain-bandwidth limitations of the given source and load impedances, which in turn results in the ultimate RF power-intake and power-delivery capacity of the amplifier. During the numerical performance assessment process, a robust tool called “Virtual Gain Optimization” is presented. In the course of performance assessment process, a new definition called “Power-Performance-Product” is introduced to measure the quality of an active device. Examples are presented to test the realizability of the given source/load-pull data and to assess the gain-bandwidth limitations of the given source/load-pull impedances for a 45W-GaN power transistor, over 0.8-3.8 GHz bandwidth.

In the second part of the thesis, we present the actual design and implementation of the novel methods in a sequential manner. As the result of the proposed methods, firstly, the power-intake and power-delivery capacity of the active device are assessed for a 10W-GaN power transistor over 800 MHz-3.0 GHz bandwidth. We determined the optimum realizable source and load impedance data via the virtual gain optimization. Then, the optimum source and load impedance data is modelled as realizable network functions. Generated realizable network functions are synthesized using the Darlington synthesis which in turn yields optimum input and output matching network topologies with component values. Eventually, the designed power amplifier

is manufactured. It is shown that the computed and the measured performance of the amplifier agrees within acceptable limits. Hence, we obtained an avaragre of 10 Watts output power with 11.4 ± 0.6 dB gain and 49% to 76 % power added efficiency.

In the third part, we introduce a new matching concept, so-called Virtual or interchangebly Fictitious Matching (FM), which may be defined between the artificially generated non-Foster passive immittances, over a lossless equalizer [E]. These immittances may not necessarily belong to physical devices, rather, they are fabricated like a source-pull or load-pull impedances to maximize the gain, the output power, the efficiency, and to minimize the output harmonics of the nonlinear-active device under consideration. In Fictitious Matching problems, equilezer [E] is constructed between the virtually produced generator immittance data K_{GF} and the load immittance data K_{LF} to optimize the power transfer in the passband. In this regard, [E] is described by means of its back-end driving point input immittance in Darlington sense, and it is determined as the outcome of the optimization process. The input and the output impedances are synthesized as commensurate transmission lines as they are cascaded. It is demonstrated that the new concept of virtual matching can be utilized to build broadband power amplifiers. In this part, solving virtual matching problem successively, the input and the output matching networks of a power amplifier are designed over 500 MHz-3 GHz with the average gain of $11.5 dB$, the output power of $40.5\ dBm$, and an average drain efficiency of 61.7%.

DOĞRUSAL OLMAYAN AKTİF ELEMANLARIN PERFORMANS ANALİZİ VE SANAL KAZANÇ OPTİMİZASYONUYLA GENİŞBANDLI MİKRODALGA GÜÇ KUVVETLENDİRİCİSİ TASARIMI

ÖZET

Bu çalışmada, geniş-bandlı mikrodalga güç kuvvetlendiricilerinin tasarımında kullanmak üzere geliştirilmiş olan bir dizi orjinal yöntem sunulmaktadır. Güç kuvvetlendiricileri, kablosuz iletişim sistemlerinde temel devre blokları arasında yer almaktadır. Bir güç kuvvetlendiricisinin temel görevi, iletilmek istenen bilgiyi barındıran taşıyıcı elektromanyetik dalgayı, antenden gönderilmeden önce son defa kuvvetlendirerek yeterli seviyeye yükseltmektir. Sivil ve askeri kablosuz haberleşme sistemlerinin yanı sıra, radar uygulamaları, medikal mikrodalga ısıtma ve görüntüleme uygulamaları da elektromanyetik dalgaların yayınımı prensibine dayandığı için güç kuvvetlendiricilerinin kullanım alanları olarak gösterilebilir. Günümüzde popüler ticari haberleşme sistemleri olan 5G, 6G, wi-fi vb. sistemler de güç kuvvetlendiricilerinin önemli bir pazarını oluşturmaktadır. Yapay uydular ve uzay sondalarındaki kablosuz sistemler de mikrodalga güç kuvvetlendiricilerinin uzay araştırmalarında ve uzay teknolojilerindeki kullanım alanlarına örnek verilebilir. Tüm bu mevcut ve gelişmekte olan farklı kablosuz haberleşme sistemleri, yeni modülasyon türleri ve kullanılan farklı frekans bandları, farklı özelliklerde güç kuvvetlendiricilerinin geliştirilmesine ihtiyaç duymaktadır. Bu durum da, mikrodalga mühendisleri için güç kuvvetlendiricisi tasarımı üzerine yapılan çalışmaları cazip hale getirmektedir.

Pratik anlamda, güç kuvvetlendiricisi tasarım süreci, güç kazancı, çıkış gücü, verimlilik, band-genişliği gibi hedeflenen tasarım parametreleri dikkate alınarak, kuvvetlendiricide kullanılacak güç transistörünün seçilmesiyle başlar. Tasarımda kullanılacak aktif eleman yani güç transistörü seçildiğinde, giriş ve çıkış uyumlaştırmasının uygun biçimde yapılabilmesi için aktif elemanın doğrusal olmayan davranışının karakterize edilmesi gereklidir. Günümüzde, katı-hal güç kuvvetlendiricisi tasarımında yüksek güç ve yüksek band genişliği sağlama kapasiteleri nedeniyle Galyum-Nitrür (GaN) transistörlerin kullanılması yaygın bir uygulamadır. Ayrıca, çeşitli amaçlarla farklı dalga boylarındaki haberleşme sistemlerini bir arada bulunduran sistemler için geniş-bandlı güç kuvvetlendiricisi tasarımı önem arz eden bir araştırma konusudur. Bununla birlikte, verici sistemin en çok güç tüketen birimi olduğundan, güç kuvvetlendiricisinin kazancının ve veriminin de geniş bir frekans bandı boyunca olabildiğince yüksek olması hedeflenir.

Aktif elemanın doğrusal olmayan davranışı, genellikle çeşitli tekniklerle modellenerek bilgisayar destekli tasarım ortamlarına aktarılır. Böylelikle kuvvetlendirici tasarımı yaparken, istenilen elektriksel giriş, çıkış ve kutuplama şartları içerisinde kuvvetlendiricinin çalışması analiz edilir. Yani bilgisayar benzeşimleri ile tasarım süreci ilerler. Aktif elemanların son derece doğrusal olmayan davranışı nedeniyle, istenen özelliklere sahip kuvvetlendiricinin tasarımı, diğer bir ifadeyle, uygun giriş ve çıkış uyumlaşım devrelerinin elde edilmesi, yalnızca devre teorisi eşitlikleriyle

mümkün olamamaktadır. Bu nedenle, günümüzde güç kuvvetlendiricisi tasarlarken, genellikle kaynak-çekme ve yük-çekme adı verilen teknikler kullanılır. Şöyle ki, belirli çalışma koşullarında tranzistor için uygun kaynak tarafı ve yük tarafı sonlandırma empedansları tespit edilir. Bu işlem, cihazı çeşitli empedans değerleri ile sonlandırarak ve her sonlandırma empedans değerinde kazanç ve verimlilik gibi önceden belirlenmiş performans kriterlerini ölçerek gerçekleştirilir. Sonlandırma empedanslarının gerçel ve sanal kısımları, optimum kaynak ve yük empedanslarını bulmak için Smith Abağı üzerindeki belirli bir empedans bölgesinde taranır, her bir tarama adımında transistörün çıkış gücü, kazancı, verimi vs. kaydedilir. Bu işlem farklı frekanslarda tekrarlanarak her bir frekans değeri için optimum kaynak/yük-çekme empedansı tespit edilir. Kaynak/Yük-çekme işlemi, laboratuvarda ölçüm ekipmanları ile yapıldığı gibi aktif elemanın modelinin kullanarak bilgisayar benzeşimleriyle de yapılabilir. Ayrıca belirli frekanslardaki optimum kaynak/yük çekme verileri, üretici firmalar tarafından elemanların kataloğunda da genellikle verilmektedir. Ölçülen kaynak/yük-çekme empedans verileri yardımıyla band genişliği dar olan bir güç kuvvetlendiricisinin tasarımı kompleks eşlenikle uyumlama metodlarıyla kolayca yapılabilir. Ancak, band-genişliği artarsa tasarım görevi zorlaşır. Geniş bandlı bir tasarım için, ilgilenilen frekans bandı içerisindeki güç kuvvetlendiricisi performansını optimize etmek amacıyla yeterince çok sayıda ayrık frekansta kaynak/yük-çekme empedans verilerini belirlememiz gerekir. Ardından, giriş uyumlama devresi ve çıkış uyumlama devresinin kaynak/yük-çekme empedans değerleri gözetilerek tasarlanması gerekmektedir. Bu amaçla tasarımcılar genellikle bir takım uyumlaşım devre topolojileri veya önceden tanımlı analitik devre fonksiyonları seçerler. Ardından fonksiyonun parametrelerini veya devrelerdeki kapasite, bobin, iletim hattı gibi pasif elemanların değerlerini hesaplar ve optimize ederler. Böylelikle ilgili kaynak/yük-çekme empedans veri setine uyan ya da empedans değerlerine olası en yakın sonucu veren eleman değerlerinin saptanması amaçlanır. Bu aşamada belirtmek gerekir ki çeşitli kuvvetlendirici parametrelerini optimize etmek üzere elde edilmiş olan ayrık kaynak/yük-çekme empedansları, istenilen bir frekans bandı boyunca gerçeklenebilir devre fonksiyonlarına karşı gelen değerler olmayabilir yani pozitif reel fonksiyonları tanımlamayabilir. Bu nedenle çalışmamızda, verilen kaynak/yük-çekme datasının belirli bir frekans bandı içerisinde pozitif reel fonksiyon olup olmadığını belirlemek için bir test prosedürü geliştirilmiştir. Daha sonra da verilen ayrık empedans datasını, devre topolojisinden bağımsız olarak gerçeklenebilir devre fonksiyonu şeklinde modellenmesni sağlayan orjinal bir yöntem önerilmiştir. Gerçel Frekans Çizgisel Hat tekniğine dayanan bu yöntem ile, verilen kaynak/yük empedansının performans analizi de yapılabilmektedir. Şöyle ki, eğer kullanılan kaynak/yük-çekme verisi gerçeklenebilir bir devre fonksiyonuna karşılık gelmiyorsa, bu veriye ilişkin kazanç-band genişliği analizi yapılarak uyumlaşım için ey iyi sonuç, diğer bir ifadeyle, band içerisinde güç aktarım seviyesi en yüksek olan çözüm elde edilebilmektedir. Böylelikle, bu tekniğin kaynak-çekme empedansına uygulanmasıyla aktif elemanın bir sinyal kaynağından güç çekme performansı tespit edilebilir. Benzer şekilde yük-çekme datasının analizi ile de aktif elemanın çıkışındaki yüke güç aktarım sınırları belirlenebilir. Bu sınırları nicel olarak ifade etmek amacıyla, çalışmada "Güç Performans Ürünü (Power, Performance Product PPP)" adı verilen yeni bir metrik tanımlaması yapılmıştır. Bu metrik ile verilen bir kaynak/yük-çekme veri seti ile, ilgili aktif elemanın istenen frekans band içerisinde kullanışlı olup olmayacağı pratik olarak analiz edilmektedir. Öyle ki Güç Performans Ürünü ifadesinin 25%'ten düşük çıkması durumunda, transistöre aktarılan ve transistörden çekilmesi istenen gücün yarıdan fazlasının aktarılamadığı, ziyan olduğu anlamına gelmektedir. Bu durumda, ilgili tranzistörün ilgili frekans bandı için kullanışsız olduğu ve değiştirilmesi gerektiği sonucu çıkarılabilir.

Çalışmada önerilen, en yüksek kazanç seviyesine ulaşmayı ve en-başarılı gerçeklenebilir kaynak/yük empedanslarını tespit etmeyi sağlayan orjinal ve kullanışlı yöntem "Sanal Kazanç Optimizasyonu" olarak adlandırılmıştır. Bu yöntemin minimize edilmek istenen hata fonksiyonunu daima yakınsak biçimde global minimuma götürdüğü ve böylelikle ilgili aktif eleman için optimum-gerçeklenebilir kaynak/yük empedanslarının tespit edildiği gösterilmiştir.

Nümerik olarak üretilen gerçeklenebilir kaynak ve yük empedansları analitik olarak modellenmektedir. Sonuç olarak, bu empedanslar optimum giriş ve çıkış uyumlaştırma devre topolojilerini elde etmek amacıyla Darlington Sentezi kullanılarak sentezlenir. ticari olarak temin edilebilen bir GaN mikrodalga tranzistörünün verilen kaynak/yük-çekme verileri kullanılarak geniş bandlı, yüksek kazançlı ve verimli güç kuvvetlendiricisi tasarımları örnek olarak sunulmuştur.

Tasarım örneği olarak, CGH40010 GaN tranzistörü kullanılmış ve bu elemanın kataloğunda yer alan kaynak/yük-çekme verilerinin gerçeklenebilirliği test edilmiştir. Daha sonra bu veriler önerilen sanal kazanç optimizasyonu yöntemiyle modellenmiştir. 0.8-3.0GHz band aralığında kazanç-band genişliği analizi de yapılarak, band içerisindeki minimum değeri en yüksek kazanç seviyesine sahip çözüm üzrinden başarılı bir tasarım yapılmıştır. İdeal pasif devre elemanlarından oluşan uyumlaşım devreleri, pratik üretime uygun olarak kısmen mikroşerit hatlara dönüştürülmüşür. Tasarlanan güç kuvvetlendiricisi, çalışma bandı boyunca 38.8dBm'den 40.05dBm'e değişen çıkış gücü, 49%'dan 70.6%'ya değişen güç-ekli verim ve TPG=11.4±0.6 dB kazanç başarımı sağlamaktadır.

Bir diğer örnekte de, olası kararlılık elemanları, bağlantı hatları, DC bağlaşım kapasiteleri, transiztörün kaynak/yük empedans verisi ile birlikte kurgusal bir uyumlaşım problemi tanımlanmış ve bu problem çözülerek tasarım yapılmıştır. Bu tasarımda uyumlaşım elemanları, kaskad bağlı eş-uzunluklu iletim hatları olarak sentezlenmiştir. Ortalama kazanç 11.5dB, çıkış gücü 40.5 dBm ve ortalama savak verimi 61.7% olacak şekilde 500 MHz-3 GHz band aralığında tasarlanmıştır.

1. INTRODUCTION

Power amplifiers are the principal building blocks of wireless communication systems. The main task of a microwave power amplifier (PA) is to amplify the carrier electromagnetic wave to a sufficient level to properly drive the transmitting antenna as it is shown in Figure 1.1.

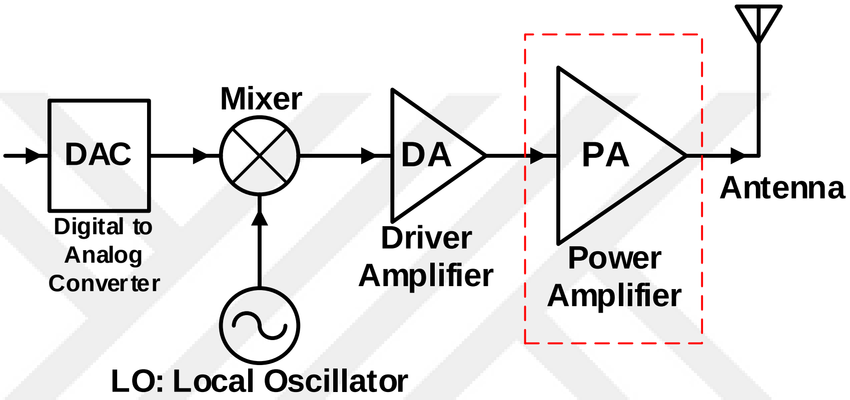

Figure 1.1 : Power amplifier on a simple microwave transmitter block diagram.

In general, power amplifiers are utilized in commercial and military systems, such as wireless communications, radar applications, microwave medical imaging and heating, etc., since all these areas requires the transmission of electromagnetic energy over the microwave frequencies [1-9]. Today's popular commercial communication systems such as 5G, 6G, and wi-fi etc. [10-15], constitute an important market for power amplifiers. Furthermore, satellite communications and wireless systems in space missions can be sorted among the major application areas of microwave power amplifiers in space exploration and space technologies [16-19]. All these existing and developing various wireless communication systems, modulation types and different frequency bands need the development of power amplifiers with different performance metrics. That is why development of new design procedures to construct power amplifiers attracts many researchers in the field of microwave engineering.

In practice, a power amplifier design process begins with the selection of a proper power transistor. At this point, it is important to consider the design parameters such as transducer power gain (TPG), output power (P_{out}), drain efficiency (η), and bandwidth (BW). When the active device is selected, it is necessary to characterize the non-linear behavior of the active element in order to match the input and the output ports properly. Nowadays, usage of Gallium-Nitride (GaN) based high electron mobility transistors (HEMTs) is common practice in solid-state power amplifier designs because of their high power and wide bandwidth capabilities [19-24]. In addition, broadband PA design is an important research topic since various communication systems with different frequencies frequently used in the same equipment [25]. However, the PA is the most power-consuming unit of the transmitter system, the power-gain and power-efficiency of the power amplifier are desired to be as high as possible over a wide frequency band.

The principal performance metrics for microwave PAs can be found in the main textbooks as [25-29]. For the sake of completeness, some of the most utilized performance metrics within the scope of the thesis can be explained as follows.

Transcuder Power gain can be defined as the ratio of the delivered output power of the amplifier to the available power (P_{av}) at the input port as

$$TPG = \frac{P_{out}}{P_{av}}. \tag{1.1}$$

In order to quantify the power consumption of a PA, drain efficiency (η) expression can be expressed as

$$\eta = \frac{P_{out}}{P_{DC}} \tag{1.2}$$

where P_{DC} is the consumed DC power to feed the active device. Most of the times, the input signal power (P_{in}) of the PA can be considerably high. Therefore power added efficiency (PAE) may be preferable to measure the power-efficiency instead, which is given as

$$PAE = \frac{P_{out} - P_{in}}{P_{DC}}. \tag{1.3}$$

To design a PA, the non-linear behavior of the active device is usually modeled with various transistor modelling techniques and transferred to computer-aided design environments [30-39]. Thus, the operation of the active device is analyzed under the desired input, output and biasing conditions on simulation tools. However, due to the highly non-linear behavior of the active device, the design of matching networks can not be possible only with the linear scattering parameter based methods. Therefore, techniques called source-pull (SP) and load-pull (LP) are generally used to determine the optimum impedance terminations for the active device from the source-end and the load-end under certain biasing conditions [26, 40-43]. This procedure is simply achieved by terminating the device with a variable-load (i.e. tuner) as shown in Figure 1.2. While sweeping the termination value, the pre-determined performance criteria such as gain and efficiency are measured at each terminating impedance point. Therefore the real and imaginary parts of the termination impedance are swept in a specific impedance region on the Smith Chart to determine the optimum source and load impedances. This process is repeated on several different frequencies to determine the optimum SP and LP impedance along the frequency band of interest. This measurement process can be carried out on the design tool using the non-linear model of the active device as well as in the laboratory with physical devices and measurement equipments. In addition, optimum SP/LP data is frequently given by the manufacturers in the catalog of the devices at certain frequencies as they are given in [44, 45]. With the usage of measured source/load-pull impedance data, a narrow-band, per say a single frequency, power amplifier can be easily designed by complex conjugate matching methods. However, the design task becomes more difficult if the bandwidth increases. For a wideband design, we need to specify source-pull and load-pull impedance data at a sufficiently large number of discrete frequencies to optimize the PA performance within the frequency band of interest. Then, the input matching network (IMN) and the output matching network (OMN) must be designed considering the SP and LP impedance values respectively. For this purpose, designers usually choose some pre-set matching network topologies composed of passive network elements such as capacitors, inductors, transmission lines and etc, as in [46-49]. Thus, it is desired to determine the element values by pre-calculations and optimizations for the best possible fit to the relevant SP/LP. At this point, it should be noted that, the collected SP/LP data placed on the Smith Chart, as shown in Figure 1.3, is so disconnected that, it may not correspond to a realizable network function over the desired frequency band. Therefore, in our study, firstly a test procedure is developed to determine whether the given source/load-pull data belongs to a positive real function within a certain frequency band, which can be realized by passive network elements in resistive termination. Then, an original method is proposed to numerically model the discrete impedance data as a realizable network function regardless of the circuit topology. The proposed method is based on the Real Frequency Line Segment Technique (RF-LST) and it allows the designer to assess the gain-bandwidth performance of the the active device employing the optimum SP and LP immittance data. That is, if the SP/LP fits to a positive real function, the best TPG hits the unity over the passband. However, if the SP/LP data does not correspond to a realizable network function, then, one should expect a deviation from perfect match to end up with realizable source and load impedance data. In this case, the ideal TPG will be less than unity ($TPG < 1$). Obviously, the target is to maximize TPG over the passband as much as possible, which in turn yields the optimum solution for the realizable source and load terminations. In this regard we propose a useful gain-bandwidth assessment algorithm to end up with realizable source and load impedance data in the form of line-segments. Thus, generation of the optimum realizable source impedance data via RF-LST, results in the best power-intake performance of the active device in least mean squared (LMS) sense. Similarly, by analyzing the LP data, the power-delivery performance of the active device can be assessed. During the numerical performance assessments process, an original tool called “Virtual Gain Optimization (VGO)” is presented. VGO enables the user to reach the highest possible gain level in LMS sense and determine the most successful realizable source/load impedances numerically. It has been shown that this method always hits the error function to be minimized to the global minimum in a convergent manner and thus optimum-realizable source/load impedances are determined for the relevant active element. In order to express performance assessment limits quantitatively, a new figure of merit called "Power, Performance Product PPP" is introduced in the following chapter. A given SP/LP data set is practically analyzed whether the relevant active device will be egligible to use in the desired frequency band. In fact, if the Power Performance Product is lower than 25%, it means that more than half of the power is wasted, since power-intake and/or power-delivery performance of the active is poor. In this case, it may be concluded that the relevant transistor is useless to operate in the desired frequency band and needs to be replaced.

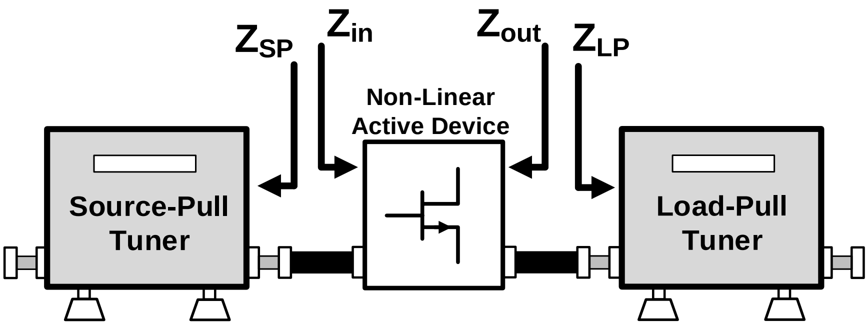

Figure 1.2 : Source-pull and load-pull procedure for the active device.

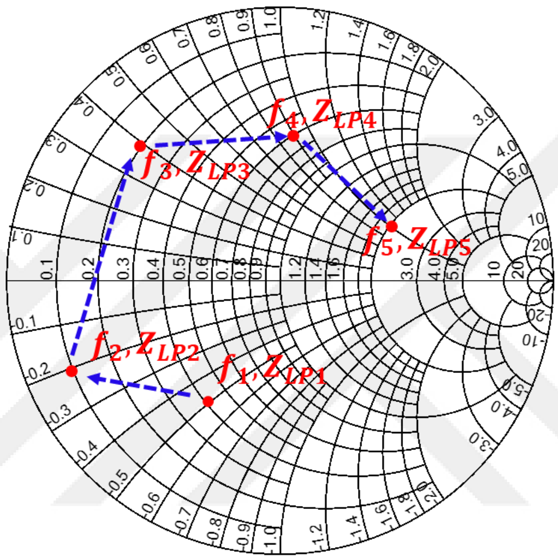

Figure 1.3 : Discrete load-pull (or source-pull) data set placed on the Smith chart.

Once the best realizable source and load impedance is numerically generated by VGO, they are analytically modeled to yield the IMN and OMN. As a result, these impedances are synthesized using Darlington Synthesis to obtain the optimum input and output matching network topologies [50-54]. Eventually, employing the proposed techniques presented in this thesis, one can design broadband PAs with high gain and high efficiency via modelling of SP/LP data given for commercially available GaN microwave transistors.

The thesis is organized as flows:

Chapter 1 introduces the objective of the thesis

In the following chapter (Chapter 2), the literature and theoretical backround is revisited to develop the performance assessment algorithm. The realizability test for the given SP/LP data and the “Virtual Gain Optimization” algorithm are introduced to perform the performance assessment for any microwave power transistor selected. A new metric called “Power Performance Product” is defined to evaluate the usability of the selected active device. Examples are presented to test the realizability of the given source/load-pull data and to assess the gain-bandwidth limitations of the given source/load pull impedances for a 45W-GaN power transistor, namely “Wolfspeed CG2H40045”, over 0.8-3.8 GHz bandwidth.

In the Chapter 3, a broadband PA design and implementation are presented employing the proposed algorithms given in Chapter 2. A commercial GaN transistor namely CGH40010F from Wolfspeed is selected for the design purpose [45]. The realizability test and gain-bandwidth analysis are performed over the 0.8-3.0GHz frequency band via the VGO tool. Then, computed optimum realizable data is modeled and a successful design is achieved with the highest gain level in the passband. Synthesized lumped-element matching networks are partially converted into microstrip lines in accordance with practical realization conditions. The designed power amplifier provides output power ranging from 38.8dBm to 40.05dBm, power-added efficiency varying from 49% to 70.6%, and TPG=11.4±0.6 dB gain throughout the band of operation.

In Chapter 4, another example, a “Fictitious Matching” problem is defined with the given SP and LP data. In this problem, some practical issues are also considered such as the stability of the transistor with connection leads, DC de-coupling capacitors attached with the source/load-pull impedance data. Hence, the above fictitious matching problem describes a double matching problem. Then, it is solved by using the Real Frequency Parametrich Approach in Richards domain (λ) , yielding driving point impedances of the IMN and OMN in Darlington sense [50-55]. Eventually, these impedances are synthesized in the form of cascaded commensurate (i.e. equal length) transmission lines. An average gain of 11.5dB, an output power of 40.5 dBm and an average drain efficiency of 61.7% are achieved over the 500 MHz-3 GHz band.

Finally, the thesis is concluded in Chapter 5.

2. BROADBAND PERFORMANCE ASSESSMENT OF A MICROWAVE POWER TRANSISTOR EMPLOYING THE REAL FREQUENCY TECHNIQUE[1]

Generation of proper source/load-pull impedances for a selected active device is essential to design an RF power amplifier for optimum gain and power added efficiency. As they are obtained, these impedances may not be realizable network functions over the desired frequency band to yield the input and the output matching networks for the amplifier. Therefore, in this chapter, first, we introduce a new method to test if a given impedance is realizable. Then, a novel “Real Frequency Line Segment Technique” based numerical procedure is introduced to assess the gain-bandwidth limitations of the given source and load impedances, which in turn results in the ultimate RF power-intake and power-delivery capacity of the amplifier. During the numerical performance assessments process, a robust tool called “Virtual Gain Optimization” is presented. Finally, a new definition called “Power-Performance-Product” is introduced to measure the quality of an active device. Examples are presented to test the realizability of the given source/load pull data and to assess the gain-bandwidth limitations of the given source/load pull impedances for a 45W-GaN power transistor, namely “Wolfspeed CG2H40045”, over 0.8-3.8 GHz bandwidth.

2.1 Introduction

For wireless communication systems, it is essential to design power amplifiers (PA) for variety of applications [26, 56-62]. Nowadays, it is a common practice to employ Gallium Nitrate (GaN) transistors due to their high-power delivering capacity [20-24]. In practice, PA design process starts with careful selection of the power transistor considering the design parameters such as the required output signal power to be delivered, power added efficiency (PAE) of the amplifier, transducer power gain

---

[1] This chapter is based on the paper "Kilinc, S, Ejaz, ME, Yarman, BS, Ozoguz, S, Srivastava, S, Nurellari, E. (2022). “Broadband performance assessment of a microwave power transistor employing the real frequency technique,” Int J Circ Theor Appl. 2022; 50(11): 3725- 3748. doi:10.1002/cta.3357".

(TPG) over the specified bandwidth, etc. Once the power transistor is selected, its nonlinear behavior is characterized by determining the optimum source-pull (SP) and load-pull (LP) impedances. This process is achieved at each frequency point by terminating the device with various impedance values, measuring the pre-set performance criteria such as gain and efficiency. The real and imaginary parts of the loading impedances are swept in a particular impedance zone on the Smith Chart to find the optimum source and load impedances. In practice, measured optimum source and load impedances are published in datasheets as in [44] One can easily make a narrow bandwidth PA design, per say, at a single frequency f_a on the measured source and load pull impedance data. However, the design task becomes difficult if the bandwidth increases. For broadband PA design, we need to determine source and load pull impedance data at sufficiently large number of discrete frequencies to optimize the PA performance inside the frequency band of interest. In this case, the resulting source and load pull impedance data sets must correspond to realizable network functions, which eventually, yield optimum input and output matching networks, when they are modelled as positive real functions [40-43].

Let $Z_{SPa}(j\omega_a) = R_{SPa}(\omega_a) + jX_{SPa}(\omega_a)$ and $Z_{LPa}(j\omega_a) = R_{LPa}(\omega_a) + jX_{LPa}(\omega_a)$ designate the discrete actual source and load pull impedance data at the actual angular frequency $\omega_a = 2\pi f_a$ with actual frequency f_a. In these notations, subscript "a" refers to measured actual values. To simplify the PA design process, measured impedance data is normalized with respect to a normalization resistance R_0 and a frequency f_{0a}. In practice, R_0 may be selected as the standard termination 50Ω and f_{0a} can be chosen at the high end of the frequency band. In this case, normalized angular frequencies are $\omega = \frac{2\pi f_a}{2\pi f_{0a}} = 2\pi f$ where f designates the normalized frequencies. Using the generic notation, a normalized impedance $Z(j\omega)$ is obtained by dividing the actual impedance $Z_a(j\omega_a) = R_a(\omega_a) + jX_a(\omega_a)$ to R_0 such that $Z(j\omega) = \frac{Z_a}{R_0} = R(\omega) + jX(\omega)$. Likewise, normalized SP and LP impedances are represented by $Z_{SP}(j\omega) = R_{SP}(\omega) + jX_{SP}(\omega)$ and $Z_{LP}(j\omega) = R_{LP}(\omega) + jX_{LP}(\omega)$ respectively. It is noted that the measured SP and LP terminations optimize the TPG as well as the PAE of the amplifier under consideration. Obviously, source and load pull impedances must be positive real (PR) functions so that one is able to analytically model the measured data and construct the front and the back-end matching networks as depicted in Figure 2.1.

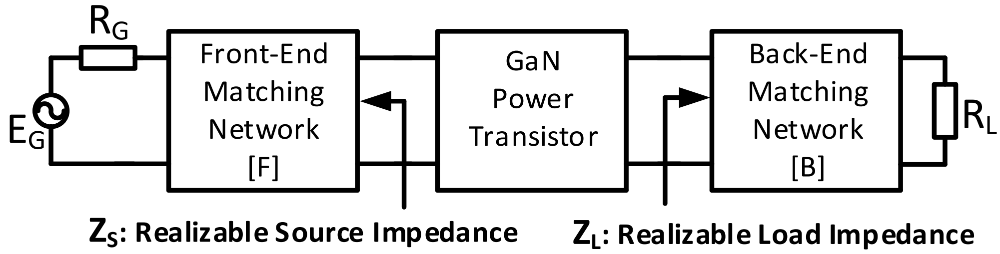

Figure 2.1 : A typical microwave power amplifier with realizable source and load impedances Z_S and Z_L.

As they are placed on the Smith Chart, discrete source and load pull impedances may not describe positive real functions over broad frequency band. In this case, one must develop a test procedure to determine if Z_{SP} and Z_{LP} are PR functions. Eventually, the best possible-realizable source and load impedances must be generated to yield the front and the back-end matching networks for the power amplifier to be designed. Therefore, in the following section, we introduce a novel numerical method to test the positive realness of a given discrete impedance data (Section 2.2). Then, examples are given to test if a measured arbitrary immittance data and the source/load pull impedances obtained from the Wolfspeed's CG2H40045 GaN power transistor, represent positive real functions (Section 2.3). In section 2.4, we propose a novel numerical process to assess the gain-bandwidth limitation of a given impedance data using the "Real Frequency-Line Segment Technique (RF-LST)" [50, 63, 64]. During the numerical performance assessments process, we introduce an original tool called "Virtual Gain Optimization (VGO)". In Section 2.5 and 2.6, "Gain-Bandwidth Limitations (GBWL)" of the source-pull and the load-pull impedances of the Wolfspeed CG2H40045 GaN power transistor is determined over $0.8GHz - 3.8GHz$ bandwidth respectively. In Section 2.7, we introduce a new definition to assess the Power-Intake and Power-Delivery performance of an active device. In section 2.8, a power amplifier design is completed by modelling the RF-LST based optimum and realizable source and load impedance data. Finally, the chapter is concluded in Section 2.9.

It may be useful to mention that the alternative performance assessment of an active device may be conducted utilizing the analytic gain-bandwidth theory. Unfortunately, the theory is not accessible as described in [65, 66].

2.2 A Numerical Approach to Test the Positive Realness of the Measured SP And LP Immittance Data

While playing with immittance data on the Smith Chart, microwave engineers may not realize that the data placed on the Smith Chart with positive real part may not necessarily represent a realizable passive immittance function over the frequency band of interest. Therefore, one needs to test the data whether it is a positive real-realizable immittance or not.

Before we introduce the realizability test algorithm for the measured Source/Load Pull immittance data, let us review some of the related concepts of the network theory such as the definition of positive real (PR) functions, minimum functions, Foster functions, Hilbert transformation and Darlington's theorem. Detailed information on these topics can be found in major textbooks such as [50, 64].

Let $p = \sigma + j\omega$ be the complex Laplace plane variable.

Definition 1: Any complex analytic function $K(p)$ is called positive real (PR) if and only if it is real for p is real (i.e., for $p = \sigma$, $K(\sigma)$ is real) and $K(\sigma) \geq 0$ when $\sigma \geq 0$.

Definition 2: A positive real function $K_m(p) = \frac{a_m(p)}{b_m(p)}$, which is free of $j\omega$ poles, is called a "minimum function". In other words, $b_m(p)$ is strictly Hurwitz, which only posses $Open - Left\ Half\ Plane$ (O-LHP) zeros.

Definition 3: A positive real function $K_F(p) = \frac{a_F(p)}{b_F(p)}$, which possess only "simple and interlacing $j\omega$ zeros and poles", is called a "Foster function".

Property 1: If $K(p) = \frac{a(p)}{b(p)}$ is PR, then it may be decomposed in to its minimum and Foster functions such that

$$K(p) = K_m(p) + K_F(p) \tag{2.1a}$$

where

$$K_m(p) = \frac{a_m(p)}{b_m(p)} = \sum_{i=1}^{n} \frac{k_i}{p - p_i} \tag{2.1b}$$

with $p_i = \sigma_i + j\omega_i$ and $p_{i+1} = \sigma_i - j\omega_i$ with $\sigma_i < 0$.

On the $j\omega$ axis, $K_F(p)$, $K(p)$, and $K_m(p)$ are expressed as

$$K_F(j\omega) = jX_F(\omega) \tag{2.2a}$$

$$K(j\omega) = R(\omega) + jX(\omega) \tag{2.2b}$$

$$K_m(j\omega) = R(\omega) + jX_m(\omega) \tag{2.2c}$$

Property 2: For a Foster function $K_F(j\omega) = jX_F(\omega)$, derivative of $X_F(\omega)$ with respect to ω is always non-negative. In other words, The Foster reactance function $X_F(\omega)$ is a monotonically increasing function. That is, $\frac{dX(\omega)}{d\,\omega} \geq 0\ ;\ \forall\omega$ with interlacing zeros and poles.

Theorem 1: A minimum function $K_m(j\omega)$ is uniquely determined from its real part $R(\omega)$ using Hilbert transformation such that

$$X_m(\omega) = R_\infty + \frac{2\omega}{\pi}\int_0^\infty \frac{R(y)}{y^2 - \omega^2}\,dy = H\{R(\omega)\} \tag{2.3}$$

In (2.3), R_∞ is the constant value of $R(\omega)$ as the frequency approaches to infinity. In practical applications, it is set to zero due to parasitic effects.

For a minimum function $K_m(j\omega)$, the relation between its real part $R(\omega)$ and its imaginary part $X(\omega)$ is called the Hilbert transformation (HT). In this study, HT operator is designated by $H\{\,.\,\}$. Thus, we say that $X_m(\omega) = H\{R(\omega)\}$.

2.2.1 Numerical evaluation of Hilbert Transformation

The real part $R(\omega)$ of a minimum function may be piece-wise linearized as shown in Figure 2.2.

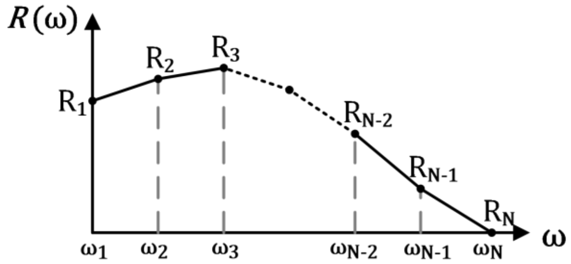

Figure 2.2 : Piecewise linearization of the Real part $R(\omega)$ of a minimum function $K_m(j\omega) = R(\omega) + jX_m(\omega)$.

In Figure 2.2, $R(\omega)$ is sampled at the break frequencies $\{\omega_1,\ \omega_2,\ \omega_3, \dots \omega_N\}$ with corresponding break points $\{R_1,\ R_2,\ R_3, \dots R_N\}$. Furthermore, it is assumed that adjacent sampled pairs $\{\omega_j, R_j\}$ and $\{\omega_{j+1}, R_{j+1}\}$ are connected by line segments. For a sufficiently large frequency placed at $\omega = \omega_N$, $R(\omega)$ becomes practically zero yielding $R_N = 0$. Based on the line-segment representation of Figure 2.2, $R(\omega)$ is simply evaluated using the following line equation. For $\omega_j \le \omega \le \omega_{j+1}$ such that $j = 1,2, \dots, (N-1)$, $R(\omega)$ is given by

$$R_j(\omega) = a_j\omega + b_j \tag{2.4}$$

where $a_j = \frac{R_j - R_{j+1}}{\omega_j - \omega_{j+1}}$ and $b_j = \frac{(R_{j+1})\,\omega_j - (R_j)\omega_{j+1}}{\omega_{j-\omega_{j+1}}}$

In the above representation of $R(\omega)$, we assume that $R_\infty = \lim_{p\to\infty} R(\omega)$ is zero. This is a practical assumption for all passband amplifier designs.

Having line-segment representation of $R(\omega)$, imaginary part $X_m(\omega)$ of (2.3) is derived as

$$X_m(\omega) = \sum_{j=1}^{N-1} \beta_j(\omega)\Delta R_j \triangleq H\{R(\omega)\} \tag{2.5a}$$

where ΔR_j and $\beta_j(\omega)$ is given by

$$\Delta R_j = R_{j+1} - R_j \tag{2.5b}$$

$$F_j(\omega) = (\omega + \omega_j)\, ln(|\omega + \omega_j|) + (\omega - \omega_j)\, ln(|\omega - \omega_j|) \tag{2.5c}$$

$$\beta_j(\omega) = \frac{1}{\pi(\omega_j - \omega_{j+1})}\left[F_{j+1}(\omega) - F_j(\omega)\right] \tag{2.5d}$$

It should be clear for the reader that, once the real part $R(\omega)$ is represented by the line segments as a continuous function of the angular frequency ω between two adjacent points, then, the Hilbert transformation (2.3) is obtained exactly on the given line-segments, specified by (2.4). Therefore, the pair (2.4) and (2.5), for sure define a realizable minimum function $K_m(j\omega) = R(\omega) + jX_m(\omega)$ by means of the line segments. In other words, at a given point ω, the value of $K_m(j\omega)$ is exactly determined from its real part $R(\omega)$.

In the following sub-section, we propose a novel numerical procedure to decompose a positive real function into its minimum and Foster functions.

2.2.2 Numerical decomposition of a measured immittance data to its minimum and Foster functions

On the real frequency axis $j\omega$, (2.1a) can be regarded as a Theorem as follows.

Theorem 2: Any immittance data $K(j\omega) = R(\omega) + jX(\omega)$ can be decomposed into its minimum $K_m(j\omega) = R(\omega) + jX_m(\omega)$ and Foster $K_F(j\omega) = jX_F(\omega)$ functions numerically such that

$$K(j\omega) = R(\omega) + jX(\omega) = K_m(j\omega) + K_F(j\omega) \tag{2.6a}$$

where

$$X_m(\omega) = H(R) \tag{2.6b}$$

$$X_F(\omega) = X(\omega) - X_m(\omega) \tag{2.6c}$$

with $\frac{dX_F(\omega)}{d\omega} \geq 0;\ \forall\omega$. Hence, (2.6) suggests the following algorithm to decompose "the measured immittance data" into its minimum and Foster functions. Then, one can test its positive realness by investigating the plot of the reactance curve $X_F(\omega)$ if it is monotonically increasing.

It is crucial to note that the measured immittance data must be extrapolated over the entire frequency band to include DC up to a frequency f_N where the real part $R(\omega_N)$ is practically zero. Likewise, the imaginary part $X(\omega)$ is also extrapolated such that $X(0) = 0$ and $X(\omega_N)$ is set to a reasonable value perhaps, by considering the immittance model, or in an ad-hoc manner to force $X_F(\omega)$ to become Foster reactance function if possible.

Based on the above derivations, let us introduce the following algorithm to separate the given immittance data to its minimum and Foster parts.

Algorithm 2.1: Extraction of the Foster Reactance part from the measured immittance data

Inputs:

FA: An array which includes actual sampling frequencies f_{ia} up to a point where the real part $R_a(f_a)$ practically vanishes and it is specified as a vector $FA = [f_{1a}\ \ f_{2a} \dots f_{Na}]$. Note that it would be preferable to select f_1 at DC (i.e., $f_1 = 0$) by extrapolating the measured immittance data.

RA: An array which includes actual sampled values of the real part of the measured immittance data $K_a(jf_a) = R_a(f_a) + jX_a(f_a)$ at the actual frequencies f_a and it is specified as a vector $RA = [R_{1a}\ \ R_{2a} \dots R_{Na}]$ (i.e. RA includes all the break points) with $R_{Na} = 0$.

XA: An array that includes actual sampled values of the imaginary part of the measured immittance data $K_a(jf_a) = R_a(f_a) + jX_a(f_a)$ at the actual frequencies f_a and it is specified as a vector $XA = [X_{1a}\ \ X_{2a} \dots X_{Na}]$. Most probably, at DC, $X_{1a} = 0$ for passive immittance data.

f_0: Actual Normalization Frequency. It may be selected at the high end of the passband such that $f_0 = f_{(N-1)a}$ where $R_{(N-1)a} > 0$ with $R_N = 0$ at f_{Na}.

R_0: Actual Normalization Resistor. It may be selected as standard termination 50Ω.

Computational Steps:

Step 1: Augment and normalize the break frequencies $WBR = FA/f_0$ to cover $\omega = 0$. The last frequency is located at a ω_N such that $RN = R(\omega_N) \cong 0$.

Step 2: Augment and normalize the real part $R(\omega)$ and $X(\omega)$.

Step 3: Compute $Xm = H\{R(\omega)\}$ on the normalized real part $R(\omega)$.

Step 4: Compute the reactance function $XF(\omega) = X(\omega) - Xm(\omega)$.

Step 5: Plot $XF(\omega)$ against the normalized angular frequency ω and check if it is monotonically increasing. If $\left\{\frac{XF(\omega)}{d\omega} \geq 0;\ \forall\omega\right\}$, $XF(\omega)$ is Foster which in turn makes the measured immittance a positive real function.

-end of the algorithm-

Now, let us run an example to implement the above algorithm in the following section.

2.3 The Realizability Test of an Impedance Data

2.3.1 The realizability test as applied on a measured impedance data

In this example, the measured impedance data $ZA(j\omega_a) = RA(\omega_a) + jXA(\omega_a)$ is depicted in Figure 2.3. Measurements cover the frequency band of $f_{1a} = 0.2\ GHz$, and $f_{2a} = 2\ GHz$. Data is normalized with respect to $R_0 = 50\Omega$ and $f_0 = 1\ GHz$. Test the measured impedance data whether it represents a positive real function.

Solution: For this purpose, Algorithm 2.1 is implemented step by step using a total number of $N_S = 11$ sampling points over 200 MHz-2 GHz bandwidth. Now, let us implement the above Algorithm.

Step 1 Frequency Augmentation: Frequency sampling points is augmented by adding two more points at the low and the high ends. The first point is placed at DC, and the second point is selected at $f_{Na} = 3\ GHz$ with R_{Na} as shown in Figure 2.3.

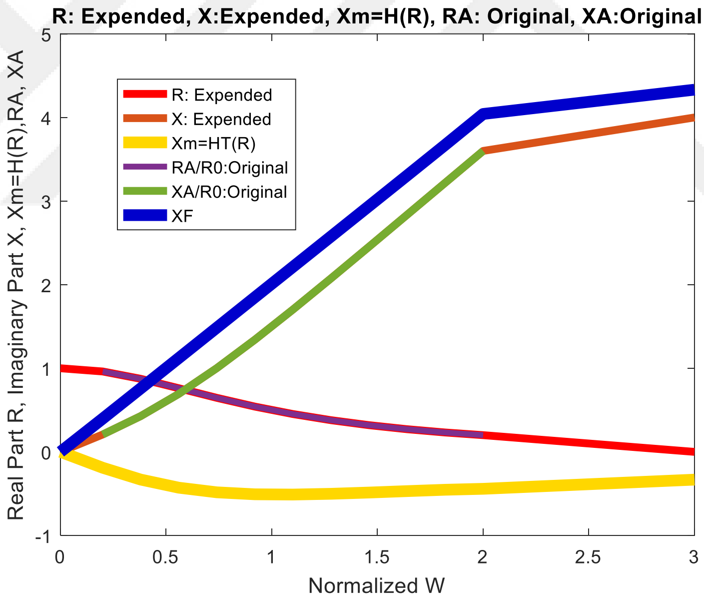

Figure 2.3 : Investigation of the measured impedance data if it is a positive real function. The answer is yes. It is PR.

Step 2 Impedance Data Augmentation: The measured real part data RA is gradually decreasing starting from 48 ohms at 200 MHz. Then, it may be appropriate to set $R1 = RA(1) = 50\Omega$ and the last break point is set to $RN = RA(N) = 0$ at 3 GHz. At DC, we assumed that the imaginary part $X(1) = 0$. Notice that at 1.82 GHz, actual reactance is $XA(1.82GHz) = 160\Omega$. At 2 GHz, $XA(2GHz) = 180\Omega$. In other words, reactance X is smoothly increasing towards 3 GHz. In this case, it may be reasonable to choose XA as $XA(3GHz) = 200\Omega$ or equivalently on the normalized scale, we set $X(3GHz) = \frac{200}{50} = 4$. Hence, augmented results are also shown in Figure 2.3.

Step 3 Generation of the imaginary part $X_m(\omega)$ of the minimum function: This step is performed using (2.5).

Step 4 Generation of Foster reactance function: This step is simply performed by $XF = X - Xm$ as in (2.6).

Step 5: Plot the results and investigate the Foster reactance function $X_F(\omega)$ if it is monotonically increasing

Computed Foster reactance function $X_F(\omega)$ is also depicted in Figure 2.3. Close examination of this figure reveals that $X_F(\omega)$ is monotonically increasing. Therefore, the measured impedance data given by Figure 2.3 belongs to a positive real impedance function. Therefore, it can be modelled as an analytic positive real function without hesitation.

2.3.2 Examination of the positive realness of the source and the load pull impedances obtained from a GaN power transistor

In this sub-section, we investigate the positive realness of the measured optimum source and load pull impedance data extracted from a GaN power transistor. The selected transistor is a $Wolfspeed - CG2H40045$, from Wolfspeed Company with nominal 45 Watts of output power [44]. As reported in [44], optimum source and load pull impedance plots are shown in Figure 2.4.

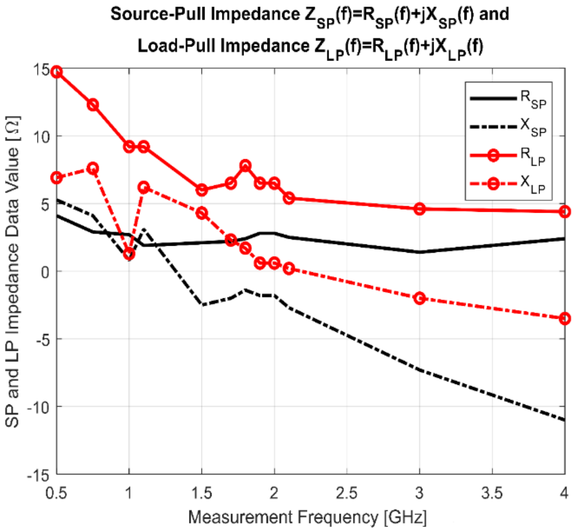

Figure 2.4 : Optimum Source-Pull and Load-Pull termination impedances.

As described in the previous section, we extrapolated the given data to cover the frequencies $F_{1a} = 0\,(DC)$ and $F_{Na} = 6\,GHz$. In extrapolating the measured source/load pull impedances, end points of the real parts (i.e., for a sufficiently large frequency point) and the first points (i.e., DC) of the imaginary parts are set to zero due to the nature of the impedance behavior. On the other hand, first points of the real parts and the last points of the imaginary parts may be predicted by linear interpolation of the given data.

At DC, we select $RSP(1) = 5\Omega$ and $XSP(1) = 0$. At $6\,GHz$, $RSP(N) = 0$ and $XSP(N) = -25\Omega$ are selected. Similarly, load pull impedance data is augmented as $RLP(1) = 20\Omega$, $RLP(N) = 0\Omega$ and $XLP(1) = 0$, $XLP(N) = -20\Omega$.

Close examination of Figure 2.5a reveals that, up to 500 MHz (Band-I), over 1.0-1.1 GHz (Band III), 1.5-1.8 GHz (Band V) and 1.9-2.0 GHz (Band VII) $X_{FSP}(\omega)$ behaves like a Foster reactance function by shape. However, over 500 MHz-1 GHz (Band II), 1.1-1.5 GHz (Band IV), 1.8-1.9 GHz (Band VI) and after 2.0 GHz (Band VIII), it is non-Foster.

Similarly, Figure 2.5b indicates that, X_{FLP} acts like a Foster reactance over DC to 750 MHz (Band-1), 1.0 GHz to 1.1GHz (Band-3), and it is non-Foster over 0.75 GHz -1.0 GHz (Band-2) and after 1.1 GHz (Band-4). Thus, we say that measured load pull impedance data behaves like a proper positive real function in Bands 1 and 3 respectively. Otherwise it is non-Foster. So far, what we have observed that due to nonlinear behavior of the GaN transistor Wolfspeed CG2H40045, reported source and load-pull impedances are not realizable network functions over the frequency bands indicated above, even though they present positive real parts. However, they can be fitted to realizable network functions as much as possible, to construct the optimum front-end (input) and back-end (output) matching networks of the power amplifier. This process leads us to the gain-bandwidth limitation of the active device under consideration. In the follow up section, we propose an algorithm to assess the gain-bandwidth limitation of the optimum source and the load pull impedances employing the real frequency line segment technique (RF-LST).

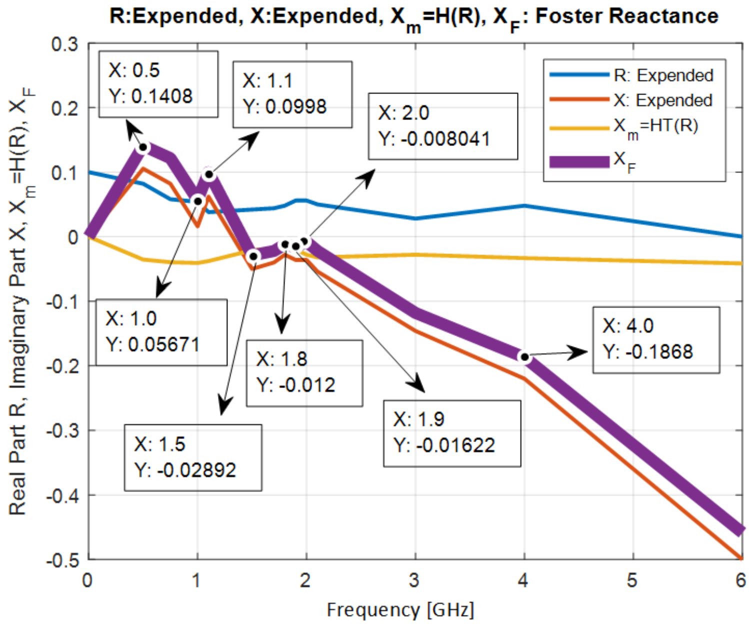

(a) Foster Part of the source-pull impedance data.

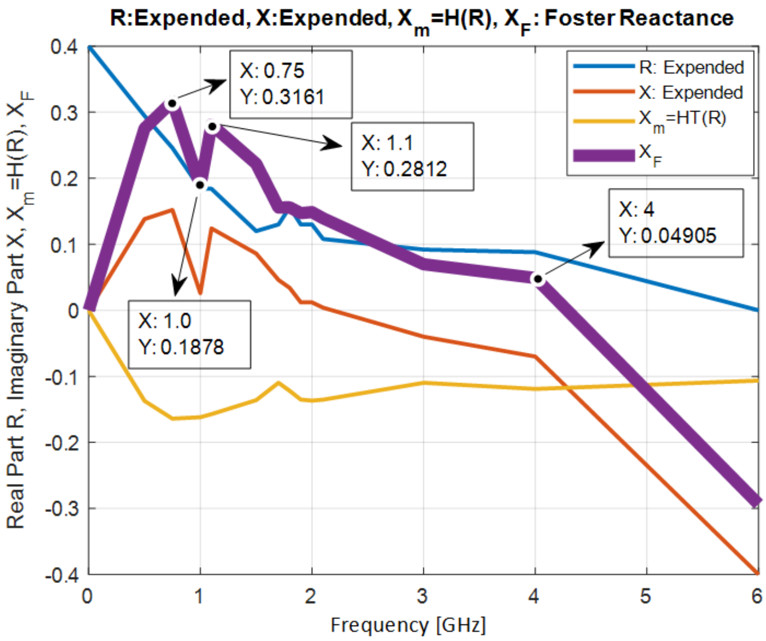

(b) Foster Part of the load-pull impedance data.

Figure 2.5 : Extraction of the Foster Reactance from the source/load pull impedances.

It is interesting to note that the imaginary part $X(\omega)$ pattern may resemble the variation of $X_F(\omega)$ if the contribution of $X_m(\omega)$ is negligible in $X(\omega) = X_F(\omega) + X_m(\omega)$.

2.4 Numerical Assessment of the Gain-Bandwidth Limitation of a Realizable Immittance

The purpose of this section is to build the best realizable line-segment model for the reported source and load pulled immittances of [44] as much as possible. The proposed method is outlined as follows.

Let $K(j\omega) = R(\omega) + jX(\omega)$ refers to either the optimum source or load-pull immittance to be modelled. In this regard, we define a virtual matching problem as shown in Figure 2.6, where the virtual load $K_{VL}(j\omega) = R_{VL}(\omega) + jX_{VL}(\omega)$ is the complex conjugate of the immittance data to be modelled using the Real Frequency Line Segment technique [50]. In this case, the virtual load $K_{VL}(j\omega)$ is expressed as

$$R_{LV}(\omega) = R(\omega) \tag{2.7a}$$

$$X_{VL} = -X(\omega) \tag{2.7b}$$

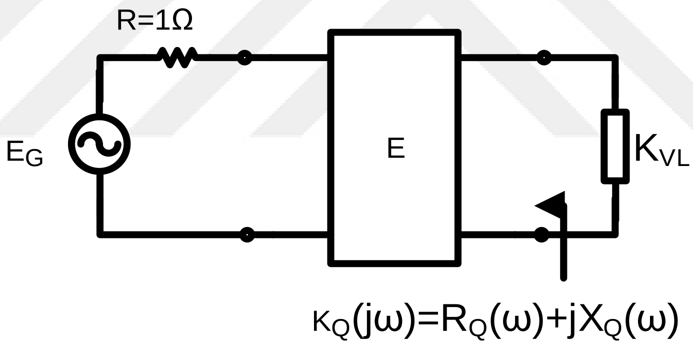

Figure 2.6 : A virtual single matching problem to model a measured immittance data $K(j\omega)$ by setting $K_{VL} = Z^*$.

Referring to Figure 2.6, in RF-LST, lossless matching network [E], is described by means of its PR driving point back-end immittance $K_Q(j\omega) = R_Q(\omega) + jX_Q(\omega)$ in Darlington sense. Furthermore, we assume that $K_Q(j\omega)$ is a minimum function. Therefore, $X_Q(\omega)$ is uniquely determined from $R_Q(\omega)$ via Hilbert Transformation as in (2.3). Referring to Figure 2.2, the unknown of the matching problem is selected as the real part $R_Q(\omega)$ and it is expressed by means of its unknown break points $RQA = [R_1\ R_2\ R_3 \ldots R_{N-1}\ R_N\ ]$, sampled at the break frequencies $WBR = [\omega_1\ \omega_2\ \omega_3 \ldots\ \omega_{N-1}\ \omega_N]$. $R_Q(\omega)$ is evaluated using (2.4) and $X_Q(\omega)$ is generated employing (2.5).

The unknown break points $[R_1\ R_2\ R_3 \ldots R_{N-1}\ R_N\ ]$ are determined to optimize the transducer power gain which is given by

$$
\begin{aligned}
T(\omega) = \frac{4R_Q R_{VL}}{\left|K_Q(j\omega) + K_{VL}(j\omega)\right|^2} = \frac{4R_Q R_{VL}}{\left(R_Q + R_{VL}\right)^2 + \left(X_Q + X_{VL}\right)^2} \\
= \frac{4R_Q R}{\left[R_Q + R\right]^2 + \left[H(R_Q) - X\right]^2}
\end{aligned}
\tag{2.8}
$$

During the optimization process, we target a flat gain level T_0 to minimize the error function $\varepsilon(\omega) = T(\omega) - T_0$ over the frequency band of interest. The ideal solution is the unity TPG (i.e., $T(\omega) = 1$) over the passband, which yields $R_Q(\omega) = R(\omega)$ and $X_Q(\omega) = -X_{LV} = X(\omega)$ as desired. As $T(\omega)$ deviates from unity gain, the trace of line segment model shifts from the original data. Therefore, we say that "quality of immittance modelling" is measured by means of the transducer power gain of the virtual matching problem. During the optimization process, the error function may be expressed in terms of the unknown break points as

$$
\begin{aligned}
\varepsilon(\omega) &= T(\omega) - T_0 \\
&= \frac{4R_Q R}{\left[R_Q(\omega) + R(\omega)\right]^2 + \left[\sum_{j=1}^{N-1} \beta_j(\omega)\Delta R_j - X(\omega)\right]^2} - T_0
\end{aligned}
\tag{2.9a}
$$

or equivalently,

$$
\varepsilon(\omega) = 4R_Q R - T_0 \left\{ \left[R_Q(\omega) + R(\omega)\right]^2 + \left[\sum_{j=1}^{N-1} \beta_j(\omega)\Delta R_j) - X(\omega)\right]^2 \right\} \tag{2.9b}
$$

In (2.9), $R(\omega)$ and $X(\omega)$ are the augmented immittance data to be modelled. $R_Q(\omega)$ is a line between the endpoints (ω_j, R_j) and (ω_{j+1}, R_{j+1}) for $\omega \in \left[\omega_j, \omega_{j+1}\right]$ as in (2.4).

It is noted that, the error expression given by (2.9a) is not an exact quadratic or convex function in terms of the unknowns R_i. On the other hand, at a fixed angular frequency point ω_j, alternative error form of (2.9b) is convex; and, as described in Section 2.4, its dependence on the angular frequency can be eliminated by using the sum of square errors, designated by ϵ, then it is minimized over the passband. In this regard, the numerical minimization process of (2.9b) is well behaved, and it is possible to hit the global minimum of ϵ with good initials. In fact, in subsection 2.4, we cover a reliable initialization method to kick the minimization process, which yields the "best solution for the break points with the highest value of the minimum of the passband gain" as shown in Figure 2.7. Based on the last statement, the following sub-section is presented to assess the numerical gain bandwidth limitation of the given immittance data.

2.4.1 The best transducer power gain T(ω)

Referring to Figure 2.6 and Figure 2.7, let $K(j\omega) = R(\omega) + jX(\omega)$ be the given immittance to be modelled as a realizable PR network function using the real frequency-line segment technique (RF-LST). Let $K_Q(j\omega) = R_Q(\omega) + jX_Q(\omega)$ be the RF-LST based minimum Driving Point Input Immittance (DPI) in Darlington sense. Let $T(\omega)$ be the transducer power gain (TPG) of the virtually matched system as specified by (2.8), which is optimized over the specified normalized angular frequency bandwidth B such that $B = [\omega_{c2} - \omega_{c1}]$.

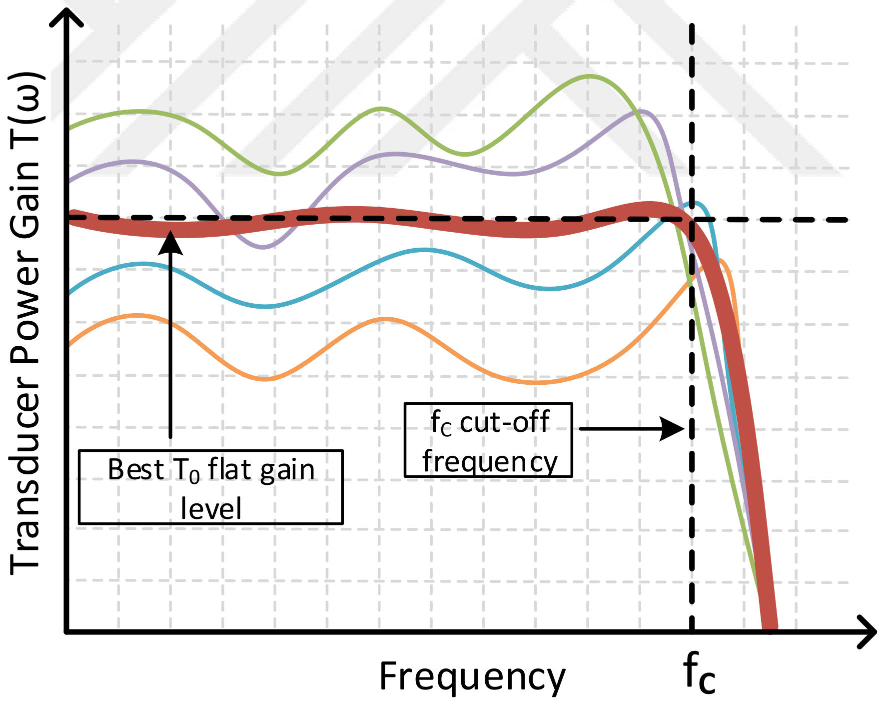

Figure 2.7 : Selection of the best GBWL by sweeping $T_0(k)$.

Let T_{min} be the minimum of $T(\omega)$ in B. Let T_{max} be the maximum of $T(\omega)$ in B. Let $T_{mean} = \frac{T_{max}+T_{min}}{2}$ be the mean value of $T(\omega)$ in B and let $\Delta T = T_{max} - T_{mean} = T_{mean} - T_{min}$ be the gain fluctuation in B.

By trial and error, one can determine a flat gain level T_0 in such a way that T_{min} reaches to its maximum value in B as depicted in Figure 2.7. This state of TPG is called the "RF-LST based Gain Bandwidth-Limitation, or in short "RFLST-GBWL" of the given complex immittance $K(j\omega)$ over the specified bandwidth B. In this state, the mean value of the transducer power gain describes the average value of the power transfer with optimum fluctuations. In this state, TPG may be expressed as $T(\omega) = T_{mean} \mp \Delta T$.

During the minimization process of (2.9), T_0 may be swept starting from the flat gain level $T_0(1) = 0.60$ upto to $T_0(n_k) = 1.00$ with small step sizes δT. For example, δT may be selected as $\delta T = 0.05$. In this case, we define an index k in a loop to minimize the error function $\varepsilon(\omega, T_0(k))$ of (2.9) for a total number $n_k + 1 = 9$ times. Then, at each step k, we store $K_Q(j\omega, k) = R_Q(\omega, k) + jX_Q(\omega, k)$, $T_{min}(k)$, $T_{max}(k)$, $T_{mean}(k)$, $\Delta T(k)$ $T(\omega, k)$ and $T_0(k)$ to determine the optimum "$gain - state$" yielding the "$RFLST\ based\ GBWL$" of the complex termination $K(j\omega) = R(\omega) + jX(\omega)$ over B, which in turn results in the best realizable-DPI in the form of line segments or equivalently as sampled data points.

For all the nonlinear optimization problems, initialization of the unknowns is always crucial. Therefore, in the next subsection we present a rule of thumb to initialize the unknown break points R_j for the minimization of the error function $\varepsilon(\omega, T_0(k))$ for a fixed T_0.

2.4.2 Initialization of the nonlinear minimization process

Before we introduce the optimization process, for a selected flat gain level T_0 and the normalized break frequencies $\{\omega_1,\ \omega_2,\ \omega_3, \dots \omega_N\}$, the unknown break points $\{R_1,\ R_2,\ R_3, \dots R_N\}$ must be initialized. In this regard, initialization of the break points can be performed using (2.8) by assuming reactance cancellation. In other words, to maximize $T(\omega)$ of (2.8), the reactance term $(X_Q - X)$ is set to zero to derive the initials break points R_{int-j} such that

$$T_0 \approx \frac{4R_Q R}{[R_Q + R]^2} \tag{2.10a}$$

or

$$R_{int-j} = R(\omega_j)\left[\frac{2 - T_0 + 2\mu\sqrt{1 - T_0}}{T_0}\right] \geq 0 \qquad (2.10b)$$

In (2.10b), μ is a unimodular constant. It is set to $\mu = +1$ for the high values of initials R_{intH-j} or it is selected as $\mu = -1$ for the low initials R_{intL-j}. One can run the optimization separately for both values of $\mu = \mp 1$, and selects the best solution which refers the value of μ. Nevertheless, for many applications, we end up with similar results regardless of what μ is.

2.4.3 Minimization of the error function: $\boldsymbol{\varepsilon(\omega, R_1, R_2, \ldots, R_{N-1})}$

In this work, we prefer to minimize the sum of squared errors of (2.9) over the passband, designated by ϵ such that

$$\epsilon = \sum_{r=1}^{Ns} [\varepsilon(\omega_r, R_1, R_2, R_3, \ldots, R_{N-1})]^2; \quad \omega_{c1} \leq \omega_r \leq \omega_{c2} \qquad (2.11)$$

In (2.11), the integer Ns is the total number of sampling points over the passband $B = [\omega_{c2} - \omega_{c1}]$ subject to optimization. The normalized angular frequencies ω_{c1} is the low-end and ω_{c2} is the high-end of the frequency band. Thus, the unknown break points $x = \{R_1, R_2, R_3, \ldots, R_{N-1}\}$ are determined to minimize the sum of squares error ϵ. Minimization is performed using the Levenberg-Marquardt algorithm [67-69].

During minimization of sum of squared errors, the first break point R_1 may be kept constant as it is initialized. This constant value may be zero for bandpass problems (i.e., $R_1 = 0$) or it may be included among the unknown break points. At the end of the minimization process, the realizable-driving point input immittance $K_Q(j\omega) = R_Q(\omega) + jX_Q(\omega)$ is obtained which is the optimum possible line-segment model for the measured immittance data $K(j\omega) = R(\omega) + jX(\omega)$.

Thus, we propose the following algorithm to assess the GBWL of the given immittance data. In the algorithm, the virtual matching problem of Figure 2.6 is considered, and its virtual gain is optimized. This process is called the "Virtual Gain Optimization" or in short "VGO".

Algorithm 2.2: Determination of the GBWL of measured immittance data via VGO

Inputs:

FA: Actual frequency array which samples the immittance data to be modelled up to a point where the real part $RA(f_{Na})$ practically vanishes. It is specified as a vector $FA = [f_{1a}\ \ f_{2a} \dots f_{Na}]$. Note that it would be preferable to select f_1 at DC (i.e., $f_1 = 0$) by extrapolating the measured immittance data.

RA: Measured real part of the immittance data. It is an array of the same size as FA. It is specified as a vector $RA = [R_{1a}\ \ R_{2a} \dots R_{Na}]$ (i.e. RA includes all the break points) with $R_{Na} = 0$.

XA: Measured imaginary part of the immittance data. It is an array of the same size as FA. it is specified as a vector $XA = [X_{1a}\ \ X_{2a} \dots X_{Na}]$. Most probably, at DC, $X_{1a} = 0$ for passive immittance data.

$R0$: Normalization resistance. It may be selected as standard termination 50Ω.

$F0$: Normalization frequency. It may be selected at the high end of the passband such that $F_0 = F_{(N-1)a}$ where $R_{(N-1)a} > 0$ with $R_N = 0$ at F_{Na}.

ω_{C1}: Low-end of the passband ($\omega_{C1} \geq 0$).

ω_{C2}: High-end of the passband ($\omega_{C2} > \omega_{C1}$).

ω_{s1}: Low-end of the stop band.

ω_{s2}: High-end of the stop band.

N: Total number of break points $[R_1, R_2, R_3, \dots, R_{N-1}\ R_N]$ and break frequencies $WBR = [\omega_1\ \omega_2\ \omega_3\ \dots\ \omega_{N-1}\ \omega_N]$.

$KFlag$: This “integer” indicates if TPG is described in terms of impedances or admittances.

- If $KFlag = 1$, TPG is impedance based.
- If $KFlag = 0$, TPG is admittance based.

$RB1$: Initial value of the first break point. Note that one may select $RB1 = 0$ for bandpass problems.

ntr: Decide whether $RB1 \geq 0$ is included among the unknowns or not.

- Choose $ntr = 1$ if $RB1$ is among the unknowns;
- otherwise set $ntr = 0$.

T_{01} and T_{02}: Beginning and end levels of the flat gain $T_0(k)$ subject to optimization.

Note that in our programs we set $T_{01} = 0.6$ and $T_{02} = 1$. The reason for these choices is that, if TPG is less than that of $T(\omega) < 0.5$ (i.e. $T(\omega)$ is less than -3dB), more than half of the available power is reflected back to the generator. In this case, termination immittance may be considered as "no good". In this case, the designer should seek a better power transistor.

δT: Incremental step size to sweep the flat gain $T_0(k)$ from T_{01} to T_{02}.

For our program, we select $\delta T = 0.05$. Therefore, the index runs from 1 to $nk + 1$ where $nk = \frac{(T_{02} - T_{01})}{\delta T} = 8$.

μ (or $sign$): It is a unimodular constant. Decide whether you wish to work with high or low values of initial break points.

- Choose $\mu = +1$ for high value
- or set it to $\mu = -1$ for low value of initial break points.

Computational Steps: Generation of the error function

Step 1: Augment and normalize the given data points with respect to $R0$ and $F0$ as in Algorithm 2.1.

In this step, normalized complex immittance termination $KLA = (RA + jXA)/R0$ is designated by its real part $RLA = RA/R0$ and its imaginary part $XLA = XA/R0$ such that $KLA = RLA + jXLA$ is a complex array. Its corresponding normalized break frequencies are designated by an array WLA which includes augmented and normalized sampling frequencies such that $WLA = [\omega_{s1}\ (FA/F0)\ \omega_{s2}]$ with, perhaps $\omega_{s1} = 0$ and $\omega_{s2} = l \times \omega_{c2}$ where l is an integer and it may be selected as $1 < l \leq 3$.

Step 2: Generation of break frequencies WBR for the unknown break points.

- Set the first break frequency as $WBR(1) = W1 = \omega_{S1} \geq 0$.
- Set the last break frequency as $WBR(N) = WN = \omega_{S2}$.

- Distribute the remaining break frequencies between ω_{C1} and ω_{C2}, perhaps uniformly.

Step 3: For a selected flat gain level $T_0(k)$, generate the initials for the break points as in (2.10) such that

$$\omega_j = WBR(j)$$

$$R_j = R_{int-j} = RLA(\omega_j)\left[\frac{2 - T_0(k) + 2\mu\sqrt{1 - T_0(k)}}{T_0}\right] \geq 0;$$

$$j = 1,2,3,\dots,N-1$$

Note that R_N is fixed at zero (i.e., $R_N = 0$).

Step 4: Generate the imaginary part $X_Q(\omega)$ of the minimum function $K_Q(j\omega)$ as an array XQA from RQA using (2.5). Where RQA is an array which includes the all the unknown break points as they are initialized under $RQA = [R_1\ R_2\ R_{3\dots}\ R_N]$.

Step 5: Generate virtual TPG as in (2.8) such that

$$T(\omega) = \frac{4R_Q(\omega)R(\omega)}{\left[R_Q(\omega) + RL(\omega)\right]^2 + \left[X_Q(\omega) - XL(\omega)\right]^2};\ \ \omega_{c1} \leq \omega \leq \omega_{c2}$$

In this step, at any point $\omega = \omega_i$, values of $R_Q(\omega)$, $R(\omega)$, $X_Q(\omega)$ and $X(\omega)$ are computed via linear interpolation.

Step 6: Generate the error function $\varepsilon(\omega_i, [R_1\ R_2\ R_{3\dots}\ R_N], T_0(k)) = T(\omega) - T_0(k)$ over the sampling points ω_i in the passband.

Step 7: Combine Step 2 through Step 6 with a nonlinear optimizer to determine the unknown break points $X = [R_1\ R_2\ R_{3\dots}\ R_N]$.

Step 8: Sweeping the flat gain level from $T_{01} = 0.6$ to $T_{02} = 1.0$, repeat Step 2 through Step 7 for each flat gain levels $T_0(k)$ and at the end of the minimization process, store the following quantities.

- $T\_min(k) = Minimum\ of\ TPG\ in\ the\ passband.$
- $T\_max(k) = Maximum\ of\ TPG\ in\ the\ passband.$
- $T\_mean(k) = (T\_max + T\_min)/2.$
- $TPGA(:,k)\ versus\ frequency.$

- $RQA(:,k)$ $versus$ $frequency$.
- $XQA(:,k)$ $versus$ $frequency$.

Step 9: Find the best solution to determine the gain-bandwidth limitation for the measured immittance data by generating the maximum value of the minimum gain $Tmin = max(T\_min(k))$ in the passband.

-end of the algorithm-

At this point, it is important to re-emphasize that the error function of (2.9b) is a convex function of the unknown break points R_i, regardless it's total numbers. Therefore, Algorithm 2.2 always hits the global minimum of the error function, which in turn yields the best solution for the selected flat gain level T_0 over the specified bandwidth. Thus, we say that RF-LST never requires to select a circuit topology nor an analytic form of a transfer function to optimize the transducer power gain of the matched structure under consideration. Hence, the ultimate gain-bandwidth limitation of the given source and load-pull impedances are automatically determined. Eventually, optimum-realizable source/load impedances are obtained as the output of Algorithm 2.2.

Now let us implement the above algorithm to generate the gain bandwidth limitations of the source and the load-pull impedances for the $Wolfspeed\_CG2H40045$ GaN power transistor.

2.5 Gain Bandwidth Limitation of the Source-Pull Impedance for Wolfspeed CG2H40045 GaN Transistor

In this section, we will investigate the "power-intake" capability of the $Wolfspeed$ $CGH240045$ GaN transistor at its input [44]. Transistor is driven by a generator with $R_0 = 50\Omega$ internal resistance. The given source-pull impedance is approximated as the driving-point back-end impedance of a lossless two-port [E] when it is terminated in the complex-conjugate of the given source pull immittance as in Figure 2.5a. In this regard, it is desired to determine the gain-bandwidth limitation of the given source-pull impedance as detailed in Algorithm 2.2. The given/augmented and the normalized source-pull impedances are depicted in Figure 2.5a. User defined passband is specified over $f_{C1} = 800MHz$ and $f_{c2} = 3.8\ GHz$. In this case, we select the normalizing frequency at $F_0 = 3.8\,GHz$. The real part of the given source-pull impedance is augmented at DC (i.e., $f = 0$) as $RSA(1) = 5\Omega$ and $RSA(N) = 0\Omega$. Similarly, the given imaginary part XSA is augmented as $XSA(1) = 0$ at DC $(i.e. ws1 = 0)$ and the end point is augmented at 6 GHz as $XSA(N) = -25\Omega$. The GBWL of the virtual matching problem of Figure 2.5a is numerically assessed via RF-LST employing the above algorithm. Inputs to the algorithm are summarized as follows.

$\omega_{C1} = \frac{0.8}{F0} = 0.2105$; $\omega_{C2} = \frac{3.8\,GHz}{F0} = 1$; $\omega_{s1} = 0.18$; $\omega_{s2} = 1.2$. We have selected $N = 21$ break points with 19 unknowns.

In the optimization process, we prefer to work with impedances. Therefore, $KFlag$ is set to 1 (i.e., $KFlag = 1$). Furthermore, $ntr = 0$ with fixed $RB1 = 0$ located at DC, since we deal with a bandpass single matching problem. Flat gain levels are swept between $T01 = 0.6$ and $T02 = 1.0$ with $\delta T = 0.05$ incremental steps. Therefore, we define the total number of 9 flat gain levels starting from $T0(1) = 0.6$ up to $T0(9) = 1.0$. Eventually, we start the optimization with low initials. Therefore, $\mu = -1$ is selected.

Execution of Algorithm 2.2 results in the RF-LST based Gain Bandwidth Limitation of the measured and augmented source pull impedance. It is noted that total execution time on MatLab is about 10.2 seconds on an i7 processor computer with 32GB RAM. Results of the sequential optimization of TPG are summarized as in Table 2.1 and depicted as in Figure 2.8 [70].

Table 2.1 : GBWL of SP impedance of Wolfspeed CG2H40045 power transistor.

$T_0(k)$	T_{mean}	$F_{max}[GHz]$	T_{max}	$F_{min}[GHz]$	T_{min}	ΔT
0.6000	0.5992	3.7930	0.6199	1.1339	0.5786	0.0206
0.6500	0.6507	0.8419	0.6624	1.1261	0.6390	0.0117
0.7000	0.6690	3.6840	0.7254	3.7852	0.6127	0.0564
0.7500	0.6772	3.6879	0.7651	3.7813	0.5892	0.0880
0.8000	0.6863	3.6957	0.7926	3.7774	0.5801	0.1062
0.8500	0.6982	3.6996	0.8155	3.7735	0.5809	0.1173
0.9000	0.7135	3.6996	0.8370	3.7697	0.5900	0.1235
0.9500	0.7355	3.7035	0.8610	3.5049	0.6101	0.1254
1.0000	0.7331	3.7074	0.8776	3.7658	0.5886	0.1445

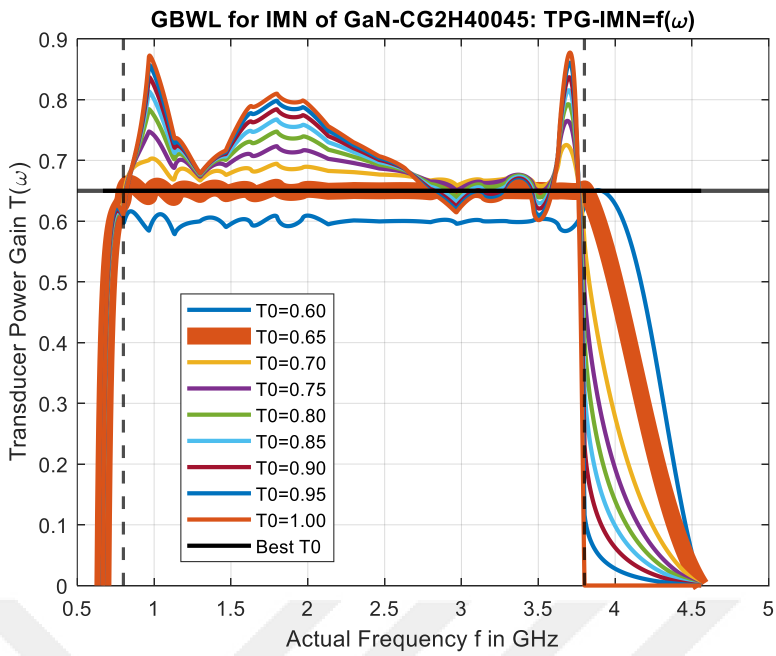

Figure 2.8 : GBWL by sweeping $T_0(k)$ obtained for the source-pull data. For $k = 7$, $T_0(k) = 0.65$ yields the best solution.

The RF-LST based Gain Bandwidth Limitation appears to be at max $(T_{min}) = 0.6390$ with loop index $k = 2$, or equivalently, $T_{mean} = 0.6507 \mp 0.0117$. Optimized break points $R_{QLST-SP}$ and its corresponding Hilbert Transform $X_{QLST-SP}$ is depicted in Figure 2.9a and Figure 2.9b respectively.

Manufacturer's published source pull impedance data and the best RF-LST based optimized source impedance $Z_{S(RF-LST)}(j\omega) = R_{S(RF-LST)}(\omega) + jX_{S(RF-LST))}(\omega)$ are shown in Figure 2.10.

Close examination of Figure 2.10 indicates that, while the imaginary parts are in good agreement, unfortunately, the real part $R_{S(RF-LST)}(\omega)$ of the "best realizable source impedance" significantly deviates from the measured data. That is the reason of the gain degradation from its ideal value 1 down to 0.65.

Referring to Table 2.1 and Figure 2.8, it is predicted that 65.07% of the available power of the generator is transferable to the input of the power transistor $CG2H40045$. In other words, GBWL of the optimum realizable source pull impedance is $T_{mean} = 0.6507$ with optimum fluctuation of $\Delta T = \mp 0.0117$.

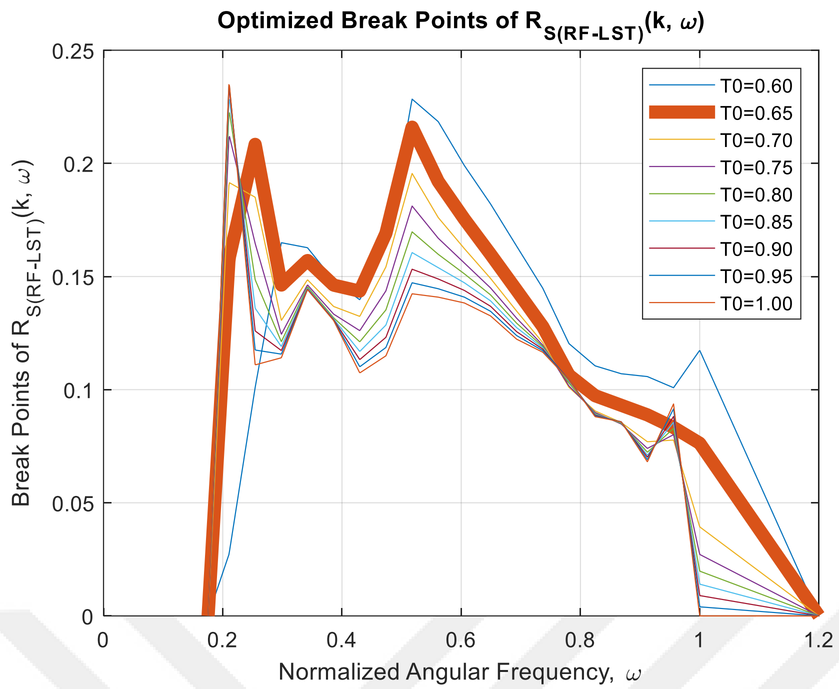

(a). Optimized real parts $R_{S(RF-LST)}(k, \omega)$ of the RF-LST based source

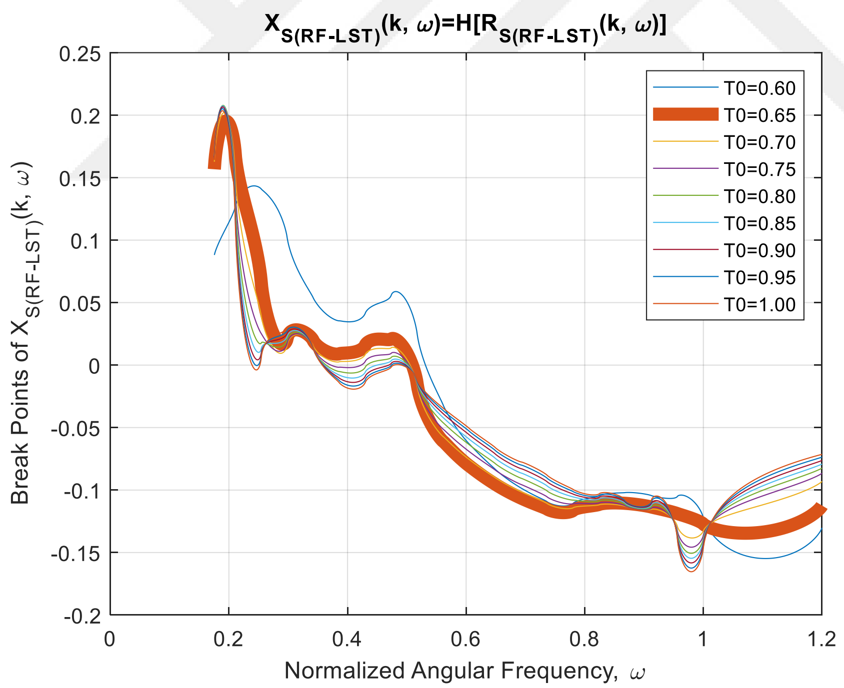

(b).Optimized imaginary parts $X_{S(RF-LST)}(k, \omega)$ of the RF-LST based source impedance.

Figure 2.9 : Optimized minimum $Z_{S(RF-LST)}(j\omega)$ for $k = 1,2,..,9$.

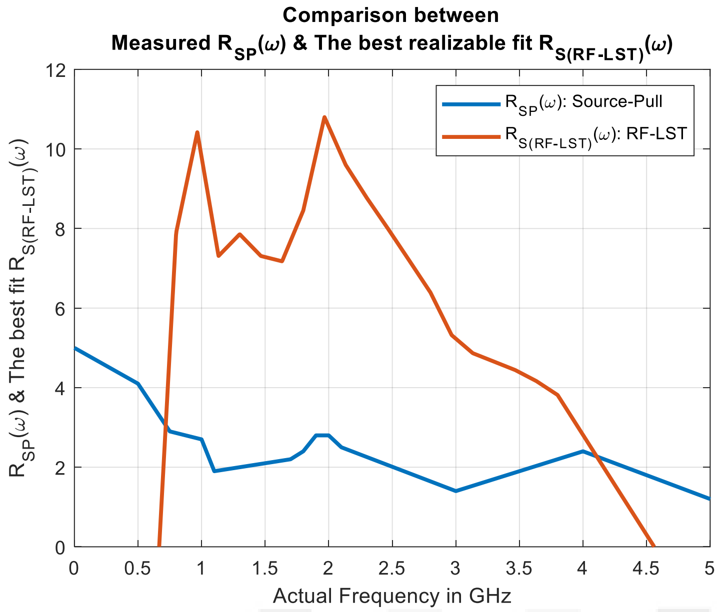

(a). The best RF-LST Based real part $R_{S(RF-LST)}(\omega)$ of the realizable SP impedance $Z_{S(RF-LST)}(j\omega) = R_{S(RF-LST)}(\omega) + jX_{S(RF-LST))}(\omega)$, obtained for $T_0(k) = 0.65$.

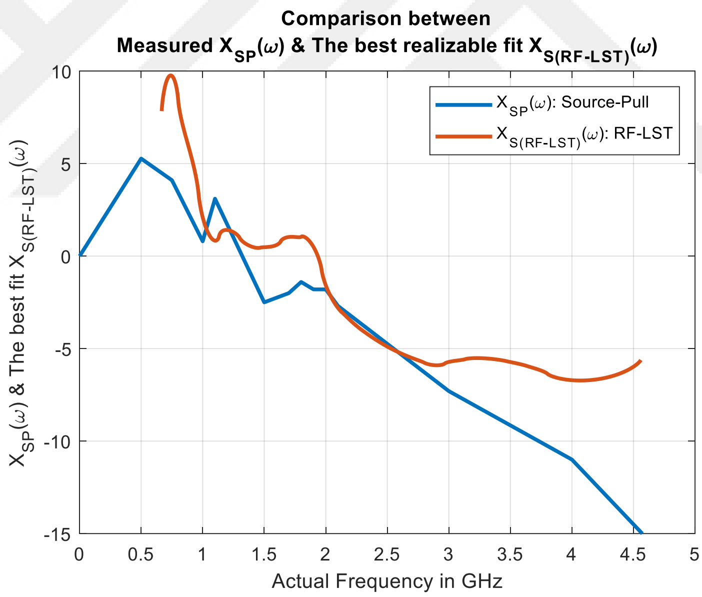

(b). Imaginary part $X_{S(RF-LST)}(\omega)$, obtained for $T_{0k} = 0.65$.

Figure 2.10 : Real and imaginary parts of the original and the RF-LST based source-pull impedance.

Let us now investigate the output power delivering capacity of the same transistor using the load-pull measured impedance data in the following section. In this regard, it is desired to determine the gain-bandwidth limitation of the optimum load-pull impedance as detailed in Algorithm 2.2. The measured/augmented and the normalized load-pull impedances are depicted in Figure 2.5b.

For the sake of further clarification, it is noted that Figure 2.10 and Figure 2.13 compare the outcome of the RF-LST based “best-realizable impedance data pair” with that of the measured source and load-pull impedances respectively. Clearly, the mismatch between the real and imaginary parts of the RF-LST based solutions and the measured source/load-pull impedance data, reflects the performance degradation, which in turn reflects in GBWL of the power amplifier under consideration as depicted in Figure 2.8 and Figur 2.11 respectively.

2.6 Gain Bandwidth Limitation of the Load-Pull Impedance for Wolfspeed CG2H40045 GaN Transistor

In this section, we will investigate the power delivering capability of the $Wolfspeed\,CG2H40045\;\;GaN$ transistor at its output-port [44]. Here, we assumed that the transistor is terminated in its modelled-realizable optimum load-pull impedance over the output matching network (OMN) while the other end of OMN is terminated in $R0 = 50\Omega$. The measured load-pull impedance is approximated as the driving-point backend impedance of a lossless two-port [E] when it is terminated in the complex-conjugate of the load-pull immittance as in Figure 2.5b.

As in the source-pull gain-bandwidth limitation computations, user defined passband is specified over $f_{C1} = 800\ MHz$ and $f_{c2} = 3.8\ GHz$. Therefore, we again set $F_0 = 3.8\ GHz$. The real part of the measured load-pull impedance is augmented at DC (i.e., $f = 0$) as $RLPA(1) = 20\Omega$ and $RLPA(N) = 0\Omega$. Similarly, the measured imaginary part $XLPA$ is augmented as $XLPA(1) = 0$ at DC $(i.e. ws1 = 0)$ and the end point is augmented at 6 GHz as $XLPA(N) = -20\Omega$.

The GBWL of the virtual matching problem of Figure 2.5b is numerically assessed via RF-LST employing Algorithm 2.2 Inputs to the algorithm is summarized as follows.

$\omega_{C1} = \frac{0.8}{F0} = 0.2105$; $\omega_{C2} = \frac{3.8\ GHz}{F0} = 1$; $\omega_{s1} = 0.18$; $\omega_{s2} = 1.1$. We have selected $N = 21$ break points with 19 unknowns. In the optimization, we prefer to work with impedances (i.e., $KFlag = 1$). Furthermore, $ntr = 0$ with fixed $RB1 = 0$ which is located at DC, since we deal with a bandpass single matching problem. The flat gain levels are swept between $T01 = 0.6$ and $T02 = 1.0$ with $\delta T = 0.05$ increamental steps. Therefore, we define the total number of 9 flat gain levels starting from $T_0(1) = 0.6$ up to $T_0(9) = 1.0$. Eventually, we start the optimization with low initials.

Therefore, $\mu = -1$ is selected. Execution of Algorithm results in the RF-LST based Gain Bandwidth Limitation of the load-pull impedance. The result of optimization is summarized as in Table 2.2 and depicted as in Figure 2.11. It is noted that total execution time on MatLab is about 3.6 seconds on an i7 processor computer with 32GB RAM [70].

Table 2.2 : GBWL of LP impedance of Wolfspeed CG2H40045 power transistor.

$T_0(k)$	T_{mean}	$F_{max}[GHz]$	T_{max}	$F_{min}[GHz]$	T_{min}	ΔT
0.6000	0.5992	1.0426	0.6133	1.1339	0.5851	0.0141
0.6500	0.6487	1.0426	0.6639	1.1339	0.6335	0.0152
0.7000	0.6982	1.0426	0.7143	1.1339	0.6821	0.0161
0.7500	0.7479	1.0391	0.7646	1.1339	0.7312	0.0167
0.8000	0.7977	1.0391	0.8146	1.1339	0.7809	0.0169
0.8500	0.8478	1.0391	0.8642	1.1339	0.8313	0.0165
0.9000	0.8980	1.0391	0.9130	1.1339	0.8829	0.0151
0.9500	0.9478	3.6776	0.9628	1.1339	0.9328	0.0150
1.0000	0.9557	3.6389	0.9952	1.1339	0.9162	0.0395

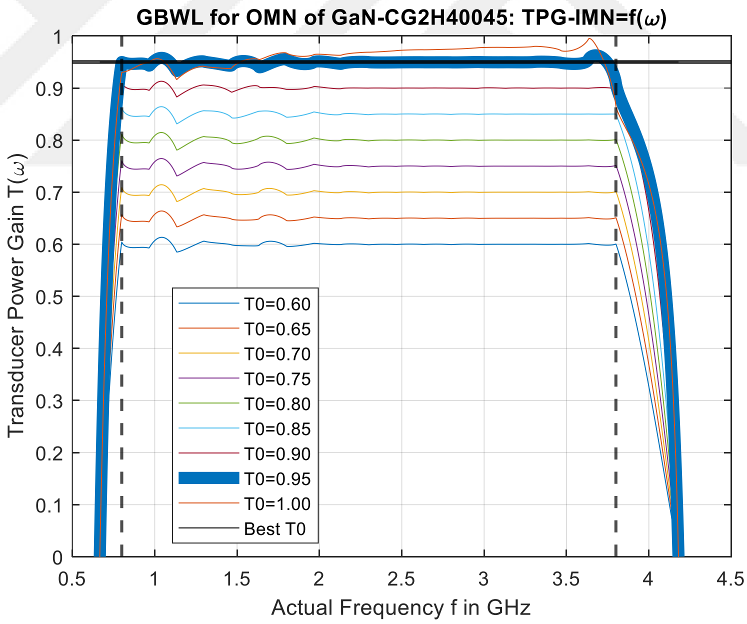

Figure 2.11 : GBWL of LP by sweeping $T_0(k)$.

The RF-LST based Gain Bandwidth Limitation appears to be at max $(T_{min}) = 0.9328$ or equivalently, $T_{mean} = 0.9478 \mp 0.015$ with corresponding loop index $k = 8$ which corresponds to $T_{0k} = 0.95$.

Optimized break points $R_{L(RF-LST)}$ and its corresponding Hilbert Transform $X_{L(RF-LST)}$ is depicted in Figure 2.12a and Figure 2.12b respectively.

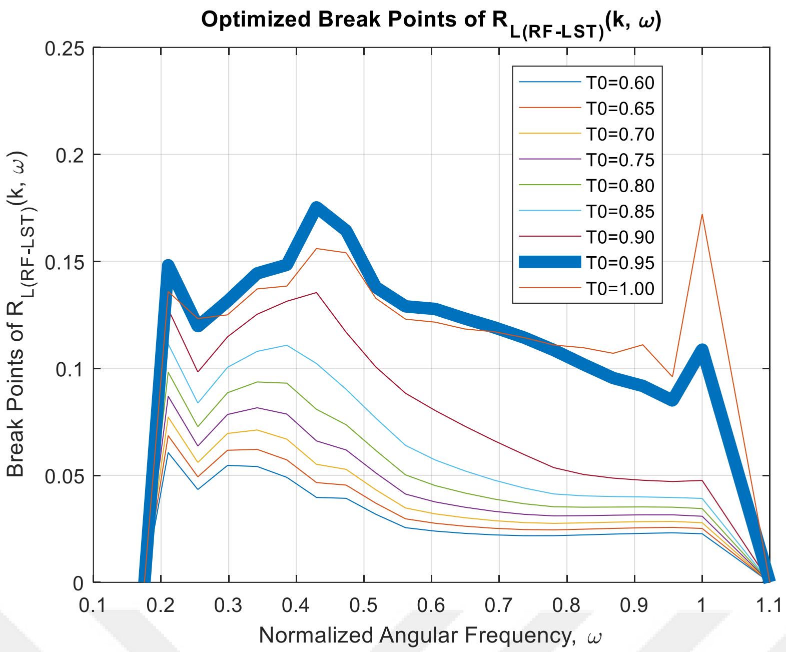

(a) Optimized real parts $R_{L(RF-LST)}(k,\omega)$ of the RF-LST based load impedance

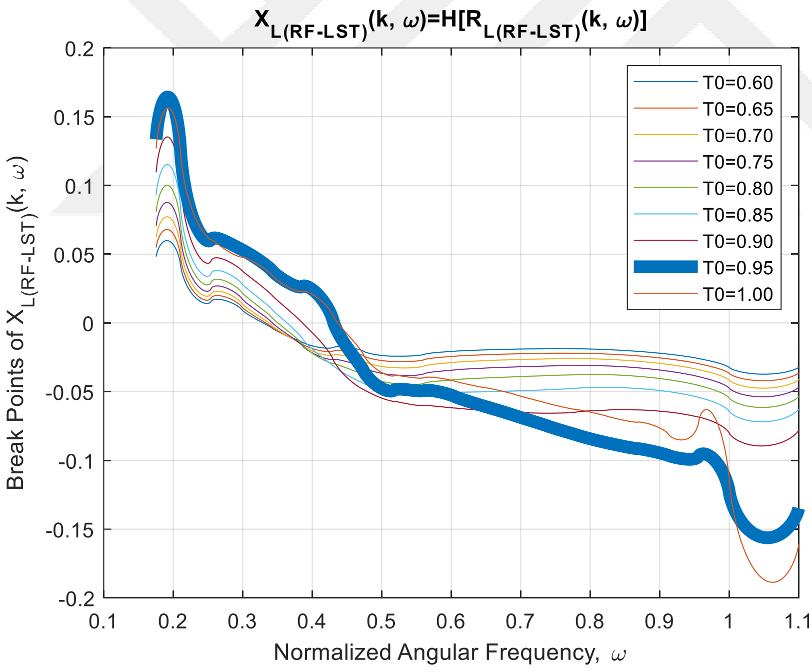

(b). Optimized imaginary parts $X_{L(RF-LST)}(k,\omega)$ of the RF-LST based load impedance.

Figure 2.12 : Optimized minimum $Z_{L(RF-LST)}(j\omega)$ for $k = 1,2,..,9$.

Real and imaginary parts of the measured load pull impedance and its analytic model $Z_L(j\omega) = R_L(\omega) + jX_L(\omega)$ are given in Figure 2.13a and Figure 2.13b respectively.

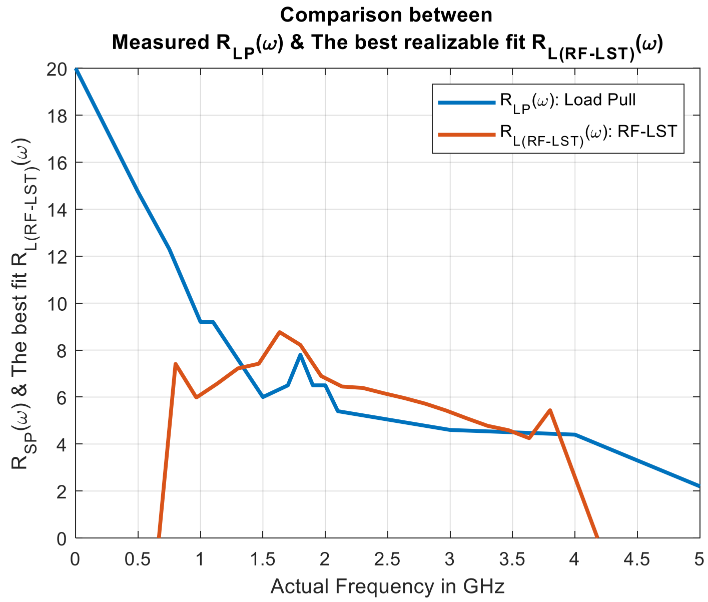

(a) The real part $R_{LP}(\omega)$ of the load pull impedance $Z_{LP}(j\omega)$ and its best fit $R_{L(RF-LST)}(k,\omega)$ for $k = 8$ via RF-LST based VGO.

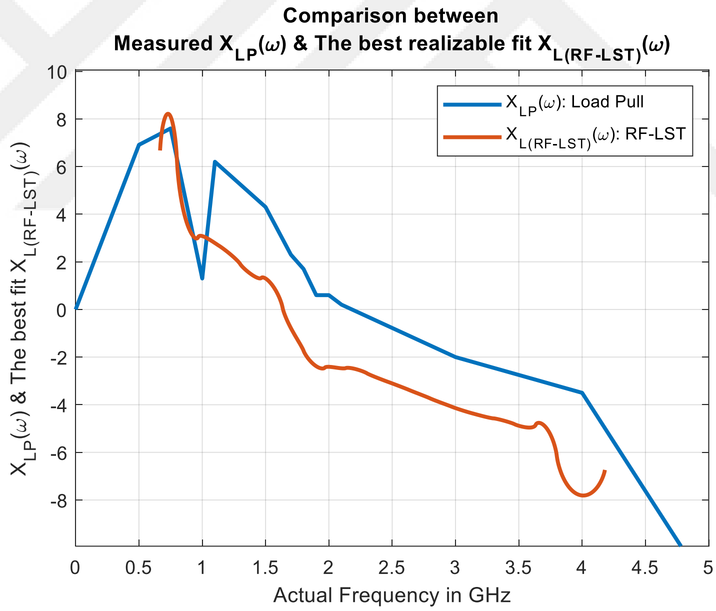

(b). The imaginary part $X_{LP}(\omega)$ of the load pull $Z_{LP}(j\omega)$ and its best fit $X_{L(RF-LST)}(k,\omega)$ via RF-LST based VGO.

Figure 2.13 : Real and imaginary parts of the original and the RF-LST based load-pull impedance.

Referring to Table 2.2 and Figure 2.11, it is predicted that 94.78% of the output power is delivered to the load-pull impedance of the power transistor $CG2H40045$. In other words, GBWL of the optimum realizable load-pull impedance is $T_{mean} = 0.9478$ with optimum fluctuation of $\Delta T = \mp 0.015$.

Figure 2.13 indicates that the best realizable load model is in good agreement with that the measured load-pull data yielding 94.78% power transfer.

At this point it would be appropriate to define the power-intake and power-delivering performance of an active device since its optimum-realizable RFT based source and load impedances refer to the ac-power absorption and power delivery capacity.

2.7 Power Performance Product of an Active Device

Considering the results of Section 2.5 and Section 2.6, we can define a new quantity called "Average Power Performance Product $(PPP)_{mean}$" of a power transistor such that

$$(PPP)_{mean} = [GBWL]_{SP} \times [GBWL]_{LP} \tag{2.12a}$$

where $[GBWL]_{SP}$ is the gain bandwidth limitation of the measured source-pull impedance and $[GBWL]_{LP}$ is the gain bandwidth limitation of the measured load-pull impedance respectively. Thus, we can say that maximum power performance product $(PPP)_{max}$ of an active device cannot exceed

$$(PPP)_{max} = [T_{max}]_{SP} \times [T_{max}]_{LP} \tag{2.12b}$$

where $[T_{max}]_{SP}$ and $[T_{max}]_{LP}$ the values of the maximum pass band gains which corresponds to $[GBWL]_{SP}$ and $[GBWL]_{LP}$ respectively.

By Table 2.1 and Table 2.2, for Wolfspeed CG2H40045, $(PPP)_{mean} = 0.6507 \times 0.9478 = 0.6167$ (i.e., ~61.7%) and $(PPP)_{max} = 0.6624 \times 0.9628 = 0.6378 = 63.8\%$.

It is noted that PPP of the amplifier varies $0\% \leq PPP \leq 100\%$. $PPP = 100\%$ corresponds to perfect match at the input and the output of the amplifier. In this case, matching networks exactly transforms the source-pull and the load-pull impedance data to 50Ω terminations meaning that, the selection of the power transistor is excellent to be utilized. However, if PPP deviates from 100%, mismatch is introduced by either IMN or OMN or for both. As designers, we do not wish to use any transistor, whose power-intake and power-delivery capacity is less than 50%, or equivalently if $(PPP)_{mean} < 25\%$. Hence, PPP can be the utilized as a figure of merit to decide whether the active device is worth using to design the power amplifier under discussion.

2.8 Construction of the Power Amplifier from the Analytic Models Built on the Optimum-Realizable RF-LST Based Source/Load Impedance Data

Once GBWL are determined for the given source and load-pull impedance data via RF-LST, resulting optimum-realizable source and load impedances of Figure 2.10 and Figure 2.13 are modelled as positive real functions as described in [50]. In this regard, the analytic form of the real part $R_{S(L)}(\omega^2)$ of the optimum source (or load) impedance, designated by $Z_{S(L)}(j\omega) = R_{S(L)}(\omega) + jX_{S(L)}(\omega)$, is given by

$$R_{S(L)}(\omega^2) = \frac{\omega^{2ndc} a_{S(L)0}^2}{B_{S(L)}(\omega^2)} \qquad (2.13a)$$

In (2.13a), the strictly positive denominator polynomial $B_{S(L)}(\omega^2)$ is defined by means of an auxiliary full polynomial $c_{S(orL)}(\omega)$ such that

$$B_{S(L)}(\omega^2) = \frac{1}{2}\left[c_{S(L)}^2(\omega) + c_{S(L)}^2(-\omega)\right] > 0;\ \forall\omega \qquad (2.13b)$$

$$c_{S(L)}(\omega) = c_{1S(L)}\omega^n + c_{2S(L)}\omega^{n-1} + \cdots + c_{nS(L)}\omega + 1; \qquad (2.13c)$$
$$c_i \neq 0; i = 1,2,\dots,n$$

In the above equations, the real part $R_{S(L)}(\omega^2)$ dictates the topology for IMN (or OMN). The integer n refers to the total number of circuit elements in the matching network under consideration. The integer ndc is the total count of the transmission zeros placed at DC (i.e., $\omega = 0$) and they appear as either series capacitors or shunt inductors. In this case, total number of transmission zeros at infinity is specified by $n_\infty = n - ndc$, and they are realized as series inductors and shunt capacitors. The optimum-realizable analytic form for the source impedance $Z_S(p)$ (or the load impedance Z_L(p)) is derived using the parametric approach [71]. Skipping the details, for selected $n = 6$, $ndc = 2$, the modelled optimum source and load impedances are found as follows.

$$a_{s0} = 3.3$$

$$c_S(\omega) = -39.6p^6 + 10.8p^5 + 56p^4 - 4.13p^3 - 16.5p^2 - 2.45p + 1$$

$$Z_S(p) = \frac{4.5p^5 + 3.5p^4 + 5.5p^3 + 1.6p^2 + 0.5p}{56p^6 + 43p^5 + 90p^4 + 38p^3 + 27p^2 + 3p + 1}$$

and

$$a_{L0} = 11.1$$

$$c_L(\omega) = 27p^6 - 13.4p^5 - 9.9p^4 - 18.2p^3 - 20.5p^2 - 6.11p + 1$$

$$Z_L(p) = \frac{2.45p^5 + 6.5p^4 + 8.1p^3 + 5.2p^2 + 0.53p}{29.1p^6 + 77.3p^5 + 112p^4 + 103p^3 + 49p^2 + 8.8p + 1}$$

Real and imaginary parts of the RF-LST based, and the modelled source and load pull impedances are depicted in Figure 2.14 and Figure 2.15 respectively. The quality of match for RF-LST based and analytically modelled impedances of source and load pair is given in Figure 2.16.

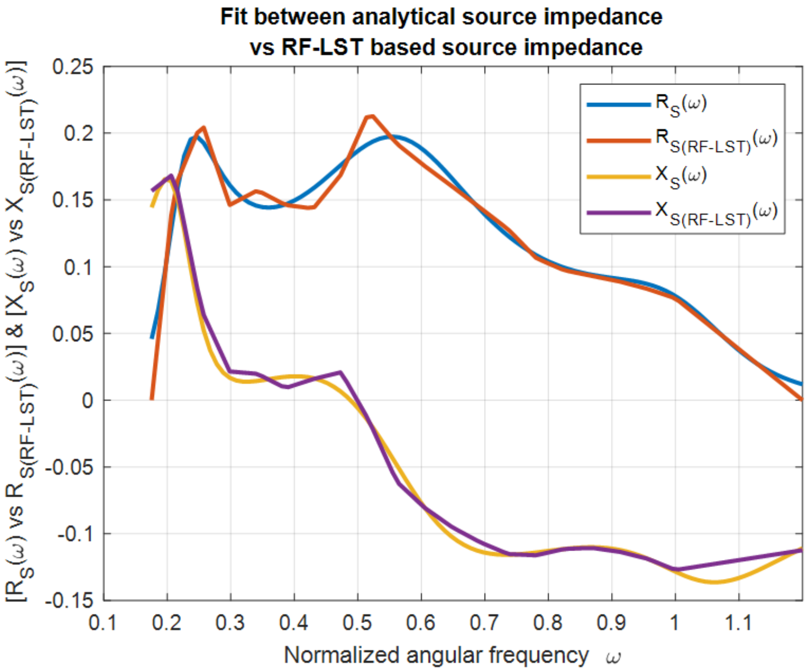

Figure 2.14 : Fit between the RF-LST based and the analytic form of the source impedances.

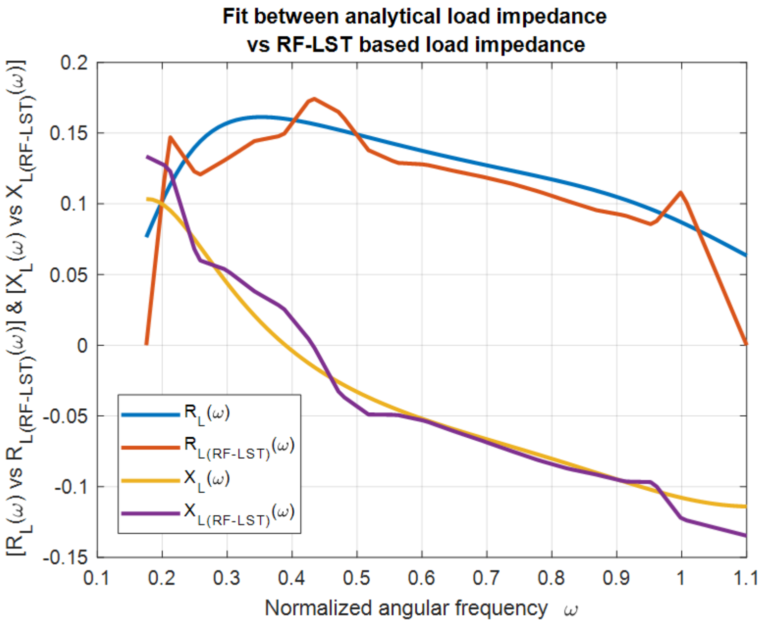

Figure 2.15 : Fit between the RF-LST based and the analytic form of the load impedances.

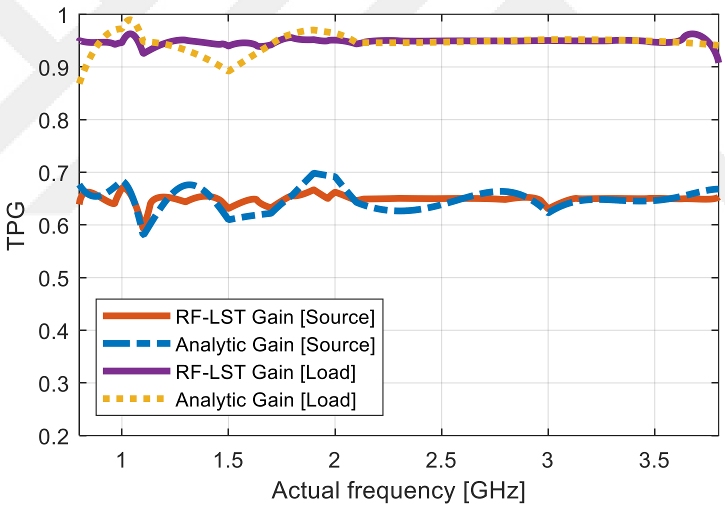

Figure 2.16 : Quality of fit comparison of RF-LST based and analytical impedance modelling.

Results obtained using RF-LST based GBWLs of Figure 2.8 and Figure 2.11 are compared with those TPGs of the IMN and IMN separately as shown in Figure 2.16. Close examination of this figure indicates that, analytic and RF-LST based TPGs are in good agreement with a less than 1% mean squared error (MSE) calculated for $N = 1000$ sample points over the passband such that

$$MSE = \frac{1}{N}\sum_{i=1}^{N}\left(TPG_{Analytic}(\omega_i) - TPG_{(RF-LST)}(\omega_i)\right)^2 \tag{2.14}$$

Using our high precision Darlington synthesis algorithm as applied on $Z_S(p)$ and $Z_L\,(p)$, IMN and OMN are constructed as shown in Figure 2.17 [54].

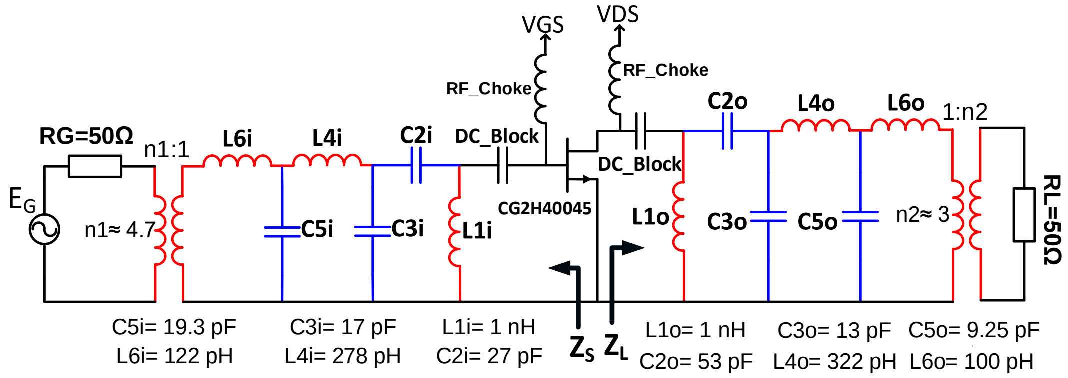

Figure 2.17 : Complete schematic of the power amplifier.

The above amplifier given in Figure 2.17 is simulated using the commercially available S/W tool ADS [72]. Biasing conditions are set as $V_{DS} = 28V; I_{DQ} = 800mA$. Constant RF input drive power $P_{in} = 36dBm$ is applied over the simulation frequency band. Resulting simulation performance is given in Figure 2.18. Close examination of Figure 2.18 reveals that, over the passband of 800 MHz-3.8 GHz, the average gain of the amplifier is TPG=11.38$dB \mp 0.75\ dB$, the average output power is $P_{out} = 47.38 \mp 0.75\ dBm$ and the average power added efficiency $PAE = 64.57 \mp 4.9$.

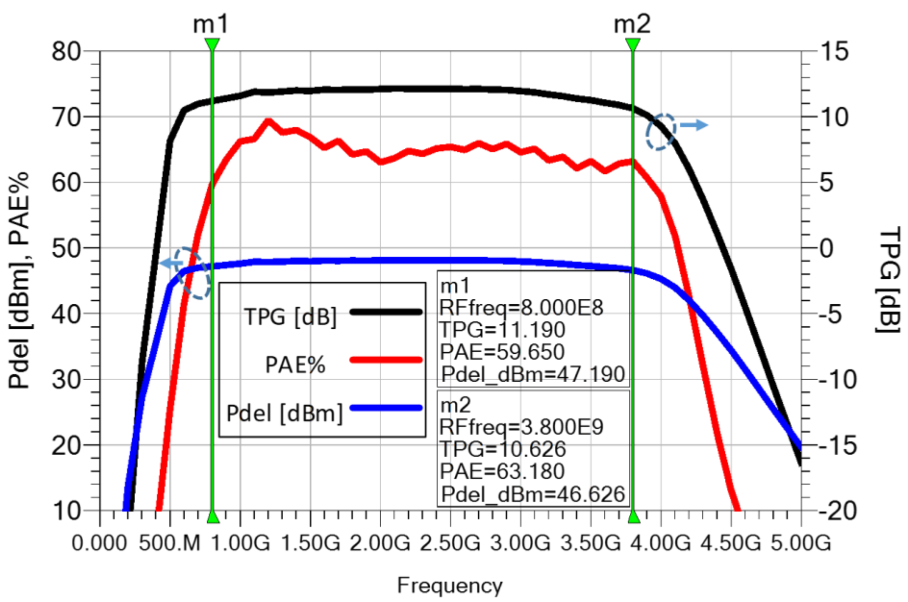

Figure 2.18 : Simulation results of the power amplifier.

2.9 Conclusion

An RF power amplifier design process starts with the characterization of the selected active device. The active device may be a GaN power transistor. In this regard, the source/load pull impedances of the active device are generated to optimize the power added efficiency (PAE) as well as the transducer power gain (TPG) of the amplifier over the frequency band of interest. Eventually, based on generated source/load pull impedances, the input and the output matching networks of the power amplifier is designed. At this point, it is crucial to note that for many practical situations, the source and the load pull impedances placed on the Smith Chart, do not necessarily belong to realizable positive functions (PRF) over the entire frequency band. In this case, one must check if these impedances are realizable. If not, it is well known that power intake and power delivery performances of the active device are penalized heavily. In this regard, the designer must evaluate the power transistor properly to decide whether it is worth using it or not. Therefore, in this chapter, first, we introduced a novel numerical method to test the given source and load pull impedances if they are realizable to construct the input and the output matching networks. Then, we introduce a new numerical method to assess the "Gain-Bandwidth Limitations (GBWL)" of the given source and load pull impedances employing the real frequency line segment technique (RF-LST), which in turn results in the best-optimum and realizable source $Z_{S(RF-LST)}$ and load $Z_{L(RF-LST)}$ impedance terminations point by point. In this context, gain bandwidth limitations of the given source and load pull impedances reveal the power-intake and the power delivery capacity of the selected active device respectively. The proposed numerical assessment method utilizes our newly developed robust "virtual gain optimization" tool called VGO. VGO minimizes a convex error function by targeting its global minimum, which in turn yields the optimum-realizable source and load terminations of the nonlinear active device under consideration. Thus, ultimate power intake and power delivery capacity of the nonlinear active device is determined. Finally, a new definition is introduced to measure the power-intake and power delivery quality of an active device, so called "Power-Performance-Product (in short PPP or 3P) based on the (GBWL) of the given source/load pull impedances.

Employing Wolfspeed's CG2H40045 GaN transistor, we exhibit the implementation of the proposed immittance realizability test procedure step by step and the design of an "optimum performance power amplifier algorithm" using the real frequency line segment technique over $0.8\text{GHz} - 3.8\text{GHz}$ bandwidth which ideally receives average of 65.07% of the available power of the resistive input excitation and delivers the 94.78% of the transistor's output power to a resistive load.

Eventually, $Z_{S(RF-LST)}$ and $Z_{L(RF-LST)}$ are modelled as analytic PRFs. Then, they are synthesized as the input matching network (IMN) and the output matching network (OMN) to construct the power amplifier. It is exhibited that, analytic and RF-LST based transducer power gains of IMN and OMN are in good agreement with less than 1% mean squared error. Thus, correctness of the RF-LST based solutions are verified.

3. A GAN MICROWAVE POWER AMPLIFIER DESIGN BASED ON THE SOURCE/LOAD PULL IMPEDANCE MODELLING VIA VIRTUAL GAIN OPTIMIZATION[1]

3.1 Introduction

Generation of proper source/load pull impedances for a selected GaN device is essential to design a microwave power amplifier for optimum gain and power-added efficiency. As they are obtained, these impedances may not be realizable network functions over the desired frequency band. Therefore, in this chapter, first we applied our newly proposed realizability test method for the SP and LP imedances of a 10W-GaN power transistor, namely “Wolfspeed CGH40010F” over 0.8-3.0 GHz bandwidth [44, 45]. Then, SP and LP impedances are modelled as realizable network functions, which in turn results in the optimum power intake and power delivering capacity for the GaN transistor used in the design. In the numerical modelling process, the robust tool called “Virtual Gain Optimization” is used. Numerically generated realizable source and load impedances are modelled analytically. Then, these impedances are synthesized using our automatic Darlington Synthesis Robot software to yield the optimum input and output matching network topologies with component values. Eventually, the power amplifier is designed and manufactured. It is shown that the computed and the measured performance of the amplifier is very close with 10 Watts output power, 11.4±0.6 dB gain and 49% to 76 % power added efficiency.

For the sake of brevity,we do not repeat the detailed theoritical aspects of this chapter since they have been already presented in the previous chapter (Chapter 2).

Therefore, in the following section, examples are given to test if a measured arbitrary immittance data and the source/load pull impedances obtained from the Wolfspeed’s CGH40010F GaN power transistor, represent positive real functions (Section 3.2). In

[1] This chapter is based on the paper "Kilinc, S., Yarman, BS., and Ozoguz, S. (2022). "A GaN Microwave Power Amplifier Design Based on the Source/Load Pull Impedance Modeling via Virtual Gain Optimization," in IEEE Access, vol. 10, pp. 50677-50691, doi: 10.1109/ACCESS.2022.3174227".

section 3.3 and in Section 3.4, we specifically investigated the power intake/power delivery performance of the source and the load pull impedance data belongs to CGH40010F over 0.8-3GHz using the “Real Frequency-Line Segment Technique (RF-LST)” [63, 64, 73, 74]. During the numerical performance assessments process, we implemented the original tool called “Virtual Gain Optimization (VGO)”. In Section 3.5, we introduce a new method to generate an analytic model for the given realizable immittance data. For the sake of completeness, in Section 3.6, the parametric method to build analytic positive real functions is summarized. In Section 3.7, the proposed analytic model technique is employed to build the rational impedance forms for the optimum source and load pull data obtained via RF-LST. In Section 3.8, the designed and constructed power amplifier is presented. Finally, the chapter is concluded in Section 3.9.

3.2 Assesment of the Realizibility of the Source and the Load Pull Impedances Obtained from a GaN Power Transistor

In this section, we investigate the positive realness of the measured optimum source and load-pull impedance data extracted from a *GaN* power transistor. The selected transistor is a, *CGH40010F* from *Wolfspeed* Company with nominal 10 Watts output power [45]. As reported in [45], optimum source and load-pull impedance plots are shown in Figure 3.1 (Black Plots: Source Pull Impedance, Red Plots: Load Pull Impedance respectively).

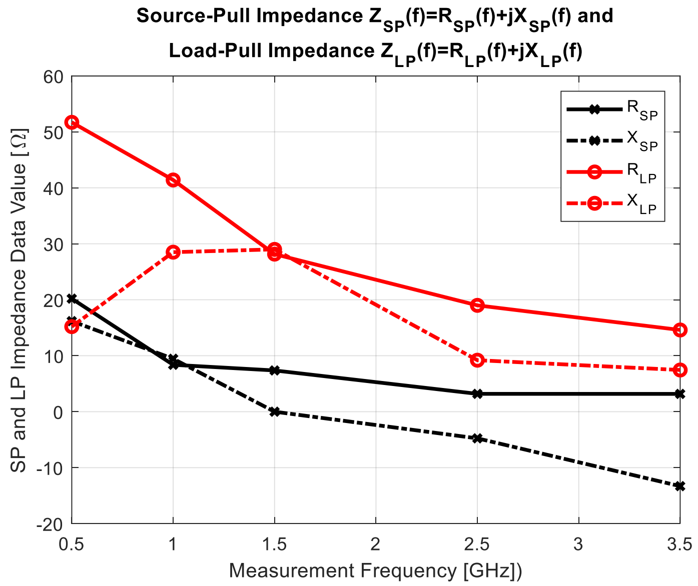

Figure 3.1 : Optimum source-pull and load-pull termination impedances.

As described in the previous chapter, we extrapolated the given data to cover the frequencies $F1a = 0\ (DC)$ and $FNa = 4\ GHz$. At DC, we select $RSP(1) = 25\Omega$ and $XSP(1) = 0$. At 4 GHz, $RSP(N) = 0$ and $XSP(N) = -13.6\Omega$ are selected. Similarly, load-pull impedance data is augmented as $RLP(1) = 61\Omega$, $RLP(N) = 0\Omega$ and $XLP(1) = 0$, $XLP(N) = 11\Omega$.

Utilizing the proposed Algorithm, we extracted the Foster reactance functions for both Source-Pull (SP) and Load-Pull (LP) impedances. Results are depicted in Figure 3.2.

Close examination of Figure 3.2a reveals that, up to 500 MHz, the extracted Foster reactance $X_{FSP}(\omega)$ is monotonically increasing (SP: Purple Plot). Then, it drastically falls. In this case, $X_{FSP}(\omega)$ behaves like a proper Foster reactance from DC to $500\ MHz$. In other words, it is possible to model the given immittance data from DC to 500MHz with an analytic positive real function which yields an exact fit (Perfect Match). Then, the data is no longer Foster function. On the other hand, computed Foster portion X_{FLP} of the measured load pull impedance is good from DC up to 1.3 GHz (Band-1). Between 1.3GHz and 2.8GHz (Band-2) it decreases. Therefore, the Band-2 region is no good; indicating that, one sacrifices gain and/or power added efficiency in this band. After 2.8GHz to 4GHz (Band-3), XF_{LP} increases monotonically. Thus, we say that measured load pull impedance data behaves like a proper positive real function in Band-1 and Band-3 which leads to perfect power delivery performance.

So far, what we have observed that, due to nonlinear behavior of the GaN transistor Wolfspeed CGH40010F, reported source and load-pull impedances are not realizable network functions over the frequency bands indicated above, even though they present positive real parts. However, they can be fitted to realizable network functions as much as possible, to construct the optimum front-end (input) and back-end (output) matching networks of the power amplifier by sacrificing the idealized gain and power added efficiency. This process leads us to the gain-bandwidth limitation of the active device under consideration.

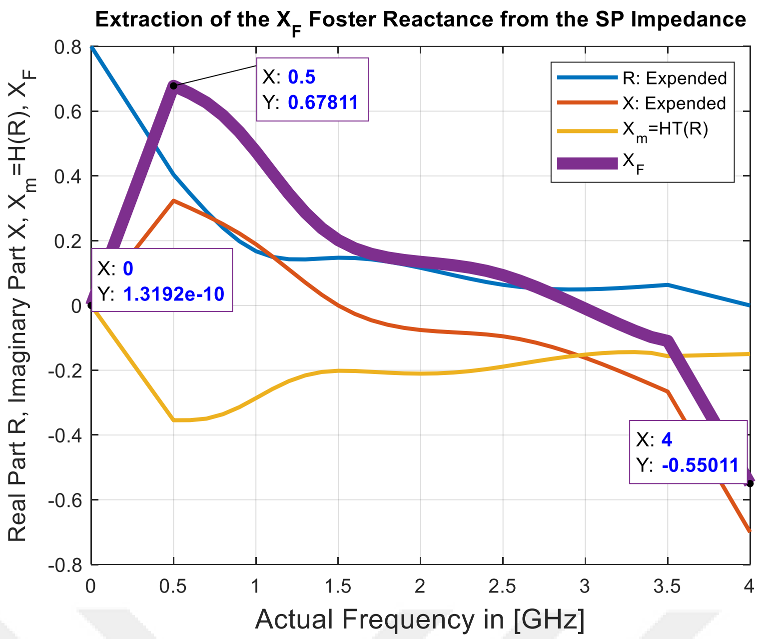

(a) Foster Part of the source pull impedance data.

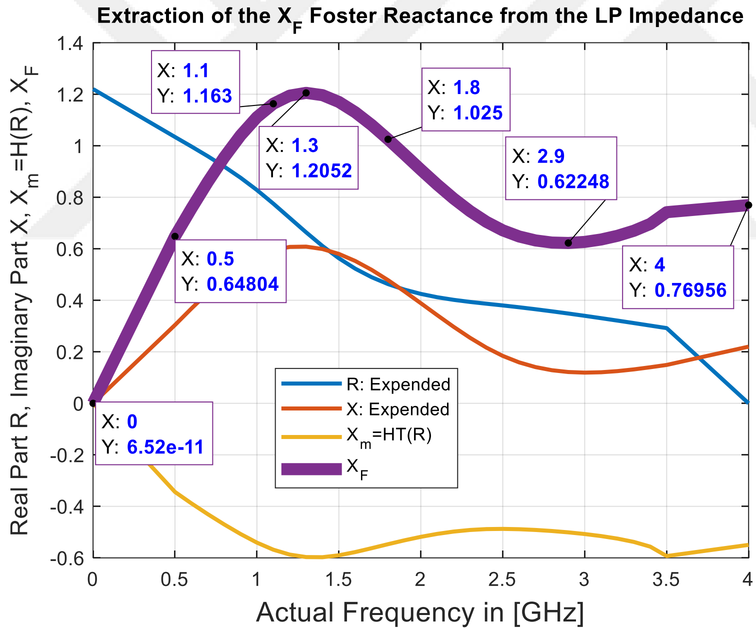

(b) Foster Part of the load pull impedance data.

Figure 3.2 : Extraction of the Foster Reactance from the source/load-pull impedances.

Now, let us implement the above minimization process to predict the power intake and power delivery performance of the source and the load pull impedances for the *Wolfspeed CGH40010F* power transistor employing the real frequency line segment technique (RF-LST).

3.3 The Power Intake Performance of a GaN Device

In this section, we will investigate the "power-intake" capability of the *Wolfspeed CGH40010F GaN* transistor at its input [45]. Transistor is driven by a resistive generator of $R_0 = 50\ Ohm$. The given source-pull impedance is approximated as the driving-point back-end impedance of a lossless two-port [E] when it is terminated in the complex-conjugate of the given source pull immittance as in Figure 3.1. In this regard, it is desired to determine the gain-bandwidth limitation of the given source-pull impedance as detailed in the above section. The given/augmented and the normalized source-pull impedances are depicted in Figure 3.2a. User defined passband is specified over $f_{C1} = 800MHz$ and $f_{c2} = 3.0\ GHz$. In this case, we select the normalizing frequency F_0 at 3.0 GHz. The real part of the given source-pull impedance is augmented at DC (i.e., $f = 0$) as $RSA(1) = 25\Omega$ and $RSA(N) = 0\Omega$. Similarly, the given imaginary part XSA is augmented as $XSA(1) = 0$ at DC $(i.e. ws1 = 0)$ and the end point is augmented at 4 GHz as $XSA(N) = -13.6\Omega$.

The GBWL of the virtual matching problem is numerically assessed via RF-LST employing the Algorithm 2.2 step by step in MatLab [70]. Inputs to the main program are summarized as follows.

$\omega_{C1} = \frac{0.8}{F0} = 0.2667$; $\omega_{C2} = \frac{3\ GHz}{F0} = 1$; $\omega_{s1} = 0$; $\omega_{s2} = \frac{4}{F0} = 1.333$. We have selected $N = 21$ break points with 19 unknowns. In the optimization process, we prefer to work with impedances. $RB1 = 0$ is fixed at DC, since we deal with a bandpass single matching problem. Flat gain levels are swept between 0.6 and 1.0 with $\delta T = 0.05$ incremental steps. Therefore, we define the total number of 9 flat gain levels. Eventually, we start the optimization with low initials by selecting $\mu = -1$.

Results of the sequential optimization of TPG are summarized as in Table 3.1 and depicted as in Figure 3.3. The best performance appears for max $(T_{min}) = 0.8212$ or equivalently, $T_{mean} = 0.8745 \mp 0.0532$. Optimized break points R_{QLST-S} and its corresponding Hilbert Transform X_{QLST-S} are depicted in Figure 3.4a and Figure 3.4b respectively as compared with the manufacturer's published source pull data.

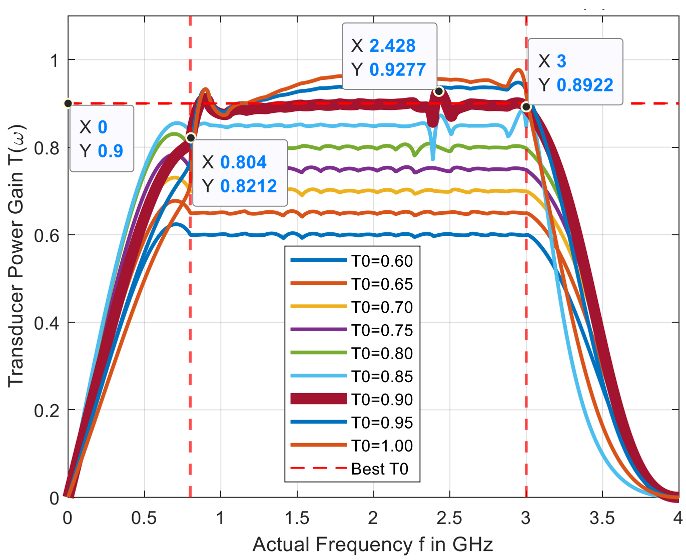

Figure 3.3 : Power-intake performance of the GaN device obtained by sweeping $T_0(k)$.

Table 3.1 : Power-intake performance of the CGH40010F power transistor.

$T_0(k)$	T_{mean}	$F_{max}[GHz]$	T_{max}	$F_{min}[GHz]$	T_{min}	ΔT
0.6000	0.5980	1.4720	0.6035	1.4080	0.5925	0.0055
0.6500	0.6476	1.4640	0.6539	1.5320	0.6412	0.0064
0.7000	0.6970	1.4560	0.7040	1.5320	0.6900	0.0070
0.7500	0.7483	2.2160	0.7546	2.2720	0.7420	0.0063
0.8000	0.7945	2.3640	0.8082	2.2680	0.7807	0.0137
0.8500	0.8280	2.9720	0.8841	2.3880	0.7719	0.0561
0.9000	0.8745	2.4280	0.9277	0.8040	0.8212	0.0532
0.9500	0.8656	2.9480	0.9477	0.8040	0.7835	0.0821
1.0000	0.8559	2.9480	0.9768	0.8040	0.7350	0.1209

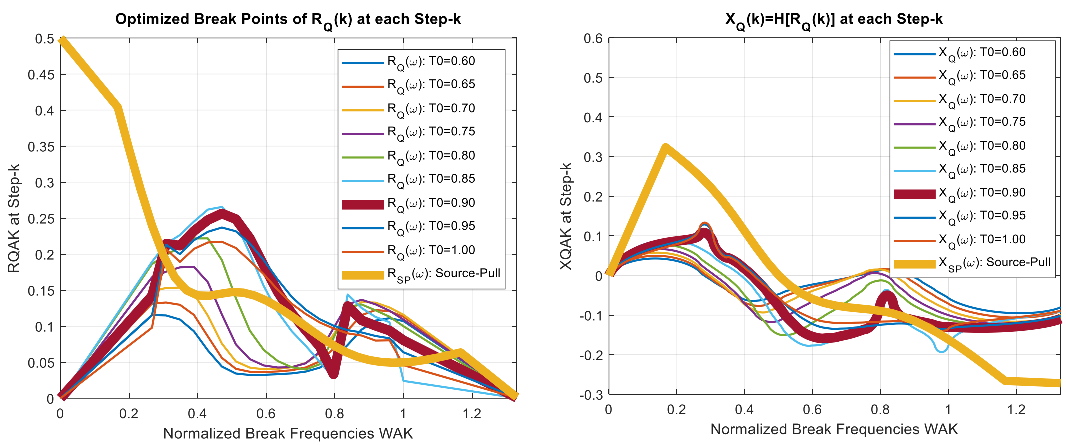

(a) RFLTS based $R_{QA}(\omega)$ and original $R_{SP}(\omega)$.

(b) RFLTS based $X_{QA}(\omega) = H\{R_{QA}(\omega)\}$ and original $X_{SP}(\omega)$.

Figure 3.4 : Real and imaginary parts of the RF-LST based and original SP impedance.

Referring to Table 3.1 and Figure 3.3, it is predicted that 87.45% of the available power of the generator is transferable to the input of the power transistor $CGH40010$F with optimum fluctuation of $\Delta T = \mp 0.0532$ in least mean square sense. Let us now investigate the output power delivery performance of the same transistor using the load-pull measured impedance data in the following section.

3.4 The Power Delivery Performance of a GaN Device

In this section, we will investigate the power delivering capability of the $Wolfspeed\ CGH40010F\ \ GaN$ transistor at its output-port [45]. Here, we assumed that the transistor is terminated in its modelled-realizable optimum load-pull impedance over the output matching network (OMN) while the other end of OMN is terminated in $R0 = 50\Omega$. The measured load-pull impedance is approximated as the driving-point backend impedance of a lossless two-port [E] when it is terminated in the complex-conjugate of the load pull immittance as in Figure 3.2b.

In the performance assessment computations, user defined passband is selected as before with $F_0 = 3.0\ GHz$. The real part of the measured load-pull impedance is augmented at DC (i.e., $f = 0$) as $RLPA(1) = 61\Omega$ and $RLPA(N) = 0\Omega$. Similarly, the measured imaginary part $XLPA$ is augmented as $XLPA(1) = 0$ at DC $(i.e. ws1 = 0)$ and the end point is augmented at 6GHz as $XLPA(N) = +11\Omega$ $(i.e., ws2 = 4/F0 = 1.333)$.

Execution of our MatLab program results in the RF-LST based Gain Bandwidth Limitation of the load-pull impedance. Results of the sequential optimization of TPG are summarized as in Table 3.2 and depicted as in Figure 3.5. The best performance appears for $\max(T_{min}) = 0.7532$ or equivalently, $T_{mean} = 0.7883 \mp 0.0351$. Optimized break points R_{QLST-L} and its corresponding Hilbert Transform X_{QLST-L} are depicted in Figure 3.6a and Figure 3.6b respectively as compared with the manufacturer's published load-pull impedance data.

Referring to Table 3.2 and Figure 3.5, it is predicted that 78.83% of the output power is delivered to the load pull impedance of the power transistor $CGH40010$. In other words, power delivery performance of the optimum realizable load pull impedance is $T_{mean} = 0.7883$ with corresponding fluctuation of $\Delta T = \mp 0.0351$.

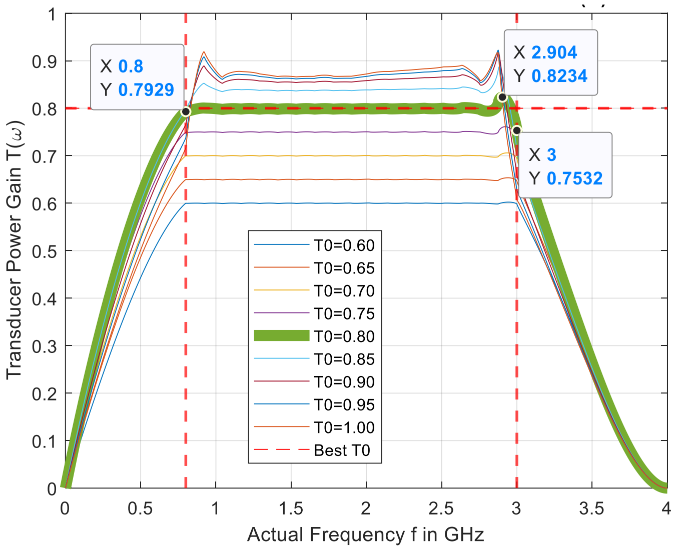

Figure 3.5 : Power-delivery performance of the GaN device obtained by sweeping $T_0(k)$.

Table 3.2 : Power-delivery performance of the CGH40010F power transistor.

$T_0(k)$	T_{mean}	$F_{max}[GHz]$	T_{max}	$F_{min}[GHz]$	T_{min}	ΔT
0.6000	0.6003	2.9440	0.6023	3.0000	0.5983	0.0020
0.6500	0.6503	2.9400	0.6536	3.0000	0.6470	0.0033
0.7000	0.7000	2.9360	0.7060	3.0000	0.6940	0.0060
0.7500	0.7483	2.9240	0.7612	3.0000	0.7354	0.0129
0.8000	0.7883	2.9040	0.8234	3.0000	0.7532	0.0351
0.8500	0.7995	2.8840	0.8871	3.0000	0.7119	0.0876
0.9000	0.7883	2.8800	0.9176	3.0000	0.6590	0.1293
0.9500	0.7747	2.8760	0.9225	3.0000	0.6269	0.1478
1.0000	0.7631	0.9200	0.9191	3.0000	0.6071	0.1560

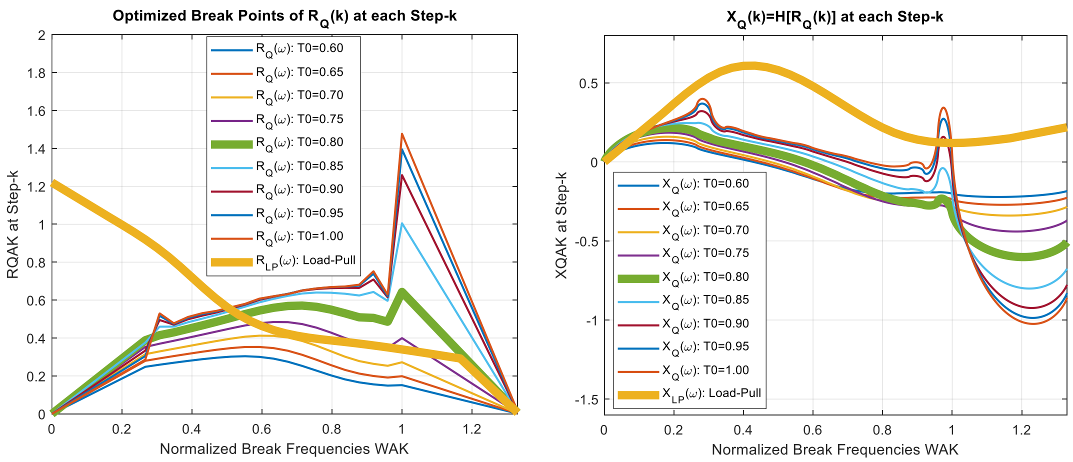

(a) RFLTS based $R_{QA}(\omega)$ and original $R_{LP}(\omega)$.

(b) RFLTS based $X_{QA}(\omega) = H\{R_{QA}(\omega)\}$ and original $X_{LP}(\omega)$.

Figure 3.6 : Real and imaginary parts of the RF-LST based and original LP impedance.

3.5 Generation of an Analytic Model for the Given Immittance Data

In the previous sections, power-intake and power delivery performance of the optimum-realizable source and load-pull immittances are determined using the real frequency-line segment technique (RF-LST). The follow-up step should be to build the best analytic immittance models for the RF-LST based terminations so that the input and the output matching networks are constructed. In this regard, the VGO method is adopted to build the analytic model for the given minimum immittance data. Referring to Figure 3.7, the load termination $K_{LA}(j\omega) = R_{LA}(\omega) + jX_{LA}(\omega)$ is described as the complex conjugate of the minimum immittance data $KA(j\omega) = RA(\omega) + jXA(\omega)$ such that

$$R_{LA}(\omega) = RA(\omega) \tag{3.1a}$$

$$X_{LA}(\omega) = -XA(\omega) \tag{3.1b}$$

Thus, the transducer power gain is given by

$$T(\omega) = \frac{4R(\omega)RA(\omega)}{[R(\omega) + RA(\omega)]^2 + [X(\omega) - XA(\omega)]^2} \tag{3.2}$$

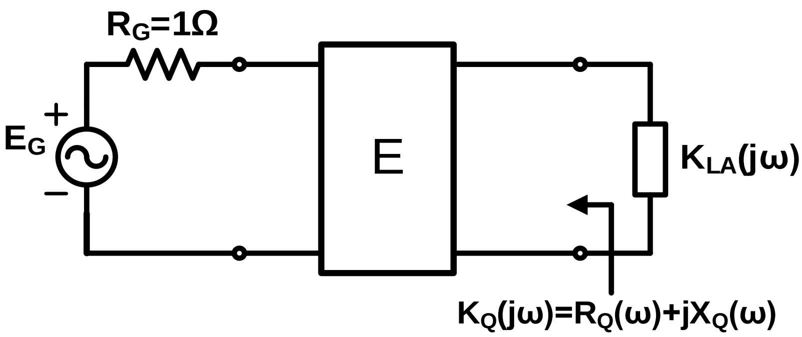

Figure 3.7 : A virtual single matching problem to model a measured immittance data $K(j\omega)$ by setting $K_{LA} = Z^*$.

In (3.2), the realizable-rational real part function $R(\omega) = R(p^2)|_{p^2=-\omega^2}$ is described in terms of an auxiliary polynomial $c(\omega) = c_1\omega^n + c_2\omega^{n-1} + \cdots + c_n\omega + 1$ such that

$$R(\omega^2) = \frac{a_0^2(-1)^{ndc}\omega^{2ndc}\prod_{i=1}^{nr}(\sigma_i^2 + \omega^2)^2\prod_{j=1}^{nz}(\omega_i^2 - \omega^2)^2}{B(\omega^2)} \tag{3.3a}$$

where

$$B(\omega^2) = \frac{1}{2}\left[c^2(\omega) + c^2(-\omega)\right] > 0;\ \forall\omega \tag{3.3b}$$

In the above formulations, n is the degree of the auxiliary polynomial which corresponds to the total number of the reactive components in the matching network when the modelled immittance is synthesized as a lossless two-port in Darlington sense. The integer ndc is the count for the total number of transmission zeros at DC. The symbol σ_i is a positive real number referring to Right Half Plane (RHP) transmission zeros. The symbol ω_i designates the finite transmission zeros on the frequency axis $j\omega$ as it comes with its complex conjugate pair. From the programming point of view, all the RHP zeros and finite frequency transmission zeros may be collected under vectors $S = [\sigma_1, \sigma_2, \cdots, \sigma_{nr}]$ and $W = [\omega_1, \omega_2, \cdots, \omega_{nz}]$ respectively. It should be emphasized that a for typical matching network, all the transmission zeros are selected by the designer as the input to the VGO program since they impose the topological structure of the matching network. In this regard, unknowns of the virtual gain optimization are selected as the real coefficients $\{c_1, c_2, c_3, \dots, c_n\}$. The real constant a_0 may as well be included among the unknowns. Once a_0 and $\{c_1, c_2, c_3, \dots, c_n\}$ are initialized, the analytic form of the minimum immittance $K(p) = \frac{a(p)}{b(p)}$ is generated using the parametric approach [63, 71, 73, 75, 76]. Eventually, for a selected constant flat gain level T_0, the error function

$$\begin{aligned}\varepsilon(\omega, c_1, c_2, c_3, \dots, c_n, a_0) &= T(\omega) - T_0 \\ &= \frac{4R(\omega)RA(\omega)}{[R(\omega) + RA(\omega)]^2 + [X(\omega) - XA(\omega)]^2} - T_0\end{aligned} \tag{3.4}$$

is minimized over the passband. In (3.4), T_0 may be set to unity since a good fit between the pairs $\{R(\omega), X(\omega)\}$ and $\{RA(\omega), XA(\omega)\}$ is sought. For the sake of completeness, let us summarize the parametric approach to construct a positive real immittance function $K(p)$ from its even part $R(\omega)$ as specified by (3.3).

3.6 A Parametric Method to Build a Positive Real Minimum Function $\boldsymbol{K(p)}$ from Its Even Part $\boldsymbol{R(p^2)}$

In this method, a minimum positive function $K(p)$ is expressed in terms of its LHP poles p_i as follows [63, 71, 73, 75, 76].

$$K(p) = \frac{a(p)}{b(p)} = R_\infty + \sum_{j=1}^{n} \frac{k_j}{p - p_j} \tag{3.5a}$$

The above form is called the parametric representation of a minimum positive real function $K(p)$.

Similarly, even part $R(p^2)$ of $K(p)$ is also expressed in parametric form as

$$R(p^2) = \frac{1}{2}[K(p) + K(-p)] = R_\infty + \sum_{j=1}^{n} \frac{k_j p_j}{p^2 - p_j^2} \tag{3.5b}$$

where the residues are given by

$$k_j = \left(p^2 - p_j^2\right)\frac{R\left(p_j^2\right)}{p_j} = \frac{A(p_j^2)}{\left(p_j\right)(-1)^n(c_1^2)\prod_{\substack{i=1 \\ i\neq j}}^{n}(p^2 - p_i^2)} \tag{3.5c}$$

$$R_\infty = \lim_{p\to\infty} R(p^2) \tag{3.5d}$$

Once the transmission zeros are selected, the arbitrary real coefficients $\{c_i; i = 1,2,..,n\}$ and a_0 are initialized, then even denominator polynomial $B(\omega^2)$ of (3.3a) are computed as

$$\begin{aligned} B(\omega^2) &= \frac{1}{2}[c^2(\omega) + c^2(-\omega)] \\ &= B_1\omega^{2n} + B_2\omega^{2(n-1)} + \cdots + B_n\omega^2 + 1 > 0\ \forall\omega \end{aligned} \tag{3.5e}$$

Afterwards, $B(p^2)$ is generated replacing ω^2 by $-p^2$. At this point, mirror-image symmetric roots of $B(p^2)$ are computed. For example, on MatLab, the command $x = roots(B)$ returns all the roots of the denominator polynomial $B(x)$ with $x = p_i^2$. Then, we set $p_i = \mp\sqrt{x}$. Let the roots of $B(p^2)$ are designated by $p = \mp p_i$; $i = 1,2,\ldots,n$. Selecting LHP roots p_j of $B(p^2)$, denominator polynomial $b(p)$ of $Z(p) = \frac{a(p)}{b(p)}$ is constructed as

$$b(p) = |c_1|\prod_{j=1}^{n}(p + p_j) \tag{3.5f}$$

Using (3.5c) and (3.5d), the residues k_j and R_∞ are computed. Then, $K(p)$ is generated as in (3.5a). Finally, its rational form is determined by algebraic manipulations to end up with the rational form of $K(p) = a(p)/b(p)$. In (3.5f), $b(p)$ is a strictly Hurwitz real polynomial. Therefore, complex roots of $b(p)$, which are specified by $p_j = -\sigma_j + j\omega_j$; $\sigma_j > 0$, must be accompanied with its complex conjugate pairs such that $p_{j+1} = -\sigma_j - j\omega_j$; $j = 1,2, \dots, n$. Thus, once the transmission zeros are selected (i.e. ndc, $W = [\omega_1, \omega_2, \cdots, \omega_{nz}]$ and $S = [\sigma_1, \sigma_2, \cdots, \sigma_{nr}]$) and the coefficients a_0 and $\{c_1, c_2, c_3, \dots, c_n\}$ of the auxiliary polynomial is initialized, minimum function $K(p) = a(p)/b(p)$ is generated employing (16). Hence, minimization of the error function of (3.4) results in the analytic form of $K(p) = \frac{a(p)}{b(p)} = \frac{a_1 p^n + a_2 p^{n-1} + a_3 p^{n-2} + \cdots + a_n p + a_{n+1}}{b_1 p^n + b_2 p^{n-1} + b_3 p^{n-2} + \cdots + b_n p + 1}$ as in (3.5). It is noted that in our computations, we take $a_1 = 0$ since $\lim_{p \to \infty} R(p) = 0$ is assumed. Furthermore, in MatLab computations, a polynomial $a(p)$ of degree n is defined as a vector $a = [a_1 \; a_2 \dots a_{n+1}]$ of n+1 tuples.

Eventually, $K(p) = \frac{a(p)}{b(p)}$ is synthesized as a lossless two-port in Darlington sense. If $K(p)$ refers to the source/load pull immittance, the lossless two-port will be the input/output matching network. Optimization and Synthesis are implemented under MatLab environment in a similar manner to that of [50-54].

3.7 Analytic Models for the RF-LST Based Source and Load Impedances

In Section 3.3 and 3.4, Power-Intake and Power-Delivery Performance of the device is obtained over the given source/load pull impedance data. In this section, we build practical analytic models for both source and load pull impedances as follows.

3.7.1 Source-pull impedance model

RF-LST based optimum source impedance data is shown in Figure 3.4 as red plot. Employing the modelling method introduced above, we obtained the realizable analytic form for the optimum source impedance $Z_{QA-SP}(p) = a(p)/b(p)$ as specified in Table 3.3 for $n = 5$ and $ndc = 1$ (a single transmission zero at dc). Data fit between the analytic impedance and the RF-LST based source impedance is depicted in Figure 3.8. In this regard, quality of the curve fitting (QF) may be evaluated by means of the virtual transducer power gain (VTPG). For example, VTPG=1 corresponds to exact fit at the given points over the passband. Otherwise, trace of the analytic function will deviate from the original RF-LST points. VTPG of the IMN is depicted in Figure 3.9 with the black curve. Close examination of this figure reveals that quality of match is about 95% but it drops down to 85% in the vicinity of the normalized frequency $\omega = 0.8$. The analytic form of $Z_{QA-SP}(p) = a(p)/b(p)$ is synthesized as in Figure 3.10.

Table 3.3 : Optimized analytic impedance function for SP model.

Optimized analytic impedance function $Z_{QA-S}(p) = a(p)/b(p)$ which best fits the RF-LST based SP impedance $Z_{QLST-S}(j\omega) = R_{QLST-S}(\omega) + jX_{QLST-S}(\omega)$.	
For $Nc = 5; ndc = 1$:	
a_{0G}	2.1208
$c(\omega)$	$[-16.2278 \quad 1.5185 \quad 21.6723 \quad 4.1441 \quad -2.3591]$
$a(p)$	$[0 \quad 1.5239 \quad 1.6028 \quad 2.1996 \quad 0.9545 \quad 0]$
$b(p)$	$[16.2278 \quad 17.0679 \quad 30.5770 \quad 17.6893 \quad 7.0166 \quad 1.0000]$
For $Nc = 8; ndc = 2$:	
a_{0G}	2.3455
$c(\omega)$	$[15.86 \quad -69.77 \quad -38.85 \quad 78.31 \quad 28.50 \quad -12.57 \quad -13.86 \quad -1.02]$
$a(p)$	$[0 \quad 1.2083 \quad 6.4653 \quad 8.1143 \quad 8.7234 \quad 5.7561 \quad 1.9264 \quad 0.3930 \quad 0]$
$b(p)$	$[15.86 \quad 84.84 \quad 112.32 \quad 145.75 \quad 113.51 \quad 60.67 \quad 25.35 \quad 4.90 \quad 1.00]$

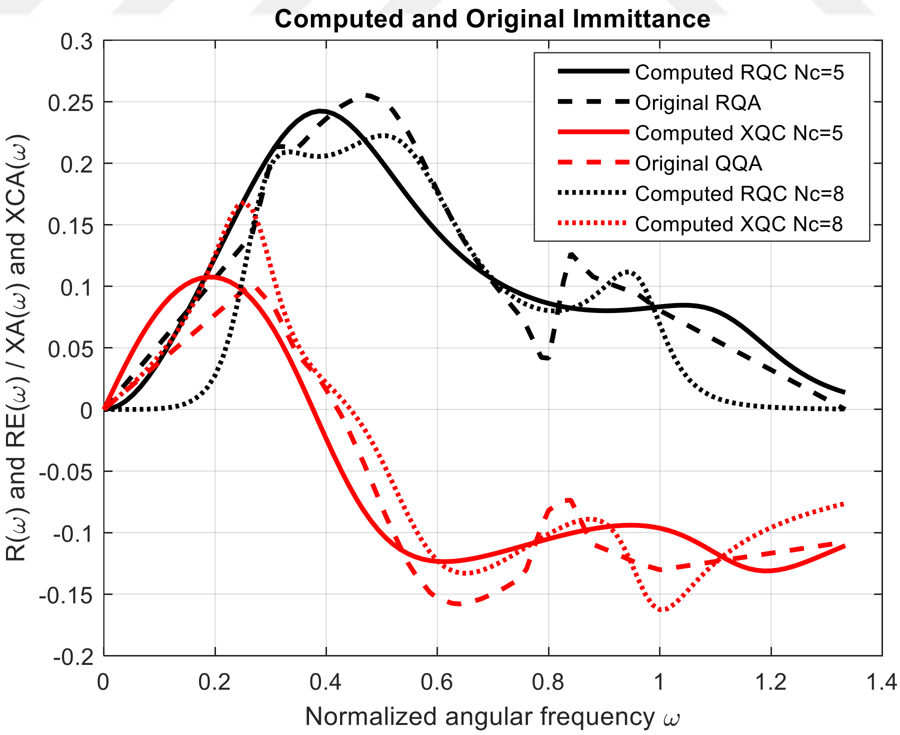

Figure 3.8 : Fit between the modeled and RF-LST based source impedance real and imaginary parts.

Synthesis is completed using our “high-precision Darlington synthesis (HPDS) methods” presented in [50-54]. In HPDS, driving point input immittance is corrected after each transmission zero extraction. In this way, one can synthsize a lossless matching network with more than 30 reactive elements with relative error less than 10^{-4} as reported in [30-34]. The alternative sysnthesis could be to use Darlington Synthesis in a straight forward manner without immittance correction. In this way, sythesis is halted after a few steps due to overflow/underflow errors occour during the computations. Another high precision synthesis method is reported in [77], which utilized the correction on the Feldkeller condtion after each transmission zeros extranction. However, this work is only good for lowpas LC ladder synthesis, and the resulting computational precion is similar to that of [30-34] upto 10 elements.

It should be mentioned that QF may be improved by increasing the total number of elements in the matching networks. For example, In Table 3.3, we present the results of VTPG optimization for $ndc = 2$, $Nc = 8$ case. Corresponding VTPG is also depicted in Figure 3.9 with blue dashed plot. As it is seen from Figure 3.9, quality of fit is slightly improved with sharpened edges. Nevertheless, for the sake of simplicity, we have selected the “5 element IMN” to construct PA.

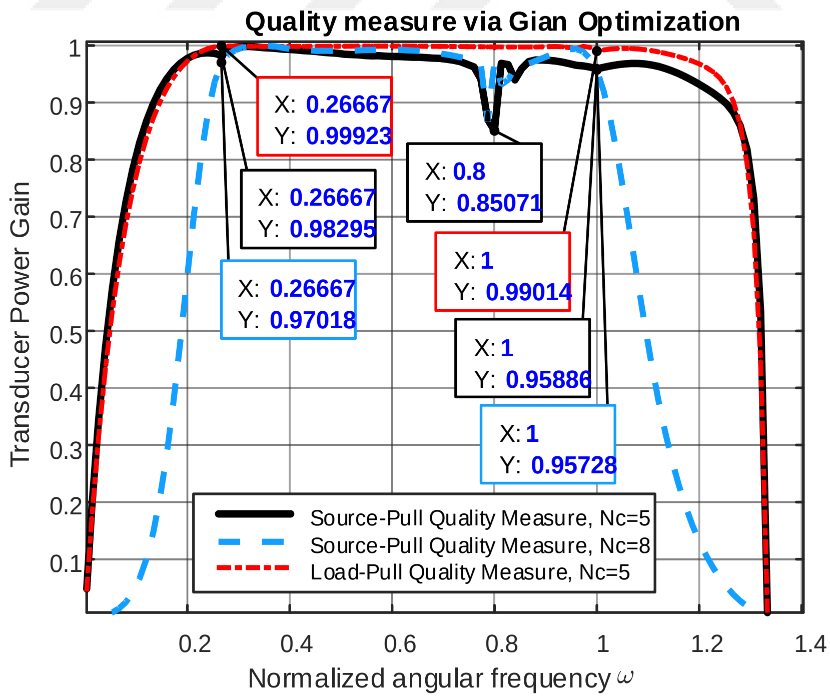

Figure 3.9 : Quality measure for the fit between optimum and modeled impedances via VGO algorithm.

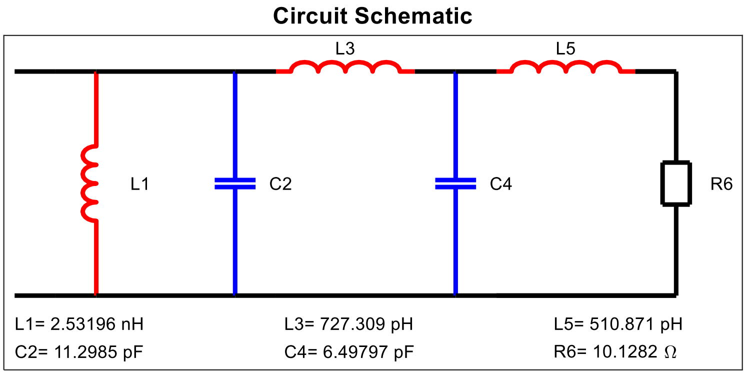

(a) 5 element network with ndc=1.

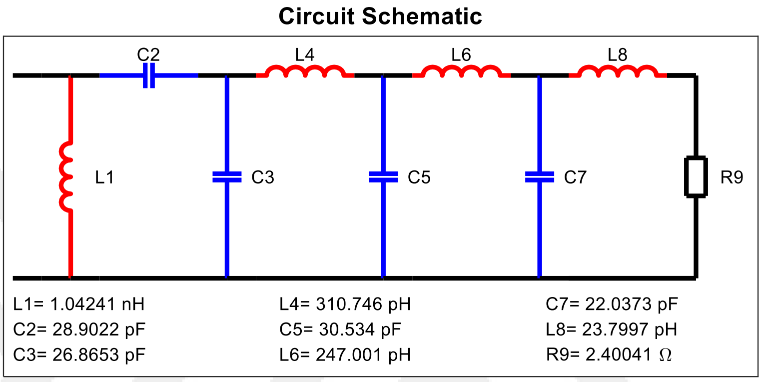

(b) 8 element network with ndc=2.

Figure 3.10 : Synthesized networks by modeling the RF-LST based source impedance.

3.7.2 Load-pull impedance model

In Figure 3.6, RF-LST based load-pull impedance data is depicted (green plot). Utilizing the analytic virtual modeling method, we end up with the positive-real function form for the load-pull impedance as listed by Table 3.4 for $ndc = 1$ and $n = 5$. The fit between the analytic form and the break points are shown in Figure 3.11. Quality of fit (QF) is depicted in Figure 3.9 with the red-dotted curve. Here in this case, QF is better than 99% over the entire frequency band. Hence, synthesis of $Z_{QA-LP}(p) = a(p)/b(p)$ is shown in Figure 3.12.

Note that, it is possible to build an exact model for the RF-LST based immittance data yielding perfect match employing the linear interpolation method of positive real functions [78]. However, this method unnecessarily complicates the matching network topology with total number of $2(N-1)$ components. In this representation, integer N refers to the count of sampling points as in Figure 2.2.

Table 3.4 : Optimized analytic impedance function for LP model.

Optimized analytic impedance function $Z_{QA-L}(p) = a(p)/b(p)$ which best fits the RF-LST based LP impedance $Z_{QLST-L}(j\omega) = R_{QLST-L}(\omega) + jX_{QLST-L}(\omega)$.	
For $Nc = 5$; $ndc = 1$	
a_{0L}	4.0827
$c(\omega)$	[3.7719 0.9181 − 0.6221 3.5809 − 4.2652]
$a(p)$	[0 1.3928 3.9380 4.7844 2.8723 0]
$b(p)$	[3.7719 10.6645 15.5864 15.2137 7.4687 1.0000]

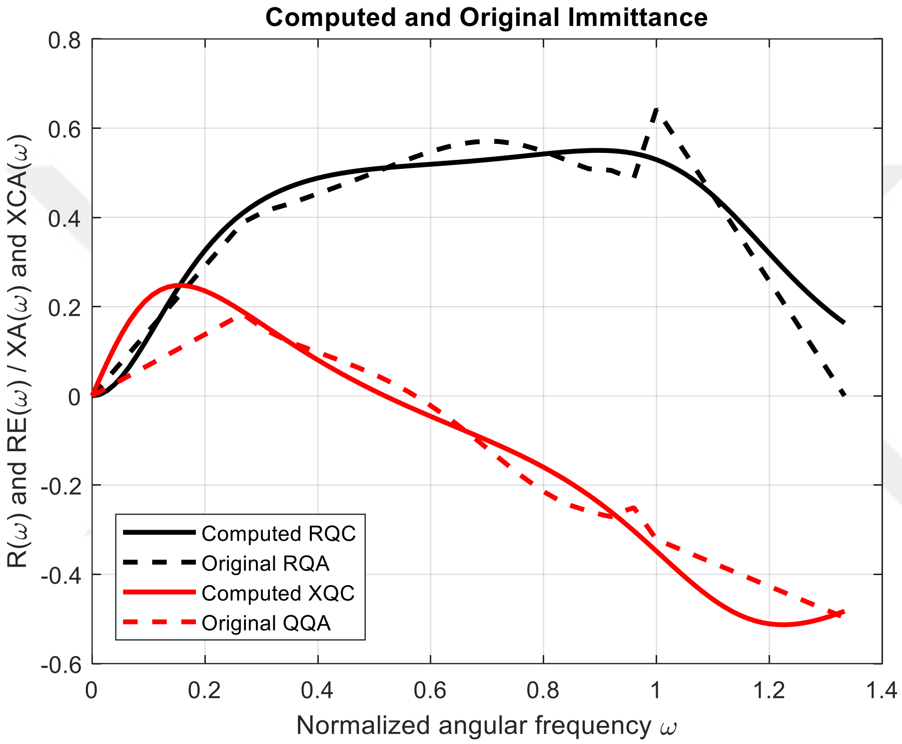

Figure 3.11 : Fit between the modeled and RF-LST based load impedance real and imaginary parts.

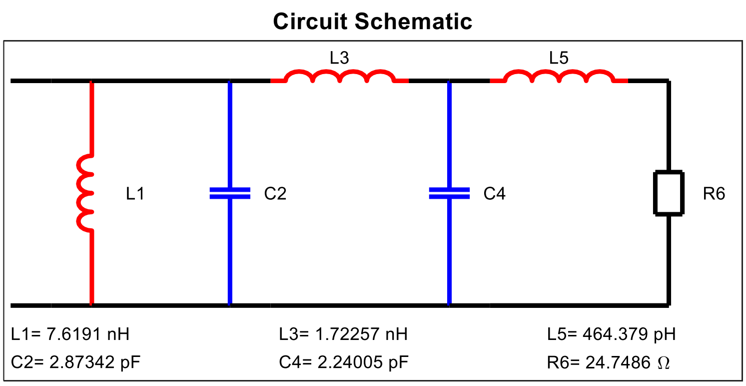

Figure 3.12 : Synthesized network by modeling the RF-LST based load impedance.

3.8 Simulation of the PA with Synthesized Matching Networks

In this section, we carried out the simulation and re-optimization process of the designed power amplifier using ADS as depicted in Figure 3.13 [72]. The circuit components of the IMN (Figure 3.10) and OMN (Figure 3.12) are re-optimized to improve the TPG and the power added efficiency of the overall amplifier to end up with practically implementable component values. Finally, the amplifier is manufactured, and its performance is measured. Details are summarized as follows.

In Figure 3.13, for AB-Class operation, the GaN transistor CGH40010F is biased with $VDD = 28\,Volts$, $VGG = -2.82\,Volts$, $IDD = 150\,mA$. Over the passband, driving input power of the amplifier is kept constant at $P_{in} = 28\ dBm$ level. Under the above conditions, simulation results are given in Figure 3.14. Close examination of this figure reveals that the average value of TPG is 13.6 dB with ∓0.6 dB fluctuation and the PEA varies between 65% down to 43% over the passband of (800MHz-3GHz). For the sake of comparison, simulation results for the synthesized IMN with $Nc = 8$ elements, is also depicted in Figure 3.14 as TPG2 and PAE2. As can be seen from this figure, the passband performance is similar to that of 5 element IMN, whereas the stop-band roll-offs is sharpened as expected.

So far, we are only concerned with the optimum data fit between the realizable analytic forms and the given source/load-pull immittance data. Therefore, we did not care about the IMN and OMN resistive terminations if they are 50 ohms or not. As a matter of fact, they are also included among the unknowns of the virtual matching problems by varying the real constant a_0 of (3.3a). Indeed, for IMN, the optimum solution is obtained for $a_{0G} = 2.12$ which yields $R_{0G} = 10.13\Omega$. Similarly, the terminating resistor of OMN is $R_{0L} = 24.75$ which refers to the real constant $a_{0L} = 4.08$. However, practical designs of IMN/OMN may require 50Ω terminations. This fact can be taken care of in ADS during the re-optimization process. Moreover, for the sake of simple PA fabrication, most of the lumped elements are converted to microstrip lines. Thus, we end-up with the final design as depicted in Figure 3.15. At this point, it is crucial to emphasized that, without using VGO method, which yields the circuit topologies with element values for IMN and OMN as depicted in Figure 3.10 and Figure 3.12, we would not be able to carry-out the re-optimization to end-up with the final design of the PA on ADS as depicted in Figure 3.15.

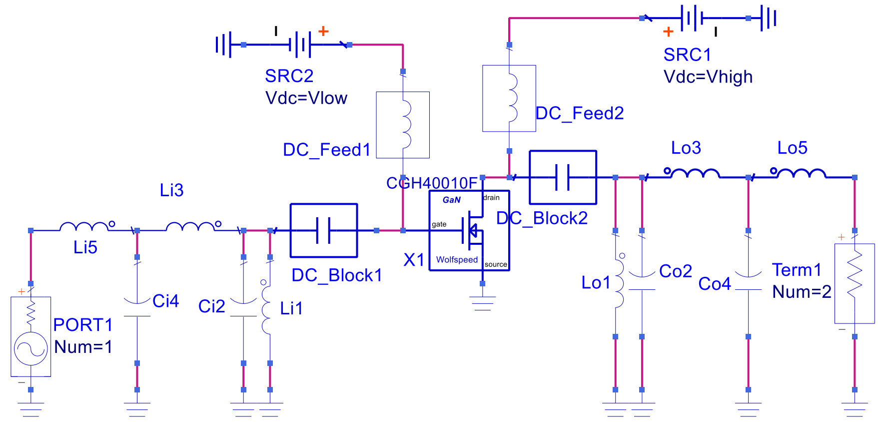

Figure 3.13 : ADS simulation schematic of the designed amplifier.

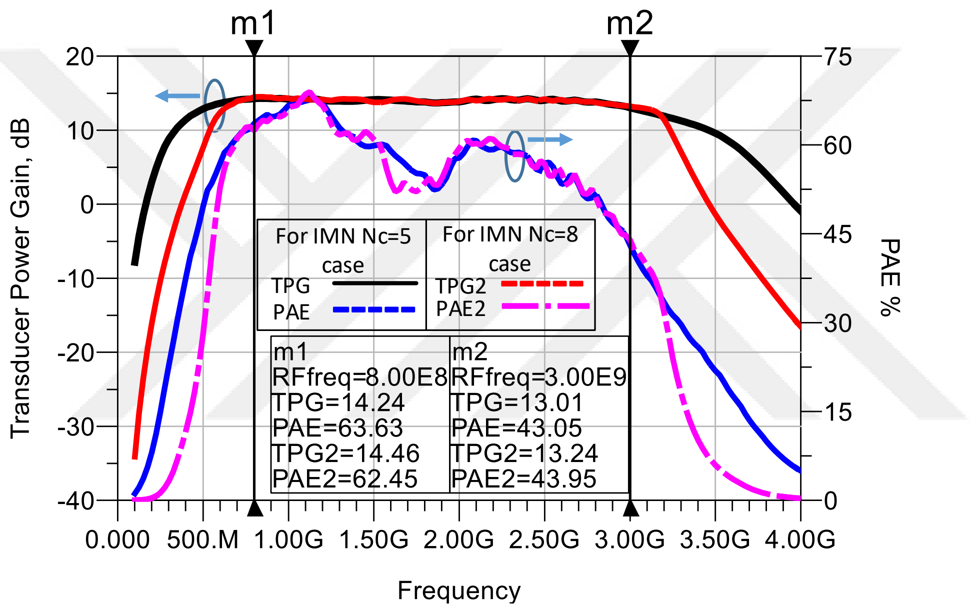

Figure 3.14 : ADS simulation results of the designed amplifier.

Referring the Figure 3.13 and Figure 3.15, capacitors and inductors can be realized as cascaded microstrip lines. The shunt inductors L_{i1} of IMN and L_{o1} of OMN are connected through the bias lines. Due to its substantial value, it is appropriate to realize the capacitor C_{i2} of IMN as a radial stub. After re-optimization, it is found that, inductors L_{i5}, L_{o5} and the capacitor C_{o2} can be disregarded due to their negligible contributions to the PA performance. The series inductors L_{i3} and L_{o3} are printed on the top surface as transmission lines TL_{i1} and TL_{o1} respectively. In a similar manner, C_{i4} of the IMN is realized as TL_{i2}. The pi section $[C_{o2} - L_{o3} - C_{o4}]$ of Figure 3.15 can be replaced with a single transmission line TL_{o2} as described in [25, 48, 49, 79-82]. Additionally, required connection lines such as bias and solder paths for gate/drain leads of the active device are inserted. Furthermore, an RC low-frequency damping circuit is included to compensate low frequency gain variations, to reduce the return loss and to improve the stability of the amplifier. As a substrate, Taconic RF35 board is used for the PA realization with dielectric constant $\epsilon = 3.5$ and $h = 30\,mil$ thickness [83]. Non-ideal discrete component models are inserted for lumped elements (i.e. for C_i and C_o, 600S series from Kyocera AVX corp. for C_G and $Li1$, GJM15 and LQW15 series from Murata respectively and for $Lo1$, 603HP series from coil-craft [84-86]). After these modifications, EM analysis and post-layout optimizations are completed with the best possible realizable form of the amplifier. The finalized schematic of the amplifier is given in Figure 3.15. The picture of the manufactured amplifier is given in Figure 3.16. The final simulation and the measurement results are given in Figure 3.17. As it is seen from the figure, the actual TPG is 11.4 ± 0.6 dB, PAE varies between 49% up to 71% and the drain efficiency (DE) varies between 52.8% and 75.3%.

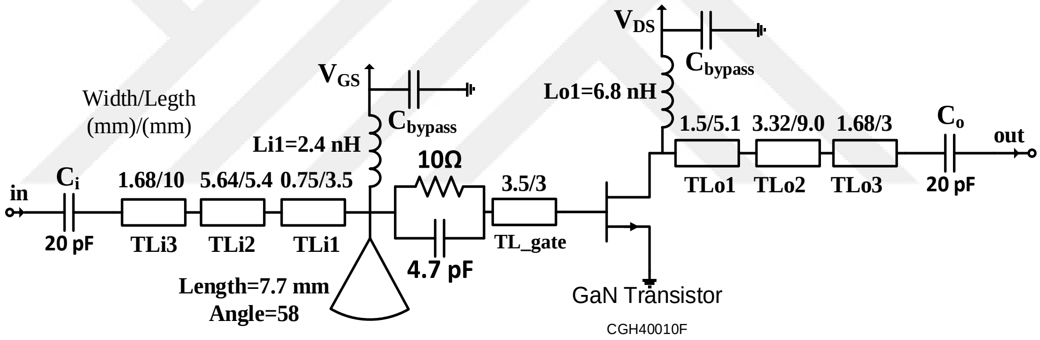

Figure 3.15 : Converted mixed equivalent of the designed amplifier.

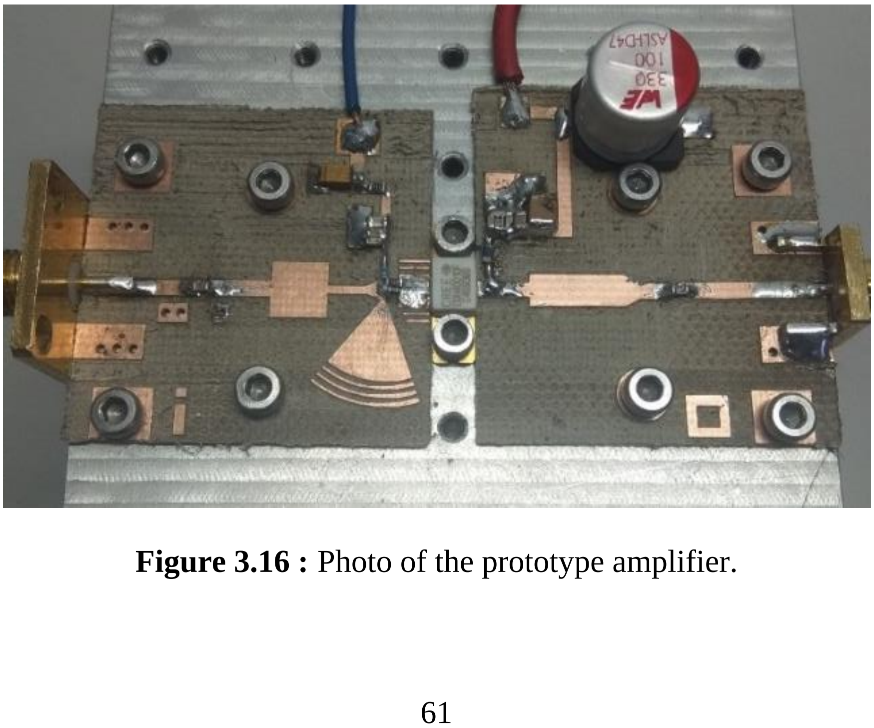

Figure 3.16 : Photo of the prototype amplifier.

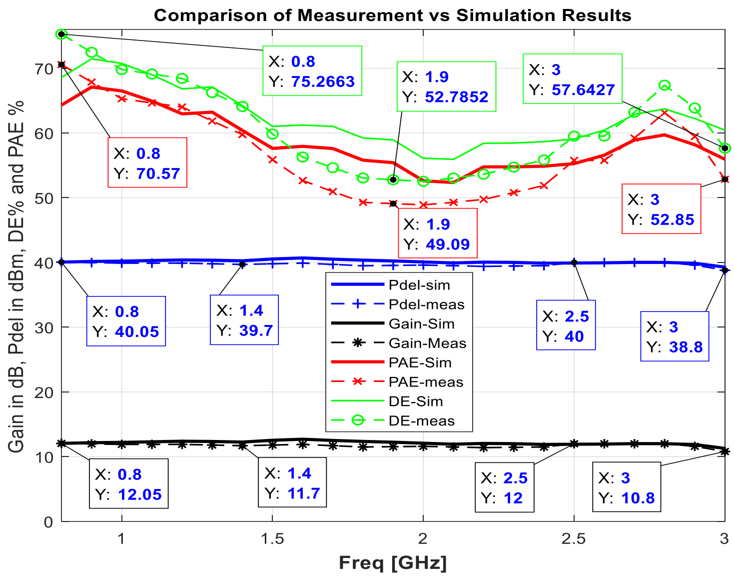

Figure 3.17 : Measurement vs simulation results.

At this point, it is useful to compare the measured performance of our amplifier with similar PAs, listed in Table 3.5. It is unveiled that, our newly proposed VGO neither requires selection of matching network topology nor demands the initialization of the element values. They are the results of the VGO method introduced in the thesis. Furthermore, our PA offers the minimum fluctuations within high average TPG in broadband.

Table 3.5 : Comparison with the recently published PAs.

[Ref]-[Year]	Frequency Band [GHz]	Gain [dB]	Pout[dBm]	DE/PAE [%]
[1]-[2022]	0.5-2.8	10-12	40-42.5	DE: 63-69
[2]-[2018]	1.2-3.6	10.5-12.5	40-42.2	DE: 60-72
[3]-[2017]	1.8-2.7	9.6-11.2	39.5-42	DE: 64-81
[4]-[2016]	0.6-3.8	9-14	40-41.9	PAE: 46-75
[5]-[2016]	0.8-3.05	9.8-13.2	40-43.2	DE: 57.4-79.1
[6]-[2014]	1.6-2.8	11.9-15.2	40-42.5	DE: 67.5-81.9
This work [2022]	0.8-3.0	10.8-12.05	38.8-40.05	DE: 52.8-75.3 PAE: 49-70.6

3.9 Conclusion

This research work proposes a structured set of sequential procedures to design power amplifiers. The power amplifier design process starts with the selection and characterization of an active device which must provide the desired output power level in demand over a prescribed frequency band. The active device may be a GaN power transistor. In this regard, the source/load pull impedances of the active device are generated to optimize the power added efficiency (PAE), and transducer power gain (TPG) while minimizing the harmonics of the amplifier over the frequency band of interest. At this point, it is crucial to note that for many practical situations, source and load pull impedances placed on the Smith Chart, do not necessarily belong to realizable positive functions (PR) over the passband. In this case, one must check if these impedances are realizable. If not, it is well known that power intake and power delivery performance of the active device is penalized heavily. Therefore, in this chapter, we applied the newly developed test procedure to determine whether the given source and load pull data are realizable network functions. Then, we introduced a new numerical method to assess the Power Intake/Delivery Performance of the given source and load pull impedances employing the real frequency line segment technique. Thus, ultimate power intake and power delivery capacity of the nonlinear active device is determined. Then, generate the optimum-realizable source and load pull impedances are as sampled data using the proposed real frequency line segment technique, which in turn results in the numerical Power-Intake and Power-Delivery Performance of these impedances. Then, we generated positive real function models for the line segment based realizable optimum source and load pull impedance data, which results in the optimum input and output matching network topologies with component values. The proposed modelling algorithm employs the method, what we call is the "virtual gain optimization, VGO". Modelled positive real functions are synthesized as the front-end and the back-end lossless matching networks, yielding the optimum power added efficiency and the transducer power gain for the power amplifier under consideration. Eventually, component values of the resulting input and output matching networks are re-computed to improve the electrical performance of the power amplifier employing a commercially available design packages such as ADS. Using GaN CGH40010F transistor, Using the proposed sequential design method step by step, we constructed an AB-Class power amplifier over $800MHz - 3GHz$ bandwidth. It is shown that the designed power amplifier offers 38.8dBm to 40.05 dBm output power, maximum of 70.6% at 800 MHz and a minimum of 49% at 3.0 GHz power added efficiency with a nearly flat transducer power gain of $T = 11.4 \pm 0.6\, dB$ over the 800MHz-3GHz bandwidth.

4. BROADBAND POWER AMPLIFIER DESIGN VIA FICTITIOUS MATCHING[1]

In this chapter, we introduce a new matching concept, so called Fictitious Matching (FM), which may be defined between the artificially generated non-Foster passive immittances, namely K_{GF} and K_{LF}, over a lossless two-port or equivalently equalizer [E]. These immittances may not necessarily belong to physical devices, rather, they are fabricated like a source-pull or load-pull impedances to maximize the gain, the output power, the efficiency, and to minimize the output harmonics of a nonlinear-active device. In FM problems, [E] is constructed to optimize the power transfer from K_{GF} to K_{LF} in the passband. In this regard, [E] is described by means of its back end driving point input immittance $K(\lambda)$ in Darlington sense, and it is determined as the outcome of the optimization process, where the complex variable $\lambda = \Sigma + j\Omega$ refers to Richards variable. Synthesis of $K(\lambda)$ results in [E], consists of commensurate transmission lines. It is demonstrated that the new concept of FM can be utilized to build broadband power amplifiers. In this work, solving FM problem successively, the input and the output matching networks of a power amplifier are designed over 500 MHz-3 GHz with the average gain of $11.5dB$, the output power of 40.5 dBm, and the average drain efficiency of 61.7%. The Power Amplifier was manufactured with microstrip lines using Wolfspeed's CGH40010F GaN transistor.

4.1 Introduction

For wireless communication systems, it is essential to design power amplifiers (PA) for a variety of applications. Recently, it is a widespread practice to employ Gallium Nitrate (GaN) transistors due to their high-power delivery capacity [1-6]. Once the power transistor is selected, its nonlinear behavior is characterized by determining it's source-pull impedance data (Z_{SPD}) and the load-pull impedance data (Z_{LPD}). It is noted

[1] This chapter is based on the paper "Kilinc, S., Yarman, B.S., and Ozoguz, S. (2022). "Broadband Power Amplifier Design via Fictitious Matching," in IEEE Transactions on Circuits and Systems II: Express Briefs, vol. 69, no. 12, pp. 4844-4848, Dec. 2022, doi: 10.1109/TCSII.2022.3207423".

Z_{SPD} and Z_{LPD} are produced to optimize the PA's transducer power gain (TPG), output power (Pout), power added efficiency (PAE) as high as possible, and to minimize the harmonics in the specified frequency band $B(\omega)$. It must be noted that any impedance $K(j\omega) = R(\omega) + jX(\omega)$, specified over the real frequencies, with positive real part $R(\omega)$ is called a "non-Foster passive impedance (NFPI) or in short a "lossy impedance" whether it is realizable or not. Therefore, the source and the load pull impedances are considered as NFPI as confirmed by definition, whether they are realizable or not [87]. Once the complex impedances Z_{SPD} and Z_{LPD} are generated, their complex conjugates are regarded as the optimum input (Z_{in}) and the output (Z_{out}) impedances for the active device under consideration. Referring to Figure 4.1, in general, a PA is designed by constructing it's lossless input and output matching networks, as they are terminated in the complex generator impedance Z_G and the complex load impedance Z_L.

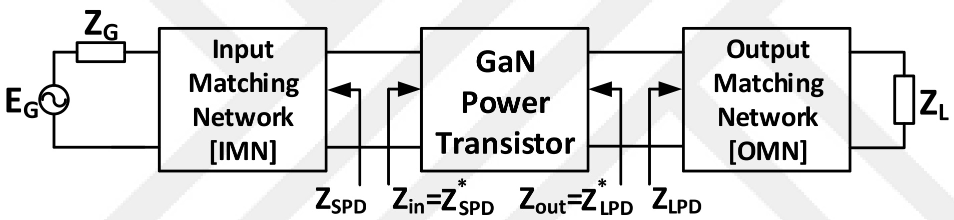

Figure 4.1 : Description of a PA by means of its Z_{SPD} and Z_{LPD}.

At this point, Z_{SPD} and Z_{LPD}, so as their complex conjugates, Z_{in} and Z_{out} may be regarded as artificially generated impedances since they are created point by point to optimize PA performance. It is not even known, if they are realizable network functions.

In this chapter, computed or equivalently generated impedances, which may not belong to proper-realizable network functions, such as the source-pull and the load-pull impedances or equivalently their complex conjugates Z_{in} and Z_{out}, are regarded as fictitious impedances. Then, a matching problem, described between the fictitious complex terminations, is called the Fictitious Double Matching Problem (FDMP). In this regard, the Input Matching Network (IMN) and the Output Matching Network (OMN) of Figure 4.1, can be designed by solving FDMP generically, since $Z_{in} = Z^*_{SPD}$ and $Z_{out} = Z^*_{LPD}$ are generated to optimize the performance of the PA. In FDMP, a lossless two-port or equivalently equalizer [E] is constructed between the complex non-Foster passive impedances designated by K_{GF} at the generator-end and K_{LF} at the load-end, to optimize TPG in the passband as described in Figure 4.2 as follows.

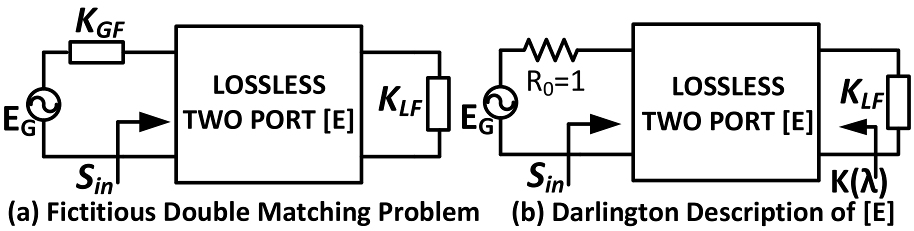

Figure 4.2 : Description of the fictitious double matching problem.

Referring to Figure 4.2a, if one constructs IMN, then the fictitious load impedance K_{LF} refers to $Z_{in} = Z_{SPD}^{*}$, and the impedance K_{GF} is set to the actual internal impedance of the generator Z_G as in Figure 4.1. Likewise, if OMN is designed, the fictitious impedance K_{GF} refers to the complex impedance of the output port specified by $Z_{out} = Z_{LPD}^{*}$, while setting K_{LF} to the original complex load impedance Z_L. Hence, design of IMN (or OMN) is handled by solving FDMP for each matching network separately. In FDMP, the goal is to design the lossless matching network [E] to maximize the TPG as flat as possible over the passband. It is noted that $TPG = 1$ corresponds to perfect match, meaning that, the equalizer $[E] = \{(IMN)\ or\ (OMN)\}$ matches the exact values of $Z_{in} = Z_{SPD}^{*}$ (or $Z_{out} = Z_{LPD}^{*}$) to those values of the actual complex termination Z_G (or Z_L) at measured frequencies point by point in the passband. Therefore, in this study, a robust numerical procedure is outlined for the solution of the fictitious double matching problem to construct $[E] = \{(IMN)\ or\ (OMN)\}$ employing the Real Frequency Technique via Parametric Approach (RFT-PA) [25, 26, 50, 71].

Referring to Figure 4.2b, in RFT-PA, the matching network [E] is described by means of its back end driving point input impedance $K(*)$ as an analytic positive real (PR) function in Darlington sense. If $K(*)$ is defined in Laplace variable $p = \sigma + j\omega$, synthesis of $K(p)$ results in [E] consist of lossless-lumped circuit elements. However, if it is given in Richards variable $\lambda = \Sigma + j\Omega$, then Richards-Synthesis of $K(\lambda)$ yields a lossless [E], which includes only commensurate transmission lines. These lines may be manufactured as microstrip lines to make the production of the PA easy and cost effective [88-90]. It is noted that the angular Richards frequency Ω is related to the angular frequency ω in Laplace domain such that $\Omega = \tan(\omega\tau)$. The Greek letter τ is known as the fixed delay lengths of the commensurate transmission lines. Let ω_{c2}

designate the normalized angular frequency of the upper end of the passband. Then, the commensurate line delays are specified by $\theta = \omega_{c2}\tau$ in degrees or in radians. For many applications, normalized ω_{c2} is kept at unity yielding $\theta = 1 \times \tau$. In practice, θ is selected by the designer satisfying the inequality of $0 < \theta < \frac{\pi}{2}$. It may be proper to select $\theta \leq \frac{\pi}{4}$, or equivalently the normalized delay length $\tau \leq \frac{\pi}{4}$. In the following sections, first, we introduce a robust numerical procedure to solve the fictitious double matching problem (Section 4.2). Then, employing FDMP successively, IMN and OMN of the PA are constructed the with equal length (i.e., commensurate) transmission lines. Eventually, the power amplifier is built by realizing commensurate transmission lines in the form of microstrip patches, printed on a selected substrate. It is shown that, simulated and measured performance of the PA agrees within acceptable tolerances. The actual average performance of the PA is measured as $TPG = 11.5 \mp 0.9\ dB$, and the average PAE is 61.7% with average output power of 40.5 dBm (Section 4.3).

In essence, Fictitious Gain Optimization (FGO) method introduced in this chapter, offers a numerically robust procedure to model the given source/load pull impedance data as positive real network functions in Richards variable λ=Σ+jΩ, resulting in the input and the output matching networks with commensurate transmission lines. Into our knowledge, FGO is the first of its kind, and it is formulated in such a way that undesirable parasitic components are imbedded in the optimization scheme, which transforms the modelling problem to a FDMP as described in Section 4.3.

4.2 A Robust Numerical Procedure to Solve FDMP

In broadband matching literature, the matching problems are studied under two major headings, namely, single, and double matching problems [50, 64, 66]. For FDMP of Figure 4.2a, the generator E_G with a fictitious internal immittance $K_{GF}(j\omega) = R_{GF}(\omega) + jX_{GF}(\omega)$, transfers its RF power to a fictitious load immittance $K_{LF} = R_{LF}(\omega) + jX_{LF}(\omega)$ over the lossless matching network [E] in the passband. Similarly, Figure 4.2b refers to a typical Fictitious Single Matching Problem (FSMP), whereas the generator's internal immittance is purely resistive (i.e., $K_{GF} = R_G = 1\Omega$). In matching problems, the goal is to construct a lossless matching network [E] to optimize the power transfer (i.e., TPG) from K_{GF} to K_{LF} as flat and as high as possible over

$B(\omega)$. In fictitious matching problems, impedances K_{GF} and/or K_{LF} may not necessarily be realizable network functions. They are rather fabricated to construct [E] to optimize the pre-selected criteria such as the TPG of the matching problem under consideration.

In the real frequency techniques (RFT), [E] is described in terms of its back end driving point input immittance $K(*)$ in Darlington sense. In this chapter, $K(\lambda)$ is expressed in Richards variable λ and it is determined as a realizable analytic function by optimizing the Fictitious Transducer Power Gain $T_{DM}(\omega)$ over the passband as follows. On the $j\Omega$ axis, $K(j\Omega)$ is expressed as

$$K(j\Omega) = R(\Omega) + jX(\Omega) \tag{4.1a}$$

In RFT-PA, the immittance function $K(\lambda)$ is assumed to be a minimum impedance or a minimum admittance. Therefore, imaginary part $X(\Omega)$ of (4.1a) is uniquely determined from the real part $R(\Omega)$ using the Hilbert Transformation (HT) [50]. Once $R(\Omega)$ is sampled at the Richards angular frequencies Ω_i, HT can be expressed as a linear numerical operator (LHT) in terms of the sampling points $R_i = R(\Omega_i)$ such that

$$X(\Omega) = \sum_{i=1}^{N} \beta(\Omega) R_i = LHT\,\{R(\Omega)\} \tag{4.1b}$$

In (4.1b), total number of sampling points N is selected in such a way that, for a large value of $\Omega \geq \Omega_N$, $R(\Omega)$ becomes zero. In other words, we set $R_N = 0$. Computational details of (4.1b) can be found in [50]. Thus, the unknown of the fictitious double matching problem is selected as the real part $R(\Omega)$. In this regard, fictitious gain $T_{DM}(\omega)$ of the FDMP is given by

$$T_{DM}(\Omega) = \frac{1 - |S_G(j\Omega)|^2}{|1 - S_{in}(j\Omega) S_G|} T_{SM}(\Omega) \tag{4.1c}$$

In (4.1c), $T_{SM}(\Omega)$ refers to the TPG of the FSMP of Figure 4.2b and it is given as

$$T_{SM}(\Omega) = \frac{4R(\Omega)R_{LF}(\omega)}{[R(\Omega) + R_{LF}(\omega)]^2 + [X(\Omega) - X_{LF}(\omega)]^2} \tag{4.1d}$$

The reflection coefficients S_G, and S_{in}, and Ω are given by

$$S_G = \mu_G \frac{K_G - 1}{K_G + 1} \tag{4.1e}$$

$$S_{in} = (-1)^{ndc} \mu_{in} \left[\frac{K_{LF}(j\omega) - K(-j\Omega)}{K_{LF}(j\omega) + K(j\Omega)} \right] \tag{4.1f}$$

$$\Omega = \tan(\omega\tau) \tag{4.1g}$$

where the unimodular constant μ_G(or μ_{in}) is set to $+1$ if K_{GF} (or K_{LF} and K) refers to an impedance function(s). Otherwise, it is set to $\mu_G(or\ \mu_{in} = -1)$ for admittance functions.

For practical matching networks constructed with commensurate transmission lines, $R(\Omega)$ may be described as

$$R(\Omega) = \frac{a_0^2(-1)^{ndc}\Omega^{2ndc}(1+\Omega^2)^m}{B(\Omega^2)} \geq 0; m + ndc \leq n \tag{4.2}$$

where $B(\Omega^2)$ is a strictly positive even polynomial and may be generated by means of an auxiliary polynomial $c(\Omega)$ to impose the realizability on $R(\Omega)$ such that

$$B(\Omega^2) = \frac{1}{2}\left[c^2(\Omega) + c^2(-\Omega)\right] > 0;\ \forall\Omega \tag{4.3a}$$

$c(\Omega)$ is a real full polynomial with non-zero coefficients in the Richard frequency Ω such that

$$c(\Omega) = c_1\Omega^n + c_2\Omega^{n-1} + \cdots + c_n\Omega + 1 \tag{4.3b}$$

In (4.2), the integer n refers to the total number of commensurate transmission lines in [E], and they are called unit Elements (UE), each of them possesses equal lengths with different characteristic impedances. These characteristic impedances are obtained as the result of the Richards Synthesis of $K(\lambda)$ [55]. The integer ndc is the total count of the transmission zeros placed at $\Omega = \omega = 0$ (i.e., at DC), and they are realized as open stubs (Richards Capacitors C_λ) in series configuration or as short stubs (Richards Inductors L_λ) in shunt configuration. The integer m is the total count for the UEs in cascaded connections, and $n_\infty = n - m - ndc$ is the total count for the transmission zeros placed at infinity (i.e., $\Omega = \omega = \infty$), and they are either realized as inductors L_λ

in series configuration or capacitors C_λ in shunt configuration. Integers n, m, and ndc are selected by the designer based on the design considerations. For the sake of simplicity, it may be preferable to select $ndc = 0$, and $n = m$ to avoid realization of transmission zeros at DC and infinity as short and open stubs. Therefore, in this study, we set $n = m$, and $ndc = 0$, so that [E] includes only cascade-connection of n Unit Elements with different characteristic impedances $\{Z_i; i = 1,2, \dots, n\}$.

In RFT-PA, the minimum immittance function $K(\lambda)$ is expressed as

$$K(\lambda) = \frac{a_m(\lambda)}{b_m(\lambda)} = \frac{a_1\lambda^n + a_2\lambda^{n-1} + \cdots + a_n\lambda + a_{n+1}}{b_1\lambda^n + b_2\lambda^{n-1} + \cdots + b_n\lambda + b_{n+1}} \tag{4.4}$$

The complex terminations Z_G and Z_L of Figure 4.1 are specified by the application. For example, if PA is designed as the output stage of a transmitter connected to an antenna, then Z_{GF} may be regarded the complex conjugate of the load pull impedance Z_{LP} of the nonlinear active device, and the load K_{LF} is considered as the actual input impedance Z_A of the antenna. Integers n, m, and ndc of (4.2) are selected by the designer. It should be kept in mind that these integers are related to the complexity of the matching network [E]. We prefer to choose $m = n$ and $ndc = 0$ with $n \leq 7$. In this case, [E] includes only total number of n UEs in cascade configuration.

The unknowns of FDMP are selected as the coefficients and $\{c_i; i = 1,2, \dots, n\}$ of (2). The real constant a_0 may be fixed as unity or it may also be included among the unknowns. To determine the unknown coefficients, we define an error function ε to be minimized such that

$$\varepsilon(\Omega, a_0, c_1, c_2, c_3, \dots, c_n, m, ndc, K_{GF}, K_{LF}) = T_{DM} - T_{0k} \tag{4.5}$$

In (4.5), T_{0k} is the target flat gain level, and it must be selected as high as possible. It may be determined by trial and error starting from the unity level down to $T_{0k} \geq 0.5$ by sweeping it. In the numerical minimization process of (4.5), we experienced that, Levenberg-Marquardt nonlinear minimization algorithm yields satisfactory results to determine the unknown coefficients of (4.5) [67, 68]. Once the analytic form of $R(\Omega)$ is determined, use of parametric approach returns with the realizable analytic form of $K(\lambda) = \frac{a_m(\lambda)}{b_m(\lambda)}$ as described in [50]. Then, $K(\lambda)$ is synthesized employing the high precision Richard synthesis algorithm to generate the matching network topology with the characteristic impedances of the commensurate transmission lines under a vector such that $Z_{UE} = [Z_1\ Z_2\ ...\ Z_n]$ as detailed in [55].

4.3 PA Design via FDMP Solution

In this section, we introduce the design of a power amplifier over 500MHz-3GHz frequency band with average output power of 10 Watts employing the GaN device of *Wolfspeed-CGH40010F*. Its source and load pull data measurement conditions are reported in [45]. As detailed in [45], the source and the load pull data measurements are made to optimize the output power, gain, saturated output power P_{Sat}, and power added efficiency. During the design process, we solved FDMP successively to build IMN and OMN with commensurate transmission lines (i.e., UEs). Eventually, UEs are realized using the microstrip technology.

4.3.1 Design of OMN by solving FDMP

In designing OMN, the output impedance of the GaN transistor is assumed to be equal to the complex conjugate of the generated-optimum load-pull impedance Z_{LP}. Moreover, a microstrip patch ($Mlin_D$) is placed at the output port for easy access to the active device. Referring to Figure 4.3, let $Z'_{out}(j\omega)$ designate the revised output port impedance. Then, the fictitious generator impedance Z_{GF} of OMN is defined as the $Z'_{out}(j\omega)$. The 50Ω termination of OMN is accessed over a series capacitor $C_0 = 27pF$ to confine the delivered power within the passband. Thus, the fictitious load termination K_{LF} is set to $Z'_L(j\omega)$, which is the series combination of C_0 with 50Ω as shown in Figure 4.3. Hence, we end up with a FDMP to construct OMN.

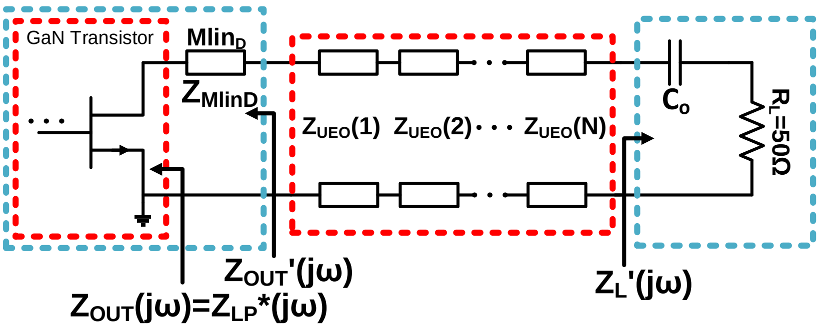

Figure 4.3 : Description of the FDMP to construct OMN.

OMN is designed as described in Section 4.2 in terms of its back-end impedance $Z_{OMN} = \frac{a_{OMN-m}}{b_{OMN-m}}$ by setting $n = 7$, $m = n$, $ndc = 0$, $\tau = 0.5$ and $T_{0k} = 0.9$. Results of the minimization process is summarized in Table 4.1 and the quality of the power transfer from the fictitious impedance Z'_{out} to the 50Ω termination is depicted in Figure 4.4 (red-dashed plot).

Table 4.1 : Optimized analytic impedance function for OMN.

a_{OMN-0}	1
c_{OMN}	$[-0.006 \;\; 124.57 \;\; 64.75 \;\; -41.51 \;\; -39.42 \;\; 9.43 \;\; 4.17]$
$a_{OMN-m}(\lambda)$	[0.3366 0.5467 0.5842 0.4375 0.2189 0.0826 0.0167 0.0020]
$b_{OMN-m}(\lambda)$	[0.0000 0.2519 0.4089 0.3819 0.2380 0.0886 0.0225 0.0020]
Z_{UE-OMN}	[79.83 13.74 121.43 14.90 97.78 30.09 54.10]

4.3.2 Design of IMN by solving FDMP

As in the OMN design case, complex conjugate of the fabricated source-pull impedance data $Z_{SP}(j\omega)$ is defined as the fictitious load impedance $Z_{in}(j\omega)$ of the active device. Moreover, the GaN transistor is accessed over a microstripline designated by $Mlin_G$ with length l =2.6mm and the width $w = 5$mm. To stabilize the power transistor, a lossy $R_g//C_g$ section with $R_g = 10\Omega$ and $C_g = 5pF$ is connected to $Mlin_G$ in series configuration. It is noted that, initial values of $Mlin_G$, R_g and C_g are determined to comfortably access and stabilize the device. Nevertheless, these initial values may be improved by re-optimization in the post-layout design stage if required. Furthermore, to confine and maximize the delivered power within the passband, a series capacitor $C_i = 27pF$ is attached to the standard generator resistor $R_G = 50\Omega$. Hence, we completed the setup of FDMP to construct IMN as depicted in Figure 4.5.

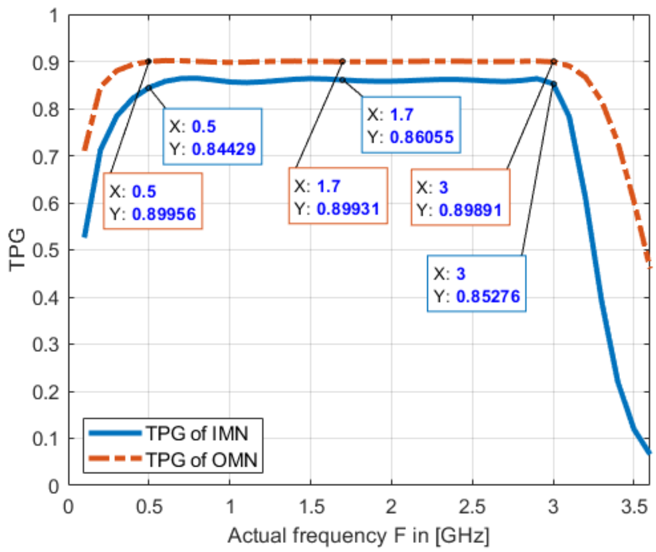

Figure 4.4 : Quality of the power transfer measured for IMN and OMN.

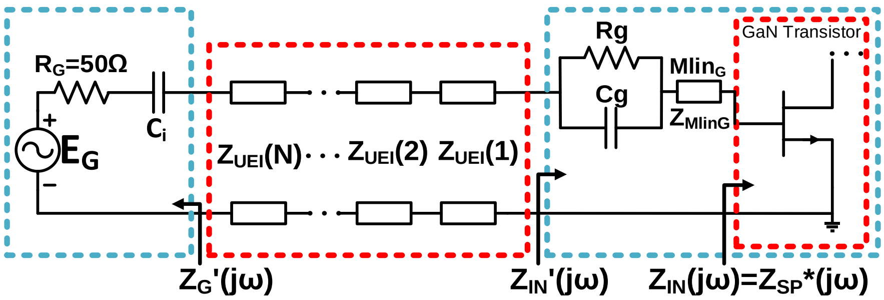

Figure 4.5 : Description of the FDMP to construct IMN.

In this case, solution to FDMP yields the back-end impedance $Z_{IMN}(\lambda) = \frac{a_{IMN-m}(\lambda)}{b_{IMN-m}(\lambda)}$ of IMN, while the other end is resistively terminated. As in the previous section, for IMN design, we set $n = 7$, $ndc = 0$, $\tau = 0.5$ and $T_{0k} = 0.85$. Results of the minimization process of (4.5) and synthesis of the optimum realizable back-end impedance $Z_{IMN}(\lambda)$ are summarized in Table 4.2.

Table 4.2 : Optimized analytic impedance function for IMN.

a_{IMN-0}	1
c_{IMN}	[0.0031 380.6 − 174.4 − 131.9 82.9 15.4 − 4.9]
$a_{IMN-m}(\lambda)$	[0.47 0.54 0.55 0.38 0.18 0.064 0.012 0.0015]
$b_{IMN-m}(\lambda)$	[0.0000 0.56 0.65 0.51 0.27 0.084 0.019 0.0015]
Z_{UE-IMN}	[52.5 12.2 133.2 12.6 120.3 21.3 61.7]

The quality of the power transfer from the fictitious generator to the input port Z'_{in} is also depicted in Figure 4.4 (blue plot). Close examination of Figure 4.4 reveals that, the generator of Figure 4.5 delivers 85% of the available power to the input port Z'_{in} of the active device CGH40010F.

TPG and the PAE of the overall PA is re-optimized and simulated in ADS [72]. PA is developed on the Rogers 4350B substrate with the relative permittivity $\varepsilon_r = 3.66$ and the thickness $h = 30mil$ [91]. Commensurate transmission lines are printed on the Roger substrate as cascaded microstrip patches with fixed lengths of $\theta = 29^0$, which corresponds to $\tau = 0.5$. A re-optimization process is carried out to compensate the effect of discontinuities between wider and thinner lines. In the re-optimization process, the minimum width of the lines was restricted to 600μm to reduce the sensitivity tolerances to the manufacturing precision. Eventually, the schematic of the final PA is given in Figure 4.6, and it is built as shown in Figure 4.7.

The GaN transistor CGH40010F was biased to operate in AB Class mode with $VDD = 28\,Volts$, $VGG = -2.82\,Volts$, $IDD = 150\,mA$. Over the passband, driving input power of the amplifier is kept constant at $P_{in} = 29\, dBm$ level. Simulated and measured PA performance are depicted in Figure 4.8. Close examination of this figure reveals that the measured average value of TPG is 11.5 dB with ∓0.9 dB fluctuation, output power is $40.5 \mp 1\, dBm$ and PEA varies between 64.9% and 49.4% in the passband. The performance of the actual amplifier is compared with those PAs listed in Table 4.3. It is understood that the power amplifier presented in this chapter, provides broadest frequency band with minimum gain fluctuation without sacrificing the output power and PAE and it is easily manufactured employing the microstripline print technology as shown in Figure 4.7.

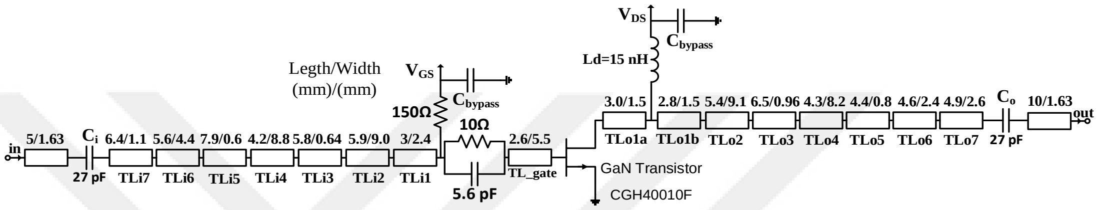

Figure 4.6 : PA schematic.

It is noted that one could have used larger series capacitors for C_i and C_0 to block DC biasing currents before the 50-ohm terminations so that IMN and OMN could have been constructed employing the Real Frequency-Parametric Approach developed for Single Matching Problems. However, in this work, we preferred to use smaller component values to confine the delivered power within the passband and to avoid parasitic effects due to large component values. Therefore, OMN and IMN were designed by solving the Double Matching problems as described by Figure 4.3 and Figure 4.5.

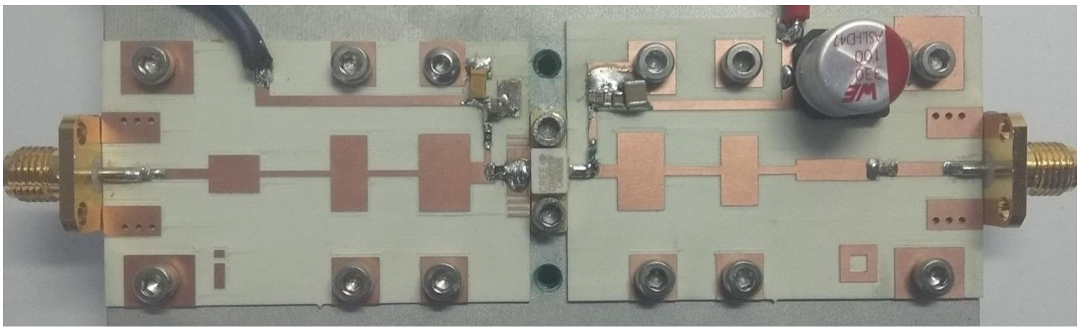

Figure 4.7 : Picture of the prototype PA.

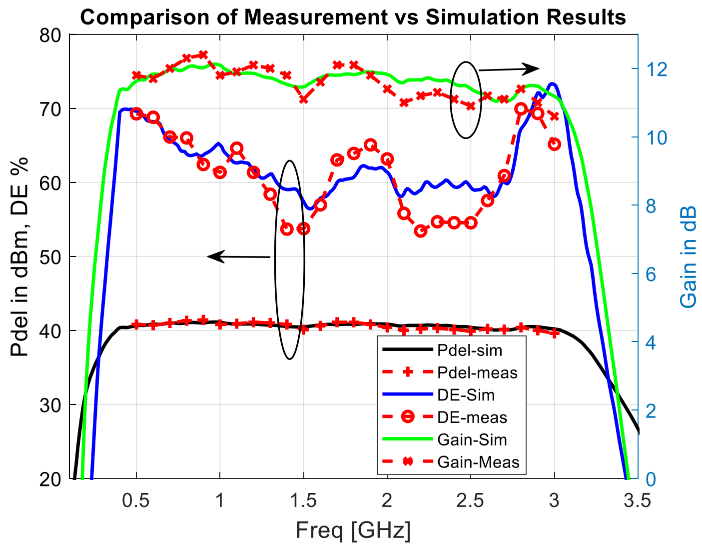

Figure 4.8 : Measured Performance of the power amplifier.

Table 4.3 : Comparison of similar PAs published in recent years.

[Ref]-[Year]	Frequency Band, [GHz]	Gain [dB]	Pout[dBm]	DE/PAE [%]
[1]-[2022]	0.5-2.8	10-12	40-42.5	DE: 63-69
[2]-[2018]	1.2-3.6	10.5-12.5	40-42.2	DE: 60-72
[3]-[2017]	1.8-2.7	9.6-11.2	39.5-42	DE: 64-81
[4]-[2016]	0.6-3.8	9-14	40-41.9	PAE: 46-75
[5]-[2016]	0.8-3.05	9.8-13.2	40-43.2	DE: 57.4-79.1
[6]-[2014]	1.6-2.8	11.9-15.2	40-42.5	DE: 67.5-81.9
This work [2022]	0.5-3.0	10.6-12.4	39.6-41.4	DE: 53.4-70 PAE: 49.4-64.9

4.4 Conclusion

This study describes the design procedure of a broadband power amplifier constructed with commensurate transmission lines using the concept of “Fictitious Double Matching Problem-FDMP”. In this regard, we designed and manufactured a power amplifier, using Cree’s GaN transistor of CGH40010F over 500MHz-3GHz bandwidth. It is exhibited that the manufactured power amplifier provides wider frequency band without sacrificing the gain, output power level and the power added efficiency over the others encountered in the recent literature. It is noted the Wolfspeed device used in this work, is not very sensitive to the second and third harmonics mismatches, but otherwise, predistortion techniques may be utilized to design the PA.

5. CONCLUSION AND RECOMMENDATIONS

In this thesis, we propose a series of novel procedures to design broadband microwave power amplifiers with high gain and high efficiency. The RF power amplifier design process starts with the selection and characterization of an active device which must provide the desired performance outcomes in demand over a prescribed frequency band. The active device may be a GaN RF power transistor. Once, the active device is selected, its non-linear behavior is modeled by means of measuring source-pull and load-pull impedance as well as non-linear transistor CAD models. Eventually, based on generated source/load pull impedances, the input and the output matching networks of the power amplifier is designed for optimum gain and efficiency. At this point, it is crucial to note that, for many practical situations, source and load-pull impedances do not necessarily belong to realizable positive real functions over the frequency band of interest. In this regard, we introduced a novel numerical method to test the given source and load-pull data if they are realizable network functions to construct the input and the output matching networks. Then, we introduced a new numerical method to assess the "Gain-Bandwidth Limitations, GBWL" of the given source and load pull impedances employing the Real Frequency Line Segment Technique. Determination of GBWL using the source-pull data the power intake performance of the active device. In a similar manner, power delivery capability can be obtained by assessing the GBWL for the load-pull data. As doing so, a reasonable way determining PI and PD capacity of the non-linear device is to go through its numerical gain-bandwidth limitations from the input and the output. This precedure leads us to obtain the best-optimum and realizable source and load impedance terminations point by point. Then, we generate positive real function models for the line-segment based realizable optimum source and load pull impedance data, which yields in the optimum input and output matching network topologies with component values. The proposed modelling algorithm employs the method, what we call is the "Virtual Gain Optimization, VGO". VGO minimizes a convex error function by targeting its global minimum, which in turn yields the optimum-realizable source and load terminations of the nonlinear active device under consideration. Thus, ultimate power-intake and power-delivery capacity of the nonlinear active device is determined. Modelled positive real functions are synthesized as the front-end and the back-end lossless matching networks, yielding the optimum power added efficiency and the transducer power gain for the power amplifier under consideration.

In the course of computations, we proposed a new figure of merit to measure the power-intake and power-delivery quality of an active device, so called “Power-Performance-Product (in short PPP or 3P) based on the (GBWL) of the given source/load pull impedances. In this regard, we concluded that, if PPP<25% the transistor is useless to design for desired frequency band.

In the research work through this thesis, we completed theree designs employing the proposed methods. In the first part, we exhibit the implementation of the proposed immittance realizability test procedure and the design of an “optimum performance power amplifier algorithm” using the Real Frequency Line Segment Technique over 0.8GHz − 3.8GHz bandwidth which ideally receives average of 65.07% of the available power of the resistive input excitation and delivers the 94.78% of the transistor’s output power to a resistive load.

In the second part, employing the proposed sequential design method step by step, we constructed an AB-Class power amplifier over $800MHz - 3GHz$ bandwidth. We determined the optimum realizable source and load impedances data via the virtual gain optimization. Then, the optimum source and load impedance data is modelled as realizable network functions. Generated realizable network functions are synthesized using the Darlington synthesis which in turn yields optimum input and output matching network topologies with component values. Eventually, the designed power amplifier is manufactured. It is shown that the designed power amplifier offers 38.8dBm to 40.05 dBm output power, maximum of 70.6% at 800 MHz and a minimum of 49% at 3.0 GHz power added efficiency with a nearly flat transducer power gain of $T = 11.4 \pm 0.6\ dB$ over the 800MHz-3GHz bandwidth.

In the third part, a broadband power amplifier is constructed with commensurate transmission lines using the concept of “Fictitious Double Matching Problem-FDMP”. It is shown that a fictitious matching problem can be defined between the artificially generated non-Foster passive immittances, over a lossless equalizer [E]. These immittances may be source-pull or load-pull impedances to design microwave power amplifier. In this regard, we designed and manufactured a power amplifier, using the GaN transistor over 500MHz-3GHz bandwidth. It is exhibited that the manufactured power amplifier provides high gain, output power level and the power added efficiency over a broadband frequency

It should be noted that, in the case of a broadband PA operation, harmonics of the fundamental signal may appear in the pass-band inevitably. This fact may increases the non-linearity of the PA and brings the definition of harmonic-tuning. The SP/LP data used in this work is generated for optimum gain, saturated-output-power Psat, and power added efficiency PAE. However, the data is determined in a way that it is not very sensitive to the second and third harmonics mismatches. Therefore, once we synthesized the input and the output matching networks, their simulation with the non-linear model of active device gives a succesful result. But otherwise there can be a performance degradation. Hence, we conclude that, to improve the success of the proposed technique, harmonically-tuned SP/LP measurement methods and predistortion techniques should be studied in the future.

REFERENCES

[1] **Liu, G., Lai, Z., Zhou, G., and Cheng, Z.** (2022). "Design of a Multi-octave Power Amplifier with a Novel Broadband Design Methodology," *IEICE Electronics Express*, vol. advpub, 19.20220073, doi: 10.1587/elex.19.20220073.

[2] **Huang, C., He, S., Shi, W., and Song, B.** (2018). "Design of Broadband High-Efficiency Power Amplifiers Based on the Hybrid Continuous Modes With Phase Shift Parameter," *IEEE Microwave and Wireless Components Letters*, vol. 28, no. 2, pp. 159-161, doi: 10.1109/LMWC.2017.2787061.

[3] **Hu, X., Meng, X., Yu, C., and Liu, Y.** "Design of highly efficient broadband harmonic-optimised GaN power amplifier via modified simplified real frequency technique," *Electronics Letters*, vol. 53, no. 21, pp. 1414-1416. [Online]. Available: https://digital-library.theiet.org/content/journals/10.1049/el.2017.2849

[4] **Rubio, J. J. M., Camarchia, V., Quaglia, R., Malaver, E. F. A., and Pirola, M.** (2016). "A 0.6–3.8 GHz GaN Power Amplifier Designed Through a Simple Strategy," *IEEE Microwave and Wireless Components Letters*, vol. 26, no. 6, pp. 446-448, doi: 10.1109/LMWC.2016.2549263.

[5] **Shi, W., He, S., Li, Q., Qi, T., and Liu, Q.** (2016). "Design of Broadband Power Amplifiers Based on Resistive-Reactive Series of Continuous Modes," *IEEE Microwave and Wireless Components Letters*, vol. 26, no. 7, pp. 519-521, doi: 10.1109/LMWC.2016.2574823.

[6] **Chen, J., He, S., You, F., Tong, R., and Peng, R.** (2014). "Design of Broadband High-Efficiency Power Amplifiers Based on a Series of Continuous Modes," *IEEE Microwave and Wireless Components Letters*, vol. 24, no. 9, pp. 631-633, doi: 10.1109/LMWC.2014.2331457.

[7] **Shealy, J. B., Lefevre, M., Anderson, B., Runton, D., Poulton, M. J., and Martin, J.** "Optimization of Gallium nitride high power technology for commercial and military applications," in *2009 IEEE Bipolar/BiCMOS Circuits and Technology Meeting*, 12-14 Oct. 2009 2009, pp. 146-153, doi: 10.1109/BIPOL.2009.5314127.

[8] **Xie, C. and Pavio, A.** "Development of GaN HEMT based High Power High Efficiency Distributed Power Amplifier for Military Applications," in *MILCOM 2007 - IEEE Military Communications Conference*, 29-31 Oct. 2007 2007, pp. 1-4, doi: 10.1109/MILCOM.2007.4455083.

[9] **Kenney, J. S. and Chen, J.** "Power Amplifier Linearization and Efficiency Improvement Techniques for Commercial and Military Applications," in *2006 International Conference on Microwaves, Radar & Wireless Communications*, 22-24 May 2006 2006, pp. 3-8, doi: 10.1109/MIKON.2006.4345092.

[10] **Moussaoui, M., Bertin, E., and Crespi, N.** "5G shortcomings and Beyond-5G/6G requirements," in *2022 1st International Conference on 6G Networking (6GNet)*, 6-8 July 2022 2022, pp. 1-8, doi: 10.1109/6GNet54646.2022.9830439.

[11] **Gustavsson, U. *et al.*** (2021). "Implementation Challenges and Opportunities in Beyond-5G and 6G Communication," *IEEE Journal of Microwaves*, vol. 1, no. 1, pp. 86-100, doi: 10.1109/JMW.2020.3034648.

[12] **Lapedus, M.** (2020). "Power Amp Wars Begin For 5G." Semiconductor Engineering. **Url** < *https://semiengineering.com/power-amp-wars-begin-for-5g/* >, date retrieved: December, 2022.

[13] **Collaert, N. *et al.*** (2020). "(Plenary) The Revival of Compound Semiconductors and How They Will Change the World in a 5G/6G Era," *ECS Transactions*, vol. 98, no. 5, p. 15, 2020/09/08, Art no., doi: 10.1149/09805.0015ecst.

[14] "Exceeding Wideband Power Amplifier Design Needs for 5G Power & Beyond." Wolfspeed. **Url** < *https://www.wolfspeed.com/knowledge-center/article/exceeding-wideband-power-amplifier-design-needs-for-5g-power-and-beyond/* >, date retrieved: December, 2022.

[15] **Bi, Q.** (2019). "Ten Trends in the Cellular Industry and an Outlook on 6G," *IEEE Communications Magazine*, vol. 57, no. 12, pp. 31-36, doi: 10.1109/MCOM.001.1900315.

[16] "Design, Manufacture & Test of a Single-chip Ka-band Doherty Power Amplifier." The European Space Agency. **Url** < *https://www.esa.int/Enabling_Support/Space_Engineering_Technology/Shaping_the_Future/Design_Manufacture_Test_of_a_Single-chip_Ka-band_Doherty_Power_Amplifier* >, date retrieved: January, 2023.

[17] **Sharma, A. *et al.*** "High efficiency 25 Watt GaN X-band SSPA for deep space missions," in *2017 IEEE Aerospace Conference*, 4-11 March 2017 2017, pp. 1-8, doi: 10.1109/AERO.2017.7943723.

[18] **Boger, W., Burgess, D., Honda, R., and Nuckolls, C.** "X-band, 17 Watt, solid-state power amplifier for space applications," in *IEEE MTT-S International Microwave Symposium Digest, 2005.*, 17-17 June 2005 2005, pp. 1379-1382, doi: 10.1109/MWSYM.2005.1516940.

[19] "Going GaN: Novel Chips Powering Space Missions." Directorate of Technology, Engineering and Quality, ESA. **Url** < https://technology.esa.int/news/going-gan-novel-chips-powering-space-missions >, date retrieved: December, 2022.

[20] **Kikkawa, T., Joshin, K., and Kanamura, M.** (2012). "GaN Device for Highly Efficient Power Amplifiers," *Fujitsu Sci. Tech. J.*, vol. 48, pp. 71-74.

[21] **Mizuno, S., Yamada, F., Yamamoto, H., Nishihara, M., Yamamoto, T., and Sano, S.** (2012). "Development of GaN HEMT for Microwave Wireless Communications," *SEI TECHNICAL REVIEW*, no. 74, pp. 71-74.

[22] **Komiak, J. J.** (2015). "GaN HEMT: Dominant Force in High-Frequency Solid-State Power Amplifiers," *IEEE Microwave Magazine*, vol. 16, no. 3, pp. 97-105, doi: 10.1109/MMM.2014.2385303.

[23] **K. Inoue, S. S., Y. Tateno, F. Yamaki, K. Ebihara, N. Ui, A. Kawano and H. Deguchi,** (2010). "Development of Gallium Nitride High Electron Mobility Transistor for Cellular Base Stations," *SEI TECHNICAL REVIEW*, no. 71, pp. 88-93.

[24] **Pengelly, R. S., Wood, S. M., Milligan, J. W., Sheppard, S. T., and Pribble, W. L.** (2012). "A Review of GaN on SiC High Electron-Mobility Power Transistors and MMICs," *IEEE Transactions on Microwave Theory and Techniques*, vol. 60, no. 6, pp. 1764-1783, doi: 10.1109/TMTT.2012.2187535.

[25] **Grebennikov, A., Kumar, N., and Yarman, B. S.** (2015). *Broadband RF and microwave amplifiers*. CRC Press.

[26] **Grebennikov, A.** (2019). *Radio Frequency and Microwave Power Amplifiers. Volume 1: Principles, Device Modeling and Matching Networks*. Institution of Engineering and Technology.

[27] **Grebennikov, A.** (2019). *Radio Frequency and Microwave Power Amplifiers. Volume 2: Efficiency and Linearity Enhancement Techniques*. Institution of Engineering and Technology.

[28] **Steve, C.** (2006). *RF Power Amplifiers for Wireless Communications*, Second Edition. Artech, p. 1.

[29] **Gonzalez, G.** (1996). *Microwave transistor amplifiers (2nd ed.): analysis and design*. Prentice-Hall, Inc.Division of Simon and Schuster One Lake Street Upper Saddle River, NJUnited States.

[30] "GaN HEMT Large Signal Models." Wolfspeed, Inc. **Url** < https://www.wolfspeed.com/knowledge-center/article/gan-hemt-large-signal-models/ >, date retrieved: January, 2023.

[31] **Dunleavy, L.** (2019). "GaN HEMT Models 101: How Do Nonlinear Models Help with GaN PA Design?" Qorvo, Inc. **Url** < *https://www.qorvo.com/design-hub/blog/gan-hemt-models-101-how-do-nonlinear-models-help-with-gan-pa-design* >, date retrieved: January, 2023.

[32] **Chen, J.** (2019). "RF GaN Model Survey and Model Parameter Extraction Flows." Keysight Technologies. **Url** < *https://keysightevent.com/190625/handout/pdf/a/1_RF_GaN_Model_Survey_and_Model_Parameter_Extraction_Flows.pdf* >, date retrieved: January, 2023.

[33] **Verspecht, J., Root, D. E., Wood, J., and Cognata, A.** "Broad-band, multi-harmonic frequency domain behavioral models from automated large-signal vectorial network measurements," in *IEEE MTT-S International Microwave Symposium Digest, 2005.*, 17-17 June 2005 2005, pp. 1975-1978, doi: 10.1109/MWSYM.2005.1517130.

[34] **Curras-Francos, M. C.** (2005). "Table-based nonlinear HEMT model extracted from time-domain large-signal measurements," *IEEE Transactions on Microwave Theory and Techniques*, vol. 53, no. 5, pp. 1593-1600, doi: 10.1109/TMTT.2005.847049.

[35] **Angelov, I., Schreurs, D., Andersson, K., Ferridahl, M., and Ingvarson, F.** "An empirical table based HBT large signal model," in *34th European Microwave Conference, 2004.*, 12-14 Oct. 2004 2004, vol. 1, pp. 229-232.

[36] **Corbella, I., Legido, J. M., and Naval, G.** (1992). "Instantaneous model of a MESFET for use in linear and nonlinear circuit simulations," *IEEE Transactions on Microwave Theory and Techniques*, vol. 40, no. 7, pp. 1410-1421, doi: 10.1109/22.146322.

[37] **Angelov, I., Zirath, H., and Rosman, N.** (1992). "A new empirical nonlinear model for HEMT and MESFET devices," *IEEE Transactions on Microwave Theory and Techniques*, vol. 40, no. 12, pp. 2258-2266, doi: 10.1109/22.179888.

[38] **Curtice, W. R. and Ettenberg, M.** (1985). "A Nonlinear GaAs FET Model for Use in the Design of Output Circuits for Power Amplifiers," *IEEE Transactions on Microwave Theory and Techniques*, vol. 33, no. 12, pp. 1383-1394, doi: 10.1109/TMTT.1985.1133229.

[39] **Curtice, W. R.** (1980). "A MESFET Model for Use in the Design of GaAs Integrated Circuits," *IEEE Transactions on Microwave Theory and Techniques*, vol. 28, no. 5, pp. 448-456, doi: 10.1109/TMTT.1980.1130099.

[40] **Maier, T., Carrubba, V., Quay, R., Raay, F. v., and Ambacher, O.** "Active harmonic source-/load-pull measurements of AlGaN/GaN HEMTs at X-band frequencies," in *83rd ARFTG Microwave Measurement Conference*, 6-6 June 2014 2014, pp. 1-4, doi: 10.1109/ARFTG.2014.6899516.

[41] **Teppati, V., Ferrero, A., and Sayed, M. V. Teppati, A. Ferrero, and M. Sayed** Eds. (2013). *Modern RF and Microwave Measurement Techniques* (The Cambridge RF and Microwave Engineering Series). Cambridge: Cambridge University Press.

[42] **Cripps, S. C.** "A Theory for the Prediction of GaAs FET Load-Pull Power Contours," in *1983 IEEE MTT-S International Microwave Symposium Digest*, 31 May-3 June 1983 1983, pp. 221-223, doi: 10.1109/MWSYM.1983.1130864.

[43] **Cusack, J., Perlow, S., and Perlman, B.** "Automatic Load Contour Mapping for Microwave Power Transistors," in *S-MTT International Microwave Symposium Digest*, 12-14 June 1974 1974, vol. 74, 1 ed., pp. 269-271, doi: 10.1109/MWSYM.1974.1123569.

[44] "Wolfspeed a Cree Company, GaN HEMT Transistor series CG2H40045." Durham, North Carolina, USA 27703. **Url** < *https://www.wolfspeed.com/cg2h40045* >, date retrieved: June, 2022.

[45] "Wolfspeed a Cree Company, GaN HEMT Transistor series CGH40010." Durham, North Carolina, USA 27703. **Url** < *https://www.wolfspeed.com/cgh40010* >, date retrieved: June, 2022.

[46] **Blum, S.** (2021). "How to Enable a Successful RF Broadband Design for a 500 – 3000 MHz Amplifier." Wolfspeed, Inc. **Url** < *https://www.wolfspeed.com/knowledge-center/article/how-to-enable-a-successful-rf-broadband-design-for-a-500-3000-mhz-amplifier/* >, date retrieved: December 2022.

[47] **Blum, S.** (2021). "Wolfspeed's GaN-on-SiC Tackles Broadband Design Challenges." Wolfspeed, Inc. **Url** < *https://www.eetimes.eu/wolfspeeds-gan-on-sic-tackles-broadband-design-challenges/* >, date retrieved: December 2022.

[48] **Rhea, R.** (2006). "The Yin-Yang of Matching: Part 1—Basic Matching Concepts," *High Frequency Electronics*, vol. 5, no. 3, pp. 16-24.

[49] **Rhea, R.** (2006). "The Yin-Yang of Matching: Part 2—Practical Matching Techniques," *High Frequency Electronics*, vol. 5, no. 4, pp. 28-40.

[50] **Yarman, B. S.** (2010). *Design of Ultra Wideband Power Transfer Networks*. John Wiley & Sons, Inc.

[51] **Yarman, B. S. *et al.*** (2016). "Computer Aided Darlington Synthesis of an All Purpose Immittance Function," *Electrica*, vol. 16, no. 1.

[52] **Yarman, B. S., Aksen, A., Kopru, R., Aydın, C., and Atilla, C.** "Computer aided high precision darlington synthesis for real frequency matching," in *2014 IEEE Benjamin Franklin Symposium on Microwave and Antenna Sub-systems for Radar, Telecommunications, and Biomedical Applications (BenMAS)*, 26-26 Sept. 2014 2014, pp. 1-3, doi: 10.1109/BenMAS.2014.7529474.

[53] **Kilinc, A. and Yarman, B. S.** (2013). "High Precision LC Ladder Synthesis Part I: Lowpass Ladder Synthesis via Parametric Approach," *IEEE Transactions on Circuits and Systems I: Regular Papers*, vol. 60, no. 8, pp. 2074-2083, doi: 10.1109/TCSI.2013.2239163.

[54] **Yarman, B. S. and Kilinc, A.** (2013). "High Precision LC Ladder Synthesis Part II: Immittance Synthesis With Transmission Zeros at DC and Infinity," *IEEE Transactions on Circuits and Systems I: Regular Papers*, vol. 60, no. 10, pp. 2719-2729, doi: 10.1109/TCSI.2013.2244315.

[55] **Yarman, B. S., Kopru, R., Kumar, N., and Prakash, C.** (2014). "High Precision Synthesis of a Richards Immittance Via Parametric Approach," *IEEE Transactions on Circuits and Systems I: Regular Papers*, vol. 61, no. 4, pp. 1055-1067, doi: 10.1109/TCSI.2013.2285913.

[56] **Li, M., Pang, J., Li, Y., and Zhu, A.** (2019). "Ultra-Wideband Dual-Mode Doherty Power Amplifier Using Reciprocal Gate Bias for 5G Applications," *IEEE Transactions on Microwave Theory and Techniques*, vol. 67, no. 10, pp. 4246-4259, doi: 10.1109/TMTT.2019.2932977.

[57] **Komatsuzaki, Y., Ma, R., Sakata, S., Nakatani, K., and Shinjo, S.** "A Dual-Mode Bias Circuit Enabled GaN Doherty Amplifier Operating in 0.85-2.05GHz and 2.4-4.2GHz," in *2020 IEEE/MTT-S International Microwave Symposium (IMS)*, 4-6 Aug. 2020 2020, pp. 277-280, doi: 10.1109/IMS30576.2020.9223999.

[58] **Formicone, G., Burger, J., Custer, J., Keshishian, R., and Veitschegger, W.** "A study for achieving high power and efficiency based on high bias operation in C- and X-band GaN power amplifiers," in *2018 IEEE Topical Conference on RF/Microwave Power Amplifiers for Radio and Wireless Applications (PAWR)*, 14-17 Jan. 2018 2018, pp. 39-42, doi: 10.1109/PAWR.2018.8310062.

[59] **Nikandish, G. R., Staszewski, R. B., and Zhu, A.** (2021). "A Fully Integrated GaN Dual-Channel Power Amplifier With Crosstalk Suppression for 5G Massive MIMO Transmitters," *IEEE Transactions on Circuits and Systems II: Express Briefs*, vol. 68, no. 1, pp. 246-250, doi: 10.1109/TCSII.2020.3008365.

[60] **Nikandish, G. R., Staszewski, R. B., and Zhu, A.** (2020). "Broadband Fully Integrated GaN Power Amplifier With Minimum-Inductance BPF Matching and Two-Transistor AM-PM Compensation," *IEEE Transactions on Circuits and Systems I: Regular Papers*, vol. 67, no. 12, pp. 4211-4223, doi: 10.1109/TCSI.2020.3002395.

[61] **Liu, B., Boon, C. C., Mao, M., Choi, P., and Guo, T.** (2021). "A 2.4–6 GHz Broadband GaN Power Amplifier for 802.11ax Application," *IEEE Transactions on Circuits and Systems I: Regular Papers*, vol. 68, no. 6, pp. 2404-2417, doi: 10.1109/TCSI.2021.3073345.

[62] **Krishnamurthy, K., Driver, T., Vetury, R., and Martin, J.** "100 W GaN HEMT power amplifier module with 60% efficiency over 100–1000 MHz bandwidth," in *2010 IEEE MTT-S International Microwave Symposium*, 23-28 May 2010 2010, pp. 940-943, doi: 10.1109/MWSYM.2010.5518242.

[63] **Carlin, H.** (1977). "A new approach to gain-bandwidth problems," *IEEE Transactions on Circuits and Systems*, vol. 24, no. 4, pp. 170-175, doi: 10.1109/TCS.1977.1084325.

[64] **Carlin, H. J. and Civalleri, P. P.** (1998). *Wideband Circuit Design*. New York: CRC Press.

[65] **Carlin, H. and Amstutz, P.** (1981). "On optimum broad-band matching," *IEEE Transactions on Circuits and Systems*, vol. 28, no. 5, pp. 401-405, doi: 10.1109/TCS.1981.1085001.

[66] **Carlin, H. and Yarman, B.** (1983). "The double matching problem: Analytic and real frequency solutions," *IEEE Transactions on Circuits and Systems*, vol. 30, no. 1, pp. 15-28, doi: 10.1109/TCS.1983.1085281.

[67] **Levenberg, K.** (1944). "A Method for The Solutionof Certain Non-Linear Problems in Least Squares," *Quarterly of Applied Mathematics*, vol. 2, no. 2, pp. 164-168. [Online]. Available: http://www.jstor.org/stable/43633451.

[68] **Marquardt, D. W.** (1963). "An Algorithm for Least-Squares Estimation of Nonlinear Parameters," *Journal of the Society for Industrial and Applied Mathematics*, vol. 11, no. 2, pp. 431-441. [Online]. Available: http://www.jstor.org/stable/2098941.

[69] **Coleman, T. F. and Li, Y.** (1996). "An Interior Trust Region Approach for Nonlinear Minimization Subject to Bounds," *SIAM J. Optim.*, vol. 6, pp. 418-445.

[70] "MatLab Software." from MathWorks Inc. **Url** < *https://www.mathworks.com/products/matlab.html* >, date retrieved: April, 2022.

[71] **Yarman, B. S. and Fettweis, A.** (1990). "Computer-aided double matching via parametric representation of Brune functions," *IEEE Transactions on Circuits and Systems*, vol. 37, no. 2, pp. 212-222, doi: 10.1109/31.45713.

[72] "PathWave Advanced Design System (ADS) from Keysight." **Url** < *https://www.keysight.com/zz/en/products/software/pathwave-design-software/pathwave-advanced-design-system.html* >, date retrieved: June, 2022.

[73] **Yarman, B. S.** (2010). in *Design of Ultra Wideband Power Transfer Networks*: John Wiley & Sons, Inc., ch. 11: Modern Approaches to Broadband Matching Problems; Real Frequency Solutions", pp. 539-586.

[74] **Yarman, B. S.** (2010). in *Design of Ultra Wideband Power Transfer Networks*: John Wiley & Sons, Inc., ch. 1: Circuit Theory for Power Transfer networks, Section 1.18 Positive Real Functions", pp. 25-33.

[75] **Fettweis, A.** (1979). "Parametric representation of brune functions," *International Journal of Circuit Theory and Applications*, vol. 7, no. 1, pp. 113-119, doi: https://doi.org/10.1002/cta.4490070112.

[76] **Pandel, J. and Fettweis, A.** "Broadband matching using parametric representations," in *IEEE Int. Symp. on Circuits and Systems*, 1985, vol. 41, pp. 143-149.

[77] **Dai, Z. *et al.*** (2019). "Lowpass Network Synthesis Using “Feldtkeller Correction Approach”," *IEEE Access*, vol. 7, pp. 27970-27982, doi: 10.1109/ACCESS.2019.2894408.

[78] **Yarman, B. S., Kilinc, A., and Aksen, A.** (2004). "Immitance data modelling via linear interpolation techniques: A classical circuit theory approach," *International Journal of Circuit Theory and Applications*, vol. 32, no. 6, pp. 537-563, doi: https://doi.org/10.1002/cta.295.

[79] **Aksen, A. and Yarman, B. S.** "A semi-analytical procedure to describe lossless two-ports with mixed lumped and distributed elements," in *Proceedings of IEEE International Symposium on Circuits and Systems - ISCAS '94*, 30 May-2 June 1994 1994, vol. 5, pp. 205-208 vol.5, doi: 10.1109/ISCAS.1994.409340.

[80] **Yarman, B. S. and Aksen, A.** (1992). "An integrated design tool to construct lossless matching networks with mixed lumped and distributed elements," *IEEE Transactions on Circuits and Systems I: Fundamental Theory and Applications*, vol. 39, no. 9, pp. 713-723, doi: 10.1109/81.250162.

[81] **Rhea, R. W.** (1994). *HF Filter Design and Computer Simulation*. Institution of Engineering and Technology.

[82] **Pozar, D. M.** (2012). *Microwave engineering*. Fourth edition. Hoboken, NJ : Wiley, [2012] ©2012.

[83] "Taconic Corp." **Url** < *http://www.taconic.co.kr/english/pages/sub02_03.php* >, date retrieved: June, 2022.

[84] "KYOCERA AVX Corp." **Url** < *https://www.kyocera-avx.com/* >, date retrieved: 2022.

[85] "Coilcraft Corp." **Url** < *https://www.coilcraft.com/* >, date retrieved: April, 2022.

[86] "Murata Corp." **Url** < *https://www.murata.com/en-eu/products* >, date retrieved: April, 2022.

[87] **Kilinc, S., Ejaz, M. E., Yarman, B. S., Ozoguz, S., Srivastava, S., and Nurellari, E.** (2022). "Broadband performance assessment of a microwave power transistor employing the real frequency technique," *International Journal of Circuit Theory and Applications*, vol. 50, no. 11, pp. 3725-3748, doi: 10.1002/cta.3357.

[88] **Nguyen, C.** (2001). *Analysis Methods for RF, Microwave, and Millimeter-Wave Planar Transmission Line Structures*. Hoboken, New Jersey: John Wiley & Sons, Inc.

[89] **Lee, T. H.** (2004). *Planar Microwave Engineering: A Practical Guide to Theory, Measurement, and Circuits*. Cambridge: Cambridge University Press.

[90] **Fooks, E. H. and Zakarevicius, R. A.** (1990). *Microwave engineering using microstrip circuits*. Prentice-Hall, Inc.

[91] "Rogers Corp." **Url** < *https://www.rogerscorp.com/* >, date retrieved: April, 2022.

CURRICULUM VITAE

Name Surname **: Sedat KILINÇ**

EDUCATION **:**

- **B.Sc.** **:** 2012, Yildiz Technical University, Faculty of Electrical and Electronics, Electronics and Communication Eng. Department
- **M.Sc.** **:** 2015, Istanbul Technical University, Graduate School of Science Engineering and Technology, Electronics and Communication Eng. Department

PROFESSIONAL EXPERIENCE AND REWARDS:

- 2012-2023, Research Assistant, Istanbul University-Cerrahpasa, Faculty of Engineering, Electrical and Electronics Eng. Department.

PUBLICATIONS, PRESENTATIONS AND PATENTS ON THE THESIS:

- **Kilinc, S.,** Ejaz, M.E., Yarman, B.S., Ozoguz, S., Srivastava, S., Nurellari, E. “Broadband performance assessment of a microwave power transistor employing the real frequency technique,” Int J Circ Theor Appl. 2022; 50(11): 3725- 3748. doi:10.1002/cta.3357.
- **Kilinc, S.,** Yarman, B.S., Ozoguz, S., "A GaN Microwave Power Amplifier Design Based on the Source/Load Pull Impedance Modeling via Virtual Gain Optimization," in IEEE Access, vol. 10, pp. 50677-50691, 2022, doi: 10.1109/ACCESS.2022.3174227.
- **Kilinc, S.,** Yarman, B.S., Ozoguz, S. "Broadband Power Amplifier Design via Fictitious Matching," in IEEE Transactions on Circuits and Systems II: Express Briefs, vol. 69, no. 12, pp. 4844-4848, Dec. 2022, doi: 10.1109/TCSII.2022.3207423.

- **Kilinc, S.,** Ejaz, M.E., Yarman, B.S., Ozoguz, S., Srivastava, S., Nurellari, E. "A Realizability Test as Applied on the Generated Source/Load-Pull Data," 2022 Microwave Mediterranean Symposium (MMS), Pizzo Calabro, Italy, 2022, pp. 1-5, doi: 10.1109/MMS55062.2022.9825589.
- **Kilinc, S.,** Ejaz, M.E., Yarman, B.S., Ozoguz, S., Srivastava, S., Nurellari, E. "A Numerical Procedure to Determine the Power Intake/Delivery Capacity of a GaN RF Power Transistor over Broadband," 2022 Microwave Mediterranean Symposium (MMS), Pizzo Calabro, Italy, 2022, pp. 1-6, doi: 10.1109/MMS55062.2022.9825519.
- **Kilinc, S.,** Yarman, B.S., Ozoguz, **S.** “Sanal Kazanç Optimizasyon Yöntemi ile Genişbandlı Mikrodalga Güç Kuvvetlendiricisi Tasarımı, Design of a Broadband Microwave Power Amplifier via Virtual Gain Optimization,” ELECO 2022 Elektrik-Elektronik ve Biyomedikal Mühendisliği Konferansı, Bursa, 24-26 Kasım 2022.

OTHER PUBLICATIONS, PRESENTATIONS AND PATENTS:

Journal Publications:

- Güreş, E., **Kılınç, S.,** Shayea, I., Ferhanoğlu, O. “Wideband and dual-polarized Twin Hilbert curve antennas for capsule endoscopy,” Microw Opt Technol Lett. 2023; 65: 169- 175. doi:10.1002/mop.33444.
- Yildiz, S., Aksen, A., **Kılınç, S.,** Yarman, BS. **“**Low pass filter design with improved stop-band suppression and synthesis with transformer-free ladders. IET Circuits Devices Syst. 15(6), 504– 510 (2021). https://doi.org/10.1049/cds2.12045.
- Alemdag, M., Kacar, F., **Kilinc, S**. “Design of a Class-F Power Amplifier with GaN Device Model and Reflection Data,” IETE Journal of Research (2020), DOI: 10.1080/03772063.2020.1859950.
- Yildiz, S., Aksen, A., **Kilinc, S.,** & Yarman, SB. “Multiband Filter Design Using Generalized Mapping Functions and Synthesis with Lumped Resonators,” RADIOENGINEERING, (2020) , vol.29, no.2, 343-352.
- Yildiz, S., Aksen, A., **Kilinc, S.** and Yarman, SB. “Dual band stop filter design via frequency transformation and synthesis with lumped resonators,” IET Circuits Devices Syst. (2020), 14: 311-315. https://doi.org/10.1049/iet-cds.2019.0411.
- Aydin, C., Atilla, DC., Kopru, R, **Kılınc, S.,** Karakuş, C., Yarman, BS. “A design technique of 50 Ω terminated bandpass matching network and its implementation to a Y-shaped monopole antenna matching” Analog Integr Circ Sig Process 89, 665–673 (2016). https://doi.org/10.1007/s10470-016-0768-3.
- Aydoğan, A., Uysal, A., Akleman, F., **Kılınç, S.,** Çağlayan, T. “Keyfi Şekilli Dielektrik Yüklü Dalga Kılavuzları için Saçılma Parametrelerinin Belirlenmesi,” EMO Bilimsel Dergi, (2017) 7 (13), 33-39. Retrieved from https://dergipark.org.tr/en/pub/emobd/issue/34416/293213.

- Kopru, R., **Kilinc, S.,** Aydin, C., Atilla, D., Karakuş, C., & Yarman, B. “Ultra wideband matching network design for a V-shaped square planar monopole antenna”, International Journal of Microwave and Wireless Technologies, (2014), 6(6), 555-564. doi:10.1017/S1759078714001081.

Conference Publications:

- Yarman, BS., **Kilinc, S.** “Kompleks Jeneratörü-Kompleks Yüke Uyumlaştırmak için Yeni Reel Frekans Tekniği New Real Frequency Technique to Match Complex Generator to Complex Load,” ELECO 2022 Elektrik-Elektronik ve Biyomedikal Mühendisliği Konferansı, Bursa, 24-26 Kasım 2022.
- Ejaz, M.E., **Kilinc, S.,** Yarman, B.S., Ozoguz, S., Srivastava, S., Nurellari, E. "A Unified Real Frequency Technique for the Solution to Broadband Matching Problems," 2022 Microwave Mediterranean Symposium (MMS), Pizzo Calabro, Italy, 2022, pp. 1-6, doi: 10.1109/MMS55062.2022.9825618.
- Ejaz, M.E., **Kilinc, S.,** Yarman, B.S., Srivastava, S., "10W GaN PA for 5G NR n78 Band Utilizing RFT Parametric Approach," Mediterranean Microwave Symposium 2020 (MMS’20) , Tanjah, Morocco, pp.1-4, 2020.
- Yildiz, S., Aksen, A., **Kilinc, S.** and Yarman, B.S. "A Triple Band Filter Design for the Commercial Bands Using Triple Band Frequency Mapping Technique," Mediterranean Microwave Symposium 2020 (MMS’20) , Tanjah, Morocco, pp.1-4, 2020.
- Yıldız, S., Aksen, A., **Kılınç, S. and** Yarman, B.S. "İki Bantlı Frekans Transformasyonu ile İki Bantlı RF Devre Tasarımları," Elektrik Elektronik Mühendisliği Kongresi 2019 (EEMKON2019) , İstanbul, Turkey, pp.379-384, 2019.
- **Kilinc, S.,** Yarman, B.S., "Design of an Ultra-Wideband GaN Power Amplifier via Real Frequency Technique," 2018 18th Mediterranean Microwave Symposium (MMS), Istanbul, Turkey, 2018, pp. 179-182, doi: 10.1109/MMS.2018.8612071.
- Yildiz, S., Aksen, A., **Kilinc, S.** and Yarman, B.S. "Dual Band Filter Design for GSM Bands Using Frequency Mapping and Real Frequency Technique," 2018 18th Mediterranean Microwave Symposium (MMS), Istanbul, Turkey, 2018, pp. 164-167, doi: 10.1109/MMS.2018.8612080.
- **Kilinc S.,** and Yarman, B.S. "A novel method to design broadband flat gain and sufficiently efficient power amplifiers using real frequency technique," 2017 24th IEEE International Conference on Electronics, Circuits and Systems (ICECS), Batumi, Georgia, 2017, pp. 30-33, doi: 10.1109/ICECS.2017.8292061.
- Kopru, R., Atilla, D., Aydin, C., **Kilinc, S.** & Yarman, B.S. "Design and realization of 8–12 GHz cascaded unit element microstrip filter for X-band," 2016 16th Mediterranean Microwave Symposium (MMS), Abu Dhabi, United Arab Emirates, 2016, pp. 1-4, doi: 10.1109/MMS.2016.7803792.
- Yildizbas, E., **Kilinc S.,** and Yarman, B.S. "GPS receiver front-end circuit layers 1.575 GHz LNA and antenna design," 2016 National Conference on Electrical, Electronics and Biomedical Engineering (ELECO), Bursa, Turkey, 2016, pp. 586-589.

- Koc, O., **Kilinc S.,** Kopru, R., and Yarman, B.S. "0.8–1.9 GHz microwave amplifier design," 2016 National Conference on Electrical, Electronics and Biomedical Engineering (ELECO), Bursa, Turkey, 2016, pp. 567-571.
- Kopru, R., Aydin, Ç., Atilla, D., **Kilinc, S.** & Yarman, B.S. "Wideband bandpass filter design for X band horn antenna via numerical techniques," 2015 IEEE 15th Mediterranean Microwave Symposium (MMS), Lecce, Italy, 2015, pp. 1-5, doi: 10.1109/MMS.2015.7375495.
- **Kilinc, S.,** Kopru, R., Aksen, A., and Yarman, B.S. "Mixed element wideband microwave amplifier design via simplified real frequency technique," Proceedings of 2014 Mediterranean Microwave Symposium (MMS2014), Marrakech, Morocco, 2014, pp. 1-3, doi: 10.1109/MMS.2014.7088951.
- Kopru, R., **Kilinc, S.,** Aksen, A., and Yarman, B.S. "Unit element bandpass filter design via simplified real frequency technique for UWB microstrip patch antenna," Proceedings of 2014 Mediterranean Microwave Symposium (MMS2014), Marrakech, Morocco, 2014, pp. 1-5, doi: 10.1109/MMS.2014.7088952.
- Kopru, R., **Kilinc, S.,** Aksen, A., and Yarman, B.S. "Design and implementation of wideband microwave amplifiers based on Normalized Gain Function," 2014 IEEE Benjamin Franklin Symposium on Microwave and Antenna Sub-systems for Radar, Telecommunications, and Biomedical Applications (BenMAS), Philadelphia, PA, USA, 2014, pp. 1-3, doi: 10.1109/BenMAS.2014.7529463.
- **Kilinc, S.,** Kopru, R., Yarman, B.S. "Design and realization of wideband matching networks in Richards domain," 2014 IEEE Benjamin Franklin Symposium on Microwave and Antenna Sub-systems for Radar, Telecommunications, and Biomedical Applications (BenMAS), Philadelphia, PA, USA, 2014, pp. 1-3, doi: 10.1109/BenMAS.2014.7529476.
- Kopru, R., **Kilinc, S.,** and Yarman, B.S. "Gerçel Frekans Tekniği Kullanarak Mikroşerit Yama Anten Uyum Devresi Tasarımı," URSI-Türkiye'2014 Bilimsel Kongresi ve Ulusal Genel Kurulu , Elazığ, Turkey, pp.1-3, 2014.
- **Kilinc, S.,** Kopru, R., Yarman, B.S. "Bir Genişband Empedans Uyum Devresinin Richards Uzayında Eş Uzunluklu Birim Elemanlar ile Sentezlenmesi," URSI-Türkiye'2014 Bilimsel Kongresi ve Ulusal Genel Kurulu , Elazığ, Turkey, pp.1-3, 2014.